NEW TECHNOLOGIES AND APPLICATIONS IN ENERGY-ABSORBING CELLULAR MATERIALS, AIRBAG PRE-DEPLOYMENT, INJURY PREDICTION TO OUT-OF-POSITION OCCUPANTS, AND ESTIMATION OF DRIVER FATALITY RATIO, FOR ENHANCING PASSIVE SAFETY OF ROAD VEHICLES IN SIDE-IMPACT ACCIDENTS

A Thesis by

Yi Yang Tay

Bachelor of Science, Wichita State University, 2012

Submitted to the Department of Mechanical Engineering
and the faculty of Graduate School of
Wichita State University
in partial fulfillment of
the requirements for the degree of
Master of Science

May 2014

© Copyright 2014 by Yi Yang Tay

All Rights Reserved

NEW TECHNOLOGIES AND APPLICATIONS IN ENERGY-ABSORBING CELLULAR MATERIALS, AIRBAG PRE-DEPLOYMENT, INJURY PREDICTION TO OUT-OF-POSITION OCCUPANTS, AND ESTIMATION OF DRIVER FATALITY RATIO, FOR ENHANCING PASSIVE SAFETY OF ROAD VEHICLES IN SIDE-IMPACT ACCIDENTS

The following faculty members have examined the final copy of this thesis for form and content, and recommend that it is accepted in partial fulfillment of the requirement for the degree of Master of Science with a major in Mechanical Engineering.

_____
Hamid Lankarani, Committee Chair

_____
Krishnan Krishna, Committee Member

_____
Davood Askari, Committee Member

DEDICATION

To my loving parents, Mr. John Tay and Mrs. Esther Aw
&
my brother, Daniel

To my advisor, Dr. Hamid Lankarani

ACKNOWLEDGMENTS

I wish to express my deepest gratitude to my advisor, Dr. Hamid Lankarani, professor of the Mechanical Engineering Department at Wichita State University. It has been a great privilege to be under his wing for the past few years. He has inspired me in many ways and has provided me with tremendous amount of opportunities to hone my engineering skills. I deeply cherish his continuous support and encouragement throughout my Master's program. This thesis would not have been possible without his professional guidance.

I would like to extend my gratitude to Dr. Krishna Krishnan and Dr. Davood Askari for serving on my thesis committee. Special thanks to Dr. Rasoul Moradi and Dr. Chee Sern Lim for their collaboration and valuable comments on my work. They have always provided me with great ideas in fine-tuning my research work.

I take this opportunity to express my sincere gratitude to my parents and brother for being my pillar of strength. I am forever grateful for them.

I would like to express my appreciation to all my colleagues and friends for creating a great working environment at the university. My appreciation goes out to all faculty and staff of the Department of Mechanical Engineering for their constant support.

ABSTRACT

The automotive industry is repeatedly tasked with improving vehicles structural strength, optimizing active and passive safety features, reducing occupant injury potential, and hitting lean manufacturing goals. The challenge is to find solutions to reduce production and research costs, and to maximize the vehicle's capability in protecting its occupants in the event of an accident. The influence of impact loading on the dynamic responses of vehicle structures and occupants require special consideration in the field of vehicle crashworthiness. The main goal of this study is to address the fundamental aspect on the impact injury biomechanics of vehicle occupants and safety performance of vehicle structures, and the development of various new technologies aimed at enhancing the passive safety of road vehicles in side-impact accidents. Four case studies related to the dissipation of crash energy, impact injury biomechanics, injury prediction model and pre-crash sensing algorithm form the basis of this thesis. The application examples include the investigation of pre-deploying airbags as a potential solution in reducing occupants' injuries at higher speed side-impact crashes; examination of the vehicle structural responses with the inclusion of high-energy absorbing cellular materials within the door panels in side-impact accidents; development of injury prediction model to out-of-position occupants from frontal- and side- airbags using Design-of-Experiment methodologies; and the estimation of the relative driver fatality risks of two colliding vehicles using some quantitative measurements. A detailed methodology is developed for each application, and the results present several new technologies that can be implemented to enhance the safety performance of road vehicles. These goals are achieved through the use of finite element approaches, multi-body dynamic analyses and Design-of-Experiment statistical methods.

TABLE OF CONTENTS

Chapter **Page**

TABLE OF CONTENTS (continued)

Chapter **Page**

TABLE OF CONTENTS (continued)

Chapter **Page**

LIST OF TABLES

Table **Page**

LIST OF TABLES (continued)

Table **Page**

LIST OF FIGURES

Figure **Page**

LIST OF FIGURES (continued)

Figure **Page**

LIST OF FIGURES (continued)

Figure **Page**

LIST OF FIGURES (continued)

Figure **Page**

ABBREVIATIONS

Symbol	Description
AIS	Abbreviated Injury Scale
AM	Aggressivity Metrics
ATD	Anthropomorphic Test Device
CONFOR Green	General Aviation Seat Cushion Foam
DAX55	General Aviation Seat Cushion Foam
DFR	Driver Fatality Ratio
DOE	Design-of-Experiments
DOF	Degrees of Freedom
FARS	Fatality Analysis Reporting Center
FEM	Finite Element Method
FMVSS	Federal Motor Vehicle Safety Standards
GSI	Gadd Severity Index
GES	General Estimate System
HIC	Head Injury Criteria
IARV	Injury Assessment Reference Values
IIHS	Insurance Institute for Highway Safety
LSTC	Livermore Software Technology Corporation
LTV	Light Trucks and Vans
MAC	Micro-agglomerated cork
MADYMO	Mathematical Dynamic Models
MDB	Moving Deformable Barrier
NASS	National Automotive Sampling System
NCAC	National Crash Analysis Center
NCSA	National Center for Statistics and Analysis
NHTSA	National Highway Traffic Safety Administration
OOP	Out-of-Position Occupants
PUF	Polyurethane Foam
RSM	Response-Surface Method
SAB	Side-Impact Airbags
SCI	Special Crash Investigation
SID	Side-Impact Dummy
TTI	Thoracic Trauma Index
TWG	The Side Airbag Out-Of-Position Injury Technical Working Group
US-NCAP	U.S. New Car Assessment Program
VC	Viscous Criteria
WSTC	Wayne State Tolerance Curve

CHAPTER ONE

INTRODUCTION

1.1 Background

A few decades ago, the design and analysis of mechanical components was purely based on trial and error from experienced machinist. Later, engineers have coupled mathematical models into the analysis of mechanical systems to enhance some of the limitations faced by trial and error methods. As part of today's engineering field, computer-aided design of mechanical systems has emerged as an important tool in designing and analyzing mechanical systems. This is due the significant advancement in computational tools in terms of hardware and software capabilities by creating more efficient and faster data processing computers. More importantly, the demand for the analysis of more complex mechanical systems and models spearheaded the development of various highly specific task oriented software. With the advancement in computer-aided analysis tools, the focus in the field of mechanical engineering has been shifted from system design to system optimization and on improving various existing formulations used to describe the behavior of mechanical systems. Still, the accuracy in the estimation of results using simulation codes greatly depends on the end-user's experience and accurate definition of engineering parameters in the numerical models.

The interaction between any mechanical components is categorized as loading condition and it can be classified into four distinct classifications, namely, static loading, dynamic loading, impact loading and fatigue loading. The dynamic and static responses of mechanical systems vary significantly when subjected different loading conditions. The focus of impact loading on the performance of vehicle crashworthiness and occupant safety outlines this study. From a contact-mechanics point-of-view, impact loading is a high force or

impulse transmitted between two colliding bodies. In general, an impact loading over a short time period, which is also denoted as impulse, generally have greater effect when compared to an impact loading of similar magnitude over a relatively longer time period. In general, an impact process can be classified into two phases, the "loading or compression" phase, and the "restitution or hysteresis" phase. During the loading phase, any two colliding bodies will deform in the direction of impact and reach a common velocity. At the point of common velocity, the two bodies are considered to have reached maximum crush or compression. The hysteresis phase takes place when the separation of the two bodies occurs. It is important to note that the energy dissipation, denoted by the force-indentation curve, is dissimilar for both phases. Hence, it is apparent that the impact-contact forces for these phases cannot be assumed to be similar. Hertz [1] pioneered the development of contact force law of two colliding sphere. Material properties such as the Poisson's ratio and Young's modulus form the basis of the Hertz contact-law. Additionally, the Hertzian contact force assumes the body to be frictionless and perfectly elastic. Using the Hertz model, Dubowsky et al. [2] presented an equation to express the penetration depth of a pin-in-a-hole as a function of contact force. Lankarani and Nikravesh [4] extended the work on contact-impact force by modifying the Hertzian law to include a hysteresis damping function to account for the dissipation of impact energy of a mechanism. Over the years, investigators have utilized the Hertzian contact law and to analyze and optimize various impact-contact mechanisms [5-10]. Two different approaches assist in solving impact contact problems in multi-body systems: the continuous and discontinuous approaches, and these two approaches are investigated in detail by Flores et al. [3]. The first approach is the continuous or penalty approach, where the forces and deformations are assumed to vary in a continuous manner and a force perpendicular to the contact plane is applied when contact is detected. The second approach, the discontinuous or restitution method, is based on the Newton principle where the impact is assumed to occur

instantaneously and the formulation of equation of motion is halted when no contact exist. The analysis of the discontinuous approach is divided into pre- and post- impact, in which the ratio of a body's velocity at pre- and post- impact yields the coefficient of restitution. This second approach is relatively efficient by eliminating the analysis in between the impact. Although this approach is widely adopted for solving intermittent problems [11], it cannot be utilized for solving instantaneous impact loading problems due to its limitations in neglecting the time between impacts.

Imperfection in mechanical joints due to manufacturing error can introduce impact in the joints clearance of mechanisms. Impacts at the joint clearances are highly undesirable because it introduces vibration and wear of the mechanism. For many impact problems, in particular structural deformation or explosive analysis, high stress levels and deformations are expected due to the application of impulse force; hence, the rigid-body analysis is no longer adequate. A more accurate result in the analysis of impact loading can be adopted using the stress-wave propagation and residual energy methods. A detailed analysis of these methods in analyzing impact phenomena is discussed in detailed by Moradi [12]. The variation or increment of local stress and strain of a solid is dependent on its mass density, speed of change in particle velocity and also the impact speeds. To solve complex system, the finite element method (FEM) can be used to capture all impact events. Additionally, FEM is highly capable in applications involving complex geometries such as vehicle or aircraft numerical models.

Studies on vehicle crashworthiness, occupant safety and structural behavior of road vehicles and aircrafts have attracted significant interest from both industry and academia. Impact loadings in vehicle crashes can be considered as an impulse condition as the impact durations are relatively short; the peak dynamic forces transmitted to the occupants in vehicle crashes are in the range of 10 to 100ms. Therefore, vehicle crashes typically undergo high

deceleration and high structural deformation that can be fatal to the occupants. Hence, the automotive industry is repeatedly challenged with reducing structural intrusion into the occupant cabin and to minimize the deceleration experienced by the occupants. Among many methods, dissipation of crash energy in an accident in a controlled manner is vital to reduce the fatality risks of occupants. Due to the complexity of vehicle or aircraft designs, FEM is highly popular for accident reconstructions and analyses of these systems. On the other hand, less complex designs such as the analysis of aircraft seat certification testing can be done using multi-body analysis. Figure 1.1 illustrates some examples of multi-body and finite element analyses of mechanical systems. With the significant stride made in both finite element analysis and multi-body approach, researchers are beginning to evaluate the performance of vehicle crashworthiness using computational coupling method. Coupling technique allows analyzing interaction between multi-body and finite element models simultaneously. In the multi-body dynamic code, MADYMO 7.4.2, the structural deformation of a system can be extracted from the finite element numerical model as "prescribed structural motion" and be used as an input for the facet numerical model in MADYMO. The primary benefit of these methods is to gain better efficiency and to reduce development cost.

Open-loop multi-body system (canadarm) [13]

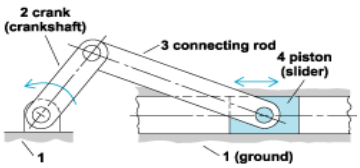

Close-loop multi-body system

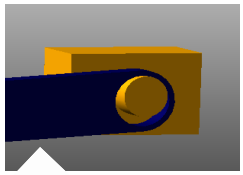

Impact in joint clearance

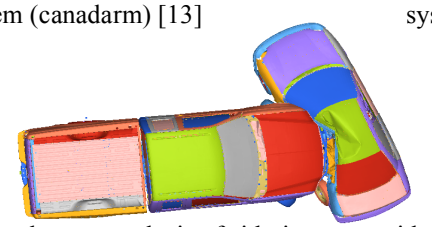

Finite element analysis of side-impact accidents

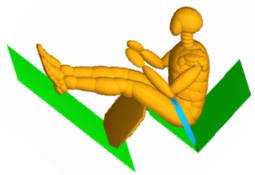

Multi-body analysis of aircraft occupants

Figure 1.1 Examples of multi-body and finite element analysis of mechanical systems

1.1.1 Vehicle side-impact protection

A basic characteristic of the structural crashworthiness of a vehicle is known as crash pulse. The crash signature is the deceleration time dependent properties measured at a location in the vehicle during impact. The crash pulse greatly differs depending on the crash configuration such as frontal, side and rear crashes. For frontal and side crashes, the crash pulse at a location on the engine-top, firewall, A- B- and C- pillars, and rocker wells are presume to accurately describe the motion and behavior of a vehicle. Therefore, various dynamic responses of the vehicle structure such as deceleration and intrusion are often measured from these locations. The characteristic of crash pulse greatly depends on the mass and structural stiffness, and structural interaction of the components.

Perhaps one of the most critical areas in the field of vehicle crashworthiness is the protection of occupants from fatal injuries in side-impact accidents. This is due to the relatively small distance separating the occupant from the point of impact. In structural terms, the limited crush zones force put occupants at higher risk of a direct impact with the interior of the vehicle. The enhancements in safety performance of occupant in frontal accidents have always surpassed that of side accidents. The depth of a fully inflated airbag system, for example, for frontal protection can provide much more cushioning effect to the occupant when compared to side-impact airbags. Unlike frontal and rear collisions where the energy absorption capacity of the structure is high due to the higher number of available load paths and structural crush zones compared to the side-structure, maximizing the crush zones in the side-structures are quite challenging.

Two primary methods can be used to improve the crashworthiness of vehicle from side-impact collisions. The first method is to increase the strength of the side-structure by using stiffer reinforcement members. The reinforcement members are designed to evenly distribute the impact energy to various supporting columns of the vehicle rather than having

the B-pillar absorb it all. The second method is to maximize the energy absorption of the side-structure using high-energy absorbing cellular foams. Ultimately, both methods must work in coherence with the sole purpose of reducing intrusion into the occupant cabin and to reduce the deceleration transmitted to the structure and the occupant.

1.1.2 Automotive occupant restraining system

Airbag system is a vital component of the occupant restraining system, and it can essentially be made up of four different components, namely, the sensor, the inflator module, the fabric bag, and the vehicle interior. The sensor module can be considered the decision-maker of the airbag system. It depicts the condition to start initiating the deployment of airbag, often through the initiation of solid chemical reactants. Additionally, the sensor has to differentiate, often within a few milliseconds, mild crashes from the severe ones, where the latter necessitate the deployment of the airbag. Advanced airbags are designed to deploy the airbag depending on the crash speeds, the crash modes, and the condition of the occupant. For example, sensors are initiated within 10-20 milliseconds for severe crashes (>35mph); 40-60 milliseconds for medium speed crashes (20-30mph). For low speed crashes, the sensor should not trigger the airbag deployment as the structures of a vehicle is designed to adequately dissipate and absorb impact energy. The fabric bag is another essential component of the airbag system. A typically bag consists of vent and holes that are designed to allow out-flow of hot gases as the occupant are compressed against the bag. In order to control the extension of the full-inflated bag, also known as airbag depth, tethers or nylon straps are installed within the bag. The folded airbag and the housing units or modular units are often called the airbag modules.

The automotive industry had initially viewed airbag systems as a replacement for safety belts but they are now designed to be used concurrently with safety belts, commonly designated as Supplemented Restrain System (SRS). One of the major issues with the use of

airbag is its tendency to induce fatal injuries to out-of-position occupants. If an occupant is very close to the airbag module, the unfolding airbag can impose high impact loading to the head and neck body region of the occupant. To avoid this issue, the airbag must be fully deployed before the occupants impact the bag. Also, it is quite obvious that by lowering the power of the deploying bag, the probability of causing injuries to out-of-position occupants can be reduced. Hence, the relevant task is to determine the deployment time threshold of the airbag, where shorter deployment time can be correlated to higher deploying force and vice versa. Conventionally, safety engineers used the rule of "5 inches minus 30 milliseconds" triggering time. This implies that the required trigger threshold can be determined by deducting 30 milliseconds from the initial time when the passenger has traveled by a distance of 5 inches. Using new technology, researchers are beginning to harvest the benefit of pre-crash sensor to pre-deploy the airbag prior to actual impact. A perspective of a complete occupant restraining system can be achieved by providing maximum restraining force over the entire range of the occupant motion. This design requires the seatbelt and airbag to work effective and coherently to bring the occupant to rest at maximum excursion. However, concept airbag system may be quite difficult to achieve as the occupants size, positions, crash modes directly influence the interaction of the occupants with the safety systems.

1.1.3 Crash compatibility and aggressivity

Crash compatibility is a measure of vehicle aggressivity and crashworthiness. In a vehicle-to-vehicle accident, crashworthiness is often referred to self-protection and reduction in aggressivity is often termed partner-protection. Vehicle aggressivity is focused on the casualties of occupants in the other vehicles involved in the accident. The aggressivity of a vehicle can be examined in three sources, the mass incompatibility, the stiffness incompatibility and the geometry incompatibility. Fueled by the increasing fleet of light trucks and vans (LTVs), researchers have quantified an aggressivity metrics (AM) that

basically evaluates the number of fatalities in the partner vehicle in a multi-vehicle collision. It is shown that fatalities counts in passenger cars are significantly higher than that of LTVs. As noted by Gabler and Hollowell [19], LTVs are 900lbs heavier than passenger car and that conservation of momentum dictates that the impact energy will be transmitted more to the passenger car. Due to the nature of LTVs, they are generally built to be stiffer than passenger car. Drawing on these two measurements, Gabler and Hollowell [19] demonstrated the relationship between mass and stiffness with the AM. Although under-ride is known in a tractor-trailer and passenger car collision, this may also occur in LTVs to passenger car crashes. Under-rides are extremely hazardous to occupants in the passenger cars as the top of the car are often crushed where head injuries and trauma or decapitation are extremely common. It is known that under-ride is directly related to the ground clearance of a vehicle.

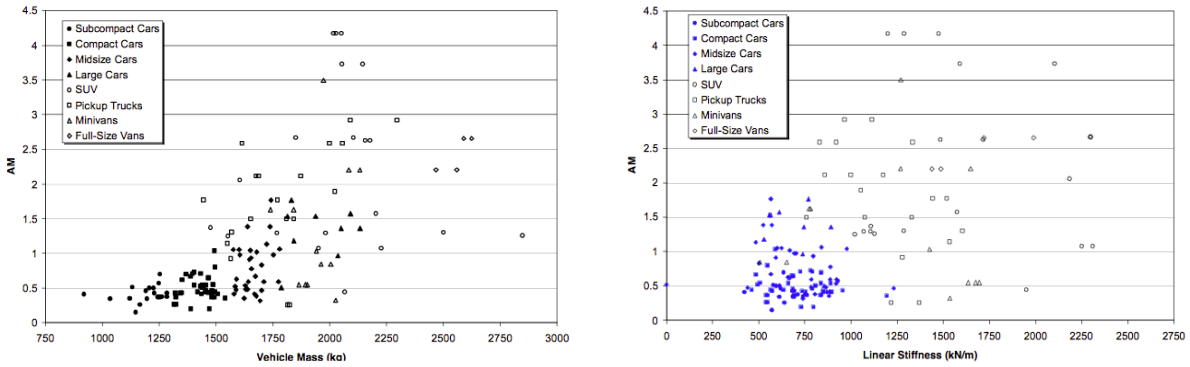

(a) AM - vehicle mass (b) AM - vehicle stiffness

Figure 1.2 Aggressivity metrics as a function of vehicle mass and stiffness [19]

1.2 Literature Review

With the significant improvement in vehicle crashworthiness, the fatality risks of vehicle occupants have been steadily decrease over the past few decades. An annual report by National Highway Traffic Safety Administration (NHTSA), as illustrated in Figure 1.3, shows that in 2010, the fatal crashes declined by approximately 60 percent compared to 2009 [14]. Although vehicle occupants fatality risk is at an all time low, the topic on vehicle safety still attracts numerous attention from both industry and academia.

In the United States, the National Center for Statistics and Analysis (NCSA) is an office of the NHTSA and it is responsible for providing a wide range of statistical and analytical reports related to motor vehicle crashes. The NCSA is a combination of the Fatality Analysis Reporting systems (FARS) and National Automotive Sampling General Estimates (GES). The first system, FARS, is probably the more popular of the two sources. FARS is established in 1975, and this system collects and publishes road fatalities on a yearly basis. GES, which is established later in 1988, contains data related to all police-reported crashes of all magnitude including fatalities and property damage. Unlike FARS, which primary function is to collect fatality counts, GES concentrate on crashes with greatest concern to highway safety and general public [15]. Besides FARS and GES databases, the Special Crash Investigations (SCI) is responsible for in depth and detailed of all types of crashes collected from a wide range of sources from routine police to insurance crash reports. The uniqueness of SCI lies in its ability to collect nationwide crash data and in perform in-depth engineering analysis, which can then be applied to improve the performance of automotive safety systems.

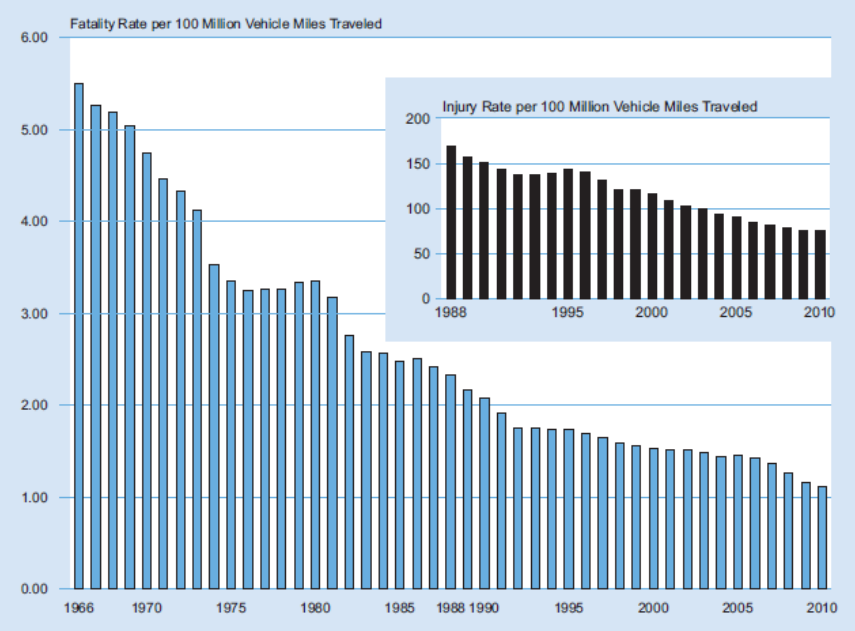

Figure 1.3 Motor vehicle fatality rates per 100 million vehicle miles traveled from 1966 – 2010 [14]

The field on vehicle crashworthiness focuses on the ability to protect occupants from an accident. In general, vehicle crashworthiness can be subdivided into two main categories, namely, occupants' injury potential and structural integrity. Crashworthiness may be assessed prospectively, using simulation models; or assessed retrospectively, by analyzing crash outcomes or historical crash data. The injury potential of an occupant in an accident is typically evaluated using criteria, which are a set of mechanical properties that correlate to injury risks. In addition to injury criteria, the structural integrity and failure of the occupant cabin also requires special attention as it protects the occupant from structural intrusion. The following topics are the primary focus of this thesis in order to determine the roadworthiness of vehicles:

a. Crash management and dissipation of impact/crash energies
b. Post-crash's occupant survivable space and injury potential
c. Kinematic and dynamic responses of occupants under different impact conditions
d. Dynamic behavior and damage of vehicle structures
e. Estimation of collision forces using some statistical or mathematical models

These topics will be examined in detailed in this literature review. Additional information on these topics is also discussed in greater details in the five case studies. The development of the four case studies is discussed later (chapter two - six).

1.2.1 Vehicular and structural crashworthiness

Vehicle crashworthiness is a term used to describe the behavior of a structure in an accident where occupants are involved in the process. Roadworthiness of a vehicle deals with meeting the acceptable safety standards of various certification programs to ensure safe transportation of occupants. A crashworthy design can be achieved when the impact energy transmitted from an accident can be dissipated efficiently equally throughout the vehicle structure and away from the occupant compartment. In recent years, researchers are

beginning to prove that this can be accomplished by incorporation of high-energy absorption material in some of the vital structural pillars such as A- and B- pillars, increase the structural load paths and increase crush zones. A strong occupant compartment is desirable to reduce the intrusion into the occupant compartment. The structural crashworthiness is often determined by the amount of intrusion into the occupant's cabin space and the deceleration experienced by the occupant.

The level of deceleration and intrusion into the occupant compartment are two measurements used to describe the crash severity. In a vehicle-to-vehicle accident, the vehicle's geometrical design, materials, crash mode, and the size difference of the two colliding vehicles often determine the crash severity. Due to the increasing fleet of light trucks and vans (LTVs) [16], NHTSA has dedicated a research program on the issue of crash compatibility and vehicle aggressivity. The crash incompatibility of two colliding vehicles causes the more aggressive vehicle to inflict greater structural damage to the less aggressive vehicle. In general, a heavy vehicle reduces the injury potential to the vehicle's occupant but increases those for the lighter vehicle's occupants [17]. Hence, it is apparent that the weight difference in two colliding vehicle contribute to the aggressivity of vehicles. In multi-vehicle crashes, the ideal crash scenario can be achieved when two identical vehicles are involved in the crash where the physical geometry, stiffness and mass are identical. Hence, LTVs are considered highly crash incompatible with passenger cars, which is reflected by the significant difference in fatality rates between LTVs and passenger cars. Overall, large vans and pickup truck are approximately three to four times more aggressive than passenger car [18]. By establishing the fact that LTVs are highly aggressive and incompatible with passenger cars, NHSA has proposed a driver fatality ratio (DFR) measurement, which represents the relative fatality risks of occupants for various LTVs-to-passenger car crash [19]. The proposed DFR is based on actual crash data gathered from Fatality Analysis

Reporting System (FARS), thus estimating the DFR for newer fleet of vehicles pose considerable challenges due to the lack of standard procedure. In recent years, researchers are beginning to correlate DFR with some quantitative measurements such as the intrusion ratio, deceleration ratio and stiffness ratio of two colliding vehicles [20].

The dynamic and injury response of the vehicle and its occupant is greatly affected by the crash mode or configuration. Some of the most widely seen crash modes are frontal, side, rear, oblique and rollover crashes. In frontal crashes, the front-end structures of the vehicle serve as energy-absorbing components and undergo approximately 20 to 30 inches of crush before crushing is initiated at the occupant cabin. In newer vehicles, the bumpers and engine of the vehicle are designed to be softer to maximize the energy-absorption capability and the occupant cabin is designed to be stiff to provide greater surviving space to the occupant. As the deformations of the engine compartment increase, the impact energy is transferred to work used to create bending and buckling. Unlike frontal-impact, the crush zone in side-impact accident is severely limited to 5 to 15 inches of crush. Hence, protecting occupant in side-impact has posted considerable challenges. The impact force to the struck-side structure put tremendous amount of mechanical stress on the A- and B- pillars of the vehicle. The most important function of these pillars is to receive loadings from the door and transfer it to the remaining structure and load paths of the vehicle. At higher crash speed, the progressive deformation of the B-pillar may cause it to fail. The failure of reinforced pillars, such as the B-pillar, is highly undesirable and should this happen; a general practice is to downgrade the safety rating of a vehicle by one grade [21]. Although side-impact crashes are known to account for higher fatality risks, the structural improvements are focused predominantly on frontal-crashes due to higher crash speed of frontal accident. In an effort to enhance the performance of a vehicle's side-structure, high-energy absorption cellular foams or

honeycomb structures can be inserted in between the door panels to increase load paths and to maximize energy absorbed by the structure.

Many regulated standards and protocols exist to evaluate the performance of occupant injury potential and structural crashworthiness in crashes. Federal Motor Vehicle Safety Standard (FMVSS) and Insurance Institute Highway Safety (IIHS) protocols are extremely popular for accident reconstruction purposes. In FMVSS 208 full-frontal protocol, the vehicle impacts a rigid wall at 35mph. This protocol seeks to address two safety concerns, 1) the response of the occupant compartment when subjected to rapid deceleration and 2) the deformation and crush of the occupant cabin space [22]. IIHS moderate and small overlap frontal tests are more vigorous frontal test compared to FMVSS 208. In the moderate and small overlap tests, the vehicle is crashed onto a deformable barrier made of aluminum honeycomb at 40 and 25 percent offset respectively [23, 24]. On both tests, the impact speed of the vehicle is 40mph. The purpose of the offset tests is to better replicate a real-life frontal accident where vehicle-to-vehicle crashes are rarely full-frontal. With the 25 percent offset test, most of the front-end crush zones are bypassed and the crash management of the vehicle can be further tested. The highly concentrated impact force evaluates the performance of seat belts and airbag designs because the occupant tends to travel in a forward and side way direction.

The FMVSS No. 214 and IIHS side-impact test protocols is to facilitate the reconstruction of side-impact accidents. In an attempt to reconstruct a T-bone accident, the FMVSS No. 214 recommends impacting a moving deformable barrier (MDB), traveling at 15mph, with the driver side of the vehicle, which is also traveling at 15mph perpendicular to the travel path of the MDB. This can be accomplished by having the MDB striking the door of the driver's side at 33.5mph crabbing at 27 degrees [25]. In 2003, IIHS developed its side-impact test protocol to account for some of the deficit of side-impact test protocols used by

the government regulatory program (FMVSS No. 214). The FMVSS No. 214 was developed by back in 1980s where the majority of on-road vehicles at that time were passenger cars, before LTVs became a major component as they are today. As the result, the current FMVSS No. 214 protocol may fail to capture all impact events for the entire fleet of on-road vehicles. Hence, IIHS initiated its own side testing by modifying the moving barrier in terms of its height, physical geometry and impact speeds. In the IIHS side testing, the moving barrier impacts the driver's side at 50km/hr and at an impact angle of 90 degrees [26].

As discussed in this section, the vehicle's stiffness, physical geometry, weight and crash configurations can greatly affect the dynamic and injury response of its occupants. It can be seen that regardless of these factors, the ultimate goal of enhancing the structural crashworthiness is to protect the occupant from fatal injuries. Therefore, an in-depth understanding of occupant response and impact injury biomechanics is equally critical.

1.2.2 Occupant protection, injury biomechanics and trauma

Occupant protection refers to the safety features designed to protect occupants from fatal injuries in the event of a crash. Occupant safety is categorized into active and passive safety designed to compensate for human reaction deficit. Active safety can be viewed as an accident prevention tool while passive safety is considered a protection tool. Active safety includes features such as pre-crash sensor, seatbelt pre-tensioning, emergency brake assistant and airbag pre-arming [27]. Features such as air bag and seat belts are often categorized as passive safety.

The development of airbag and seat belt systems are perhaps the two most important inventions in the history of vehicle safety. The most commonly used seat belt in a passenger vehicle is a three-point seat belt and air bag can be categorized into two main categories, namely, frontal and side airbags. The purpose of seat belt is to properly restrain from any uncontrolled free-flying motion during an accident. During the course of a collision, an

occupant in free-flying motion has greater potential for injury due to the greater probability of secondary impact with the interior of the vehicle. Studies have shown that the use of seat belt alone has saved 6,540 lives in year 2000 [28] and the combined use of airbag and seatbelt system can reduce fatality risks up to 60 - 80 percent [29, 30]. In a frontal crash, injuries to the chest and head body regions typically occurred as the result of secondary impact with the vehicle interior [40]. Contrast to frontal crashes, occupants injuries sustain from side-impact is mainly due to primary impact to the side panels. Therefore, the use of seatbelts and airbags are of extreme importance by reducing the probability or force of secondary impact.

Although current studies have proven the effectiveness of airbag and seatbelt systems, fatalities caused by a deploying airbag may still occur. From 2000 to 2007, NHTSA reported that as many as 122 occupant were killed despite the use of seat belt and airbags [30]. Also reported in the study are the crash configurations of these 122 cases were rarely full-frontal crash, in which the structural integrity of the vehicle is severity compromised. However, NHTSA argued that although the use of seat belt and airbags are highly effective and can reduce fatalities by 61 percent – but "61 percent is not 100 percent".

Injury biomechanics is developed to facilitate the understanding of trauma and injury mechanisms as well as the human tolerance to pain and injury. Given an impact loading, the human body typically reacts in a non-linear fashion, understanding the kinematic responses of the human body is also embedded in this discipline. In the field of injury biomechanics, the human body anatomy of interest can be divided into four body regions, head, chest, neck and pelvic regions. The head is considered the most critical body parts due to its irreversible nature of injuries in a car crash. Over the years, research has been undertaken to evaluate the injury criteria and tolerances of the head. The Wayne State Tolerance Curve (WSTC) is developed to understand the head tolerance to impact force [31]. By performing cadaver

testing, the WSTC correlates the acceleration level and the pulse duration with the human tolerance level. Several impact severity index such as Gadd Severity Index (GSI) [32] and Head Injury Criteria (HIC) [33] is an extension of the WSTC. Currently, the most widely used severity index for head injury is the HIC. The HIC is given as:

$$HIC = \left\{ t_2 - t_1 \left[\frac{1}{t_2 - t_1} \int_{t_1}^{t_2} a(t) dt \right]^{2.5} \right\}_{max} \tag{1.1}$$

where $a(t)$ is the resultant head acceleration, t_2 and t_1 are the final and initial time that correspond to the maximum HIC value. Currently, the HIC threshold set by the automotive industry is 1000 for a 50th percentile male and the maximum time interval should not exceed 36ms [34].

The thoracic injury criteria is developed to evaluate the tolerance and fatality threshold of vehicle occupants in an event of an accident. The thoracic injury mechanism for side-impact and frontal-impact differs significantly. In side-impact accidents, the thoracic body region experience primary impact with the vehicle side-structures where high impact force can cause significant injuries to the chest. As for frontal-impact accidents, the primary form of chest injury is torso compression caused by seatbelts. Three main principle of thoracic injury are compression loading, viscous response and inertia loading. In terms of quantifying these principles, the chest deflection is used to evaluate the compression loading, the chest acceleration and force used to evaluate viscous response and the viscous criterion is related to the viscous response and inertia loading. Some of the earliest work to quantify thoracic injury levels was conducted on cadavers. In 1986, Lau and Viano [35] proposed an injury severity measurement using the viscous criteria method (VC). The product of chest deformation and velocity of deflection form the basis of the VC:

$$VC = \frac{D(t) \cdot \dot{D}(t)}{D_i} \tag{1.2}$$

where $D(t)$ is the instantaneous deformation of the torso; $\dot{D}(t)$ is the instantaneous compression velocity and D_i is the initial thickness of the torso.

Currently, the VC threshold used in the automotive industry is 1.0 m/s, which correlates to 50 percent of AIS 3+ or 25 percent of AIS 4+ thoracic injury. Another widely used measurement used to evaluate thoracic injury is the Thoracic Trauma Index (TTI). The formulation of TTI for human is given as:

$$TTI = 1.4 \times A\,GE + \frac{1}{2}(RIB_{lat} + T12_{lat}) + \frac{MASS}{Mstd} \quad (1.3)$$

where $A\,GE$ represent the age of the occupant; RIB_{lat} is the maximum lateral acceleration of the 4th and 8th rib; $T12_{lat}$ is the maximum lateral acceleration of the 12th vertebra; MASS is the weight of the occupant and $Mstd$ is the standard reference weight of 75kg. The threshold for TTI is 90G's for 2 door vehicle and 85G's for 4-door vehicle. In 1997, Pintar et al. [36] analyzed 26 human cadaver using Heidelberg sled system and proposed the formulation of $TTI \times C$, where C is the average chest deflection. Additionally, Equation (1.3) can be further modified to $TTI(d)$ to be used for the 50th percentile male dummy:

$$TTI(d) = \frac{1}{2}(G_R + G_{LS}) \quad (1.4)$$

where G_R is the absolute maximum acceleration of either upper or lower rib and G_{LS} is the peak acceleration of the lower spine. Over the last decade, many researchers have proven that other quantitative measurements such as chest deflection, upper spine acceleration and energy method are a better injury predictor than the TTI [37-39]. Therefore, the automotive industry has excluded the use of TTI as a requirement for measuring torso injuries. The torso deflection and rate of deflection are also used to serve as an injury predictor for the torso. Currently, the threshold for torso deflection and deflection rate is 42mm and 8.20m/s. At 50mm deflection, the occupant risks 80 percent of serious rib fracture. At above 50mm, the occupant risks more than 90 percent of serious rib fracture and fatality [41].

During a vehicular accident, the neck body region undergoes various motions and loadings. The anatomical terms for neck motions can be divided into neutral, flexion, extension, lateral bending and rotation. The various motions of the neck are illustrated in Figure 1.4. In addition to the neck motions, the neck loadings also induce injury potential. As shown in Figure 1.5, the neck loadings can generally be categorized into bending, tension, compression, torque and shear loadings. In frontal accident, a sudden deceleration, -G_x loading, to the occupant can cause the head to rotate forward excessively and tension force is applied to the occipital condyle. This condition is denoted as hyper-flexion of the neck. On the contrary, occupants usually experience +G_x loading for a rear-end collision. Using the similar concept, the neck initially comes into hyper-extension, in which the head is rotated backward and the neck is under tension force, and the secondary motion where the head rotate forward is caused by the rebound force by the cushion seat. This injury mechanism is often informally described as a whiplash injury or formally described as the cervical acceleration-deceleration. In an attempt to quantify the neck injuries, experimental tests were often conducted to evaluate the pain tolerance of necks [42-44]. The neck flexion and extension corridors developed by Mertz and Patrick [44] are currently the most widely used injury criteria for the neck. These corridors formed the basis for the development of the N_{ij} injury criteria. The N_{ij} describes the combined loading and moment of the neck measured about the occipital condyle. Currently, the N_{ij} limit of 1.0 is used to describe the limit threshold regardless of occupant size. The formulation of N_{ij} is:

$$N_{ij} = \frac{F_z}{F_{int}} + \frac{M_Y}{M_{int}} \tag{1.5}$$

where F_z is the axial loading along the sagittal plane; F_{int} is the critical intercept value for neck; M_Y is the neck bending moment about the occipital condyle and M_{int} is the critical intercept value for moment. The critical intercept values and peak neck loadings can be referred from the NHTSA's injury criteria report [45].

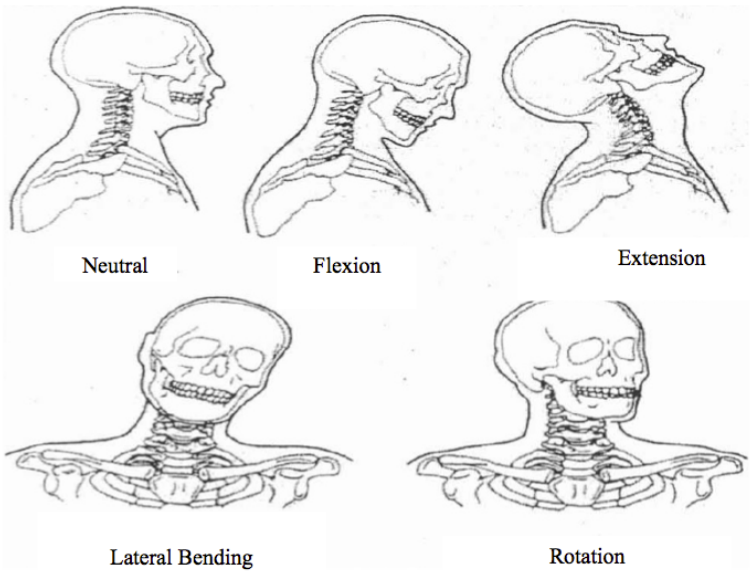

Figure 1.4. Anatomical terms for neck motion [46]

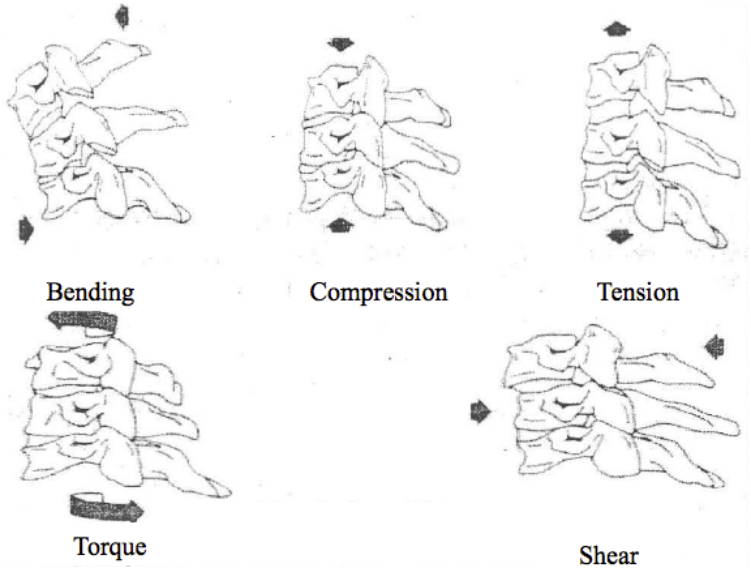

Figure 1.5. Anatomical terms for neck loadings [46]

1.2.3 Kinematic and dynamic analysis of multi-body systems

A mechanical system is a collection of bodies interconnected with some sort of mechanical joints, in which each link may undergo large amount of translational and/or rotational movements. Mechanical system can be of a simple mechanism such as the simple pendulum system (planar problem) shown in Figure 1.6(a) or of a more complex system such as a vehicle's suspension system (spatial problem) as shown in Figure 1.6(b). Essentially, two types of analysis can be performed in dealing with multi-body systems, namely, kinematic and dynamic analysis. Kinematic analysis is the study of a system's motion independently

from the forces that produce the motion. More precisely, kinematics is mostly utilized in predicting the position, velocity and acceleration of a mechanism through a set of constraint equations. Constraint equations are a set of algebraic model that defines the relative motion between two bodies. However, the solution to the kinematic analysis is typically non-trivial as non-linear behavior exists within the formulation of the constraint equations. Solving simple non-linear system by hand calculation may be possible for small problems. However, mechanical systems generally consist of multiple unknown and variables; thus, solving by hand is tedious and the likelihood to succeed is small. Computer programs are the obvious choice for faster and more accurate estimation of solutions.

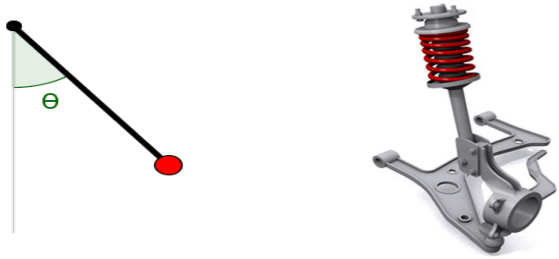

a. A single pendulum b. Mcpherson strut suspension

Figure 1.6. Comparison of a simple and a complex mechanical system

The dynamic analysis of multi-body system is aimed at understanding the motion or response of mechanical bodies when forces are introduced to the system. The dynamic analysis of a system is usually performed after the kinematic analysis once the general geometry of motion is understood. The dynamic analysis also provides the estimation of external forces, such as external forces exerted by springs, actuators and dampers, and reaction forces at mechanical joints due to the interaction between the system components.

A kinematic constraint equation, denoted by Φ, describes the relative motion between two connected bodies and to reduce the number of degree-of-freedom (DOF) in a system. A DOF is the minimum number of parameters required to fully describe the configuration of a system. A revolute and translational joint in planar dimension is discussed to illustrate the constraint equation.

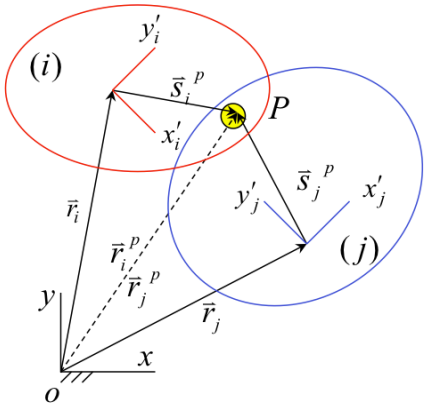

Figure 1.7. Illustration of a revolute joint connecting body i and j

Illustrated in Figure 1.7 is the revolute joint located at point P connecting body i and j. A revolute joint is a coincidence point between two bodies that allows only relative rotation by constraining the relative translation. Relative to the global coordinate, denoted by point O, the location of body i and j can be described by the two vectors $\underline{s}_i^P$ and $\underline{s}_j^P$ where $\underline{s}_i^P = [x_i'^p, y_i'^p]^T$ and $\underline{s}_j^P = [x_j'^p, y_j'^p]^T$. The constraint equation can be determined using the vector loop method as:

$$\underline{r}_i + \underline{s}_i^P = \underline{r}_j + \underline{s}_j^P \tag{1.6}$$

which can also be represented as:

$$\underline{\Phi}^{(r,2)} = \underline{r}_i + \underline{A}\underline{s}_i^P - \underline{r}_j + \underline{A}\underline{s}_j^P \tag{1.7}$$

$\underline{A}$ is the rotational transformation matrix for body and it is represented as:

$$\underline{A} = \begin{bmatrix} cos\phi & -sin\phi \\ sin\phi & cos\phi \end{bmatrix} \tag{1.8}$$

The revolute joint constraint equation shown in Equation (1.7) reduces the number of DOF of a system by 2 DOF. Therefore, two bodies connected by a revolute joint in planar dimension has 4 DOF.

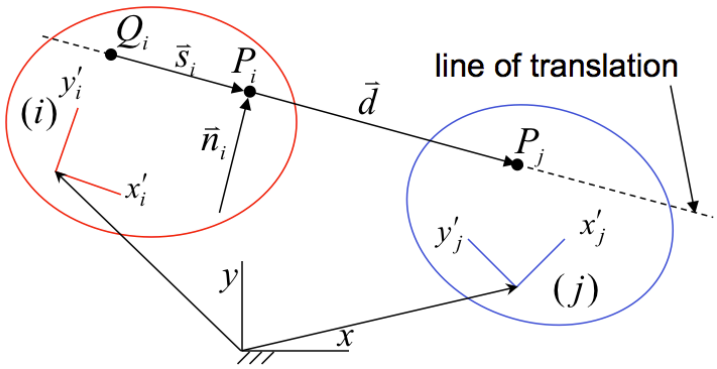

Figure 1.8. Illustration of a translational joint connecting body i and j

The illustration of a translational joint is shown in Figure 1.8. Similar to a revolute joint, a translational joint reduces the number of DOF by 2 by eliminating a relative rotation between two bodies. The line of translation is an infinite vector in which two bodies translate relative to each other. The constraint equations for the translational joint between two bodies can be defined in terms of its relative angle and relative motion. The constraint equation to define its relative angle can be provided as:

$$\phi_i - \phi_j = \phi_i^0 - \phi_j^0 \tag{1.9}$$

where ϕ_i^0 and ϕ_j^0 are the initial rotational angles for both bodies. In order to eliminate the relative translation in the direction perpendicular to line of translation, the vector $\bar{s}_i$ must be parallel to the vector $\bar{d}$. Another alternative is to define $\bar{n}_i$ to be perpendicular to vector $\bar{d}$, that is

$$\underline{n}_i^T \underline{d} = 0 \tag{1.10}$$

where $n_i = \begin{bmatrix} -(y_i^P - y_Q^P) \\ x_i^P - x_Q^P \end{bmatrix}$ if $\underline{n}_i = \underline{s}_i$

In turn, the constraint equation is given as:

$$\Phi^{(t,2)} = \begin{bmatrix} (x_i^P - x_i^Q)(y_j^p - y_i^p) - (y_j^p - y_i^Q)(x_j^p - x_i^p) \\ \phi_i - \phi_j - (\phi_i^0 - \phi_j^0) \end{bmatrix} = \begin{bmatrix} 0 \\ 0 \end{bmatrix} \tag{1.11}$$

With these two illustrations, a large class of multi-body systems and mechanisms can be modeled and analyzed. For additional formulations on other class of kinematic joints, the work of Nikravesh [47] can be referred.

When a multi-body system configuration is defined by Cartesian coordinates, a set of m holonomic independent constraints can be written as [47]:

$$\underline{\Phi}\left(\underline{q}, t\right) = 0 \tag{1.12}$$

where $\underline{q}$ and t are the vector of generalized coordinates and t is the time variable. This compact form is also denoted as position analysis and it is non-linear in terms of $\underline{q}$. The velocity and acceleration analysis can be obtained by taking the first derivatives of Equation (1.12) followed by the second derivatives of Equation (1.13):

$$\underline{\dot{\Phi}}_{\underline{q}} = \underline{\Phi}_{\underline{q}}\underline{\dot{q}} = 0 \tag{1.13}$$

where $\underline{\Phi}_{\underline{q}}$is the constraint Jacobian matrix which has a matrix dimension of $m \times n$ and m is the linear velocity equation in $\underline{\dot{q}}$.

$$\underline{\ddot{\Phi}}_{\underline{q}} = \underline{\Phi}_{\underline{q}}\underline{\ddot{q}} + (\underline{\Phi}_{\underline{q}}\underline{\dot{q}})_{\underline{q}}\underline{\dot{q}} = 0 \tag{1.14}$$

where $\underline{\ddot{q}}$ is the acceleration vector. The position analysis equation shown in Equation (1.12) are generally non-linear and are usually solve using iteration methods such as Newton-Raphson method. The velocity and acceleration equations shown in Equations (1.13) and (1.14) respectively are linear and can be solved by employing the usual linear equation method. In addition to the kinematic analysis, the dynamic analysis can further describe the mechanical system by a set of differential equations-of-motion (EoM). The EoM of multi-body system are given as [48]:

$$\underline{M}\underline{\ddot{q}} = \underline{g} + \underline{g}^{(c)} \; ; \; \underline{g}^{(c)} = \underline{\Phi}_{\underline{q}}^{T}\underline{\lambda} \tag{1.15}$$

where $\underline{M}$ is the system mass matrix, $\underline{\ddot{q}}$ is the system acceleration vector, $\underline{g}$ is the system vector of forces or the applied forces and $\underline{g}^{(c)}$ is the constraint reaction forces. The constraint force, $\underline{g}^{(c)}$, is expressed in terms of Jacobian matrix and contains the vector of Lagrange multipliers, $\underline{\lambda}$. The Lagrage multipliers are physically associated to reaction forces and moments produced at the kinematic joints.

Once the kinematic analysis is performed, the dynamic analysis can be developed. If kinematic joint is not present at the system, the system is studied as an unconstrained system. On the other hand, the system is considered a constrained system if one or more joints are present. In the formulation of EoM, spring, actuators and dampers are not considered as bodies but a force element. This assumption is made based on the negligible mass of force elements when compared to the total mass of the system. Shown in Figure 1.9 is an illustrative example of an unconstrained and a constrained mechanical systems.

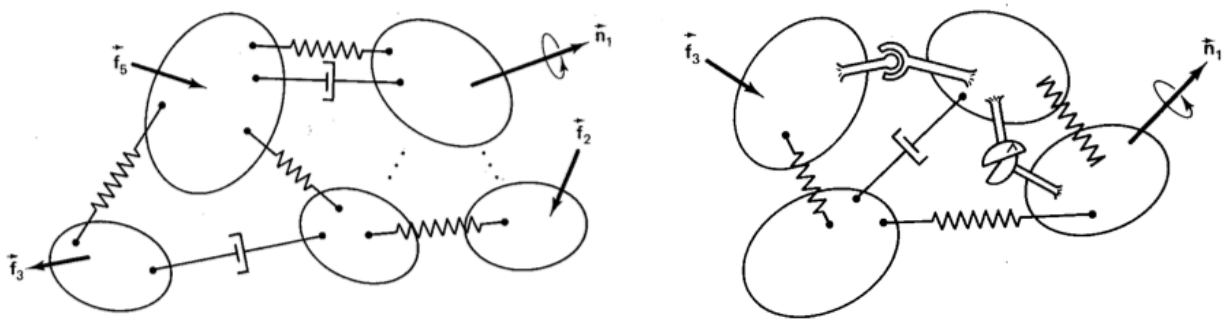

a. An unconstrained system b. A constrained system

Figure 1.9. Comparison of an unconstrained and a constrained system

For an unconstrained system such as two bodies connected using dampers and springs, the system acceleration vector can be solved as:

$$\underline{\ddot{q}} = \underline{M}^{-1}\underline{g} \tag{1.16}$$

However, for solving a constrained system, the constraint equations and differential EoM are typically analyzed simultaneously. The mathematical model for constrained multi-body system requires the solution for a n set of differential EoM and a set of m algebraic equation.

This combination of equation is also denoted as mixed differential algebraic EoM and it is illustrated as:

$$\begin{bmatrix} \underline{M} & \underline{\Phi_q^T} \\ \underline{\Phi_q} & 0 \end{bmatrix} \begin{bmatrix} \underline{\ddot{q}} \\ \underline{\lambda} \end{bmatrix} = \begin{bmatrix} g \\ \gamma \end{bmatrix} \tag{1.17}$$

where $\underline{M}$ is a constant, $\underline{\Phi_q}$ is a function of $\underline{q}$, g, and γ are functions of $\underline{q}$ and $\underline{\dot{q}}$. By solving for $\underline{\ddot{q}}$ and $\underline{\lambda}$, the acceleration and reaction forces can be solved. In order to evaluate the system velocities and positions, integration of $\underline{\ddot{q}}$ and $\underline{\dot{q}}$ can be performed for each integration time step. For a complete analysis, this formulation is repeated until the designated termination time is reached.

The integration of EoM can be approached using various methods, namely, the Baumgarte Stabalization Method [49], Coordinate Partitioning Method [50] and Augmented Lagragian Formulation. The general summary of EoM integration methods is discussed by Moradi [12] and Flores [51]. Among these integration methods, the Baumgarte Stabilization Method is popular due to its simplicity for computational implementation. As the name suggest, this method incorporate feedback to control the constraint violation. Therefore, slight constraint violation is allowed and corrective feedback is taken to reduce the violation. If exact solution exists in mechanical problem, this method allows the numerical results to oscillate around the exact solution. By modifying Equation (1.17), the Baumgarte Stabilization Method can be described as [12]:

$$\begin{bmatrix} \underline{M} & \underline{\Phi_q^T} \\ \underline{\Phi_q} & 0 \end{bmatrix} \begin{bmatrix} \underline{\ddot{q}} \\ \underline{\lambda} \end{bmatrix} = \begin{bmatrix} g \\ \gamma - 2\alpha\dot{\Phi} - \beta^2\Phi \end{bmatrix} \tag{1.18}$$

where α and β are the feedback control. One of the drawbacks of using this method is the arbitrariness in choosing the feedback controls. The author suggests employing trial-an-error method in determining the feedback controls [52].

The kinematic and dynamic analysis of mechanical systems can be automatically simulated using various multi-body dynamic software such as MSC ADAMS [53], MADYMO [54] and MotionSim [55].

The application of multi-body dynamics in injury biomechanics is vast. To name a few, multi-body dynamics is utilized to analyze skeletal model of active walking [56]. The skeletal walking model can be analyzed by a system of differential algebraic equation. Also, since the model is in intermittent contact with the ground, contact between the ground and legs can be analyzed using the coefficient of restitution method. In aiding the analysis of occupant movement subjected to an aircraft crash pulse, the Euler parameters method has been utilized to predict the path of the head of the occupant and the seat is subjected to some acceleration loadings [57]. The use of multi-body dynamics also extends to applications on accident reconstructions to evaluate the injury levels of mathematical dummies when subjected to various impact conditions [57-59]. Additionally, multi-body dynamics is also used concurrently with finite element method to obtain the best results. In the field of vehicle crashworthiness, finite element method is typically used to model the vehicle structures while multi-body is typically used to model crash dummies. This method is generally referred to as coupling [60-62].

1.3 Objectives of Thesis

The primary objective of this thesis work is to contribute to the body of knowledge on vehicle crashworthiness and occupant safety on frontal- and side- impact crashes. The medium of investigation is to utilize a combination of multi-body and finite element analysis to examine several proposed methodologies. The ultimate goal embedded in this thesis work is aimed at proposing several new technologies to enhance the passive safety of road vehicles in side-impact accidents. The outline of this thesis work can be summarized as:

-

- To evaluate the performance of high-energy absorption materials in increasing the occupant survival space and reducing the dynamic response transmitted to a vehicle's side structure using side-impact test protocol.
- To investigate the pre-crash sensing algorithm and its potential use in the development of advance side-airbag systems. The protection capability of the airbag the implementation of the pre-crash sensing algorithm is also evaluated at crash speeds above the required regulatory requirement.
- To implement a response-surface methodology to predict the combined effect of various injuries parameters to out-of-position occupants in a static frontal- and side-airbag deployment environment.
- To evaluate the crash aggressivity and compatibility of vehicles in a multi-vehicle crashes configuration, and to develop a quantitative measurements in order to estimate the driver fatality risks of occupants for side-impact accidents.

1.4 General Approach and Methodology

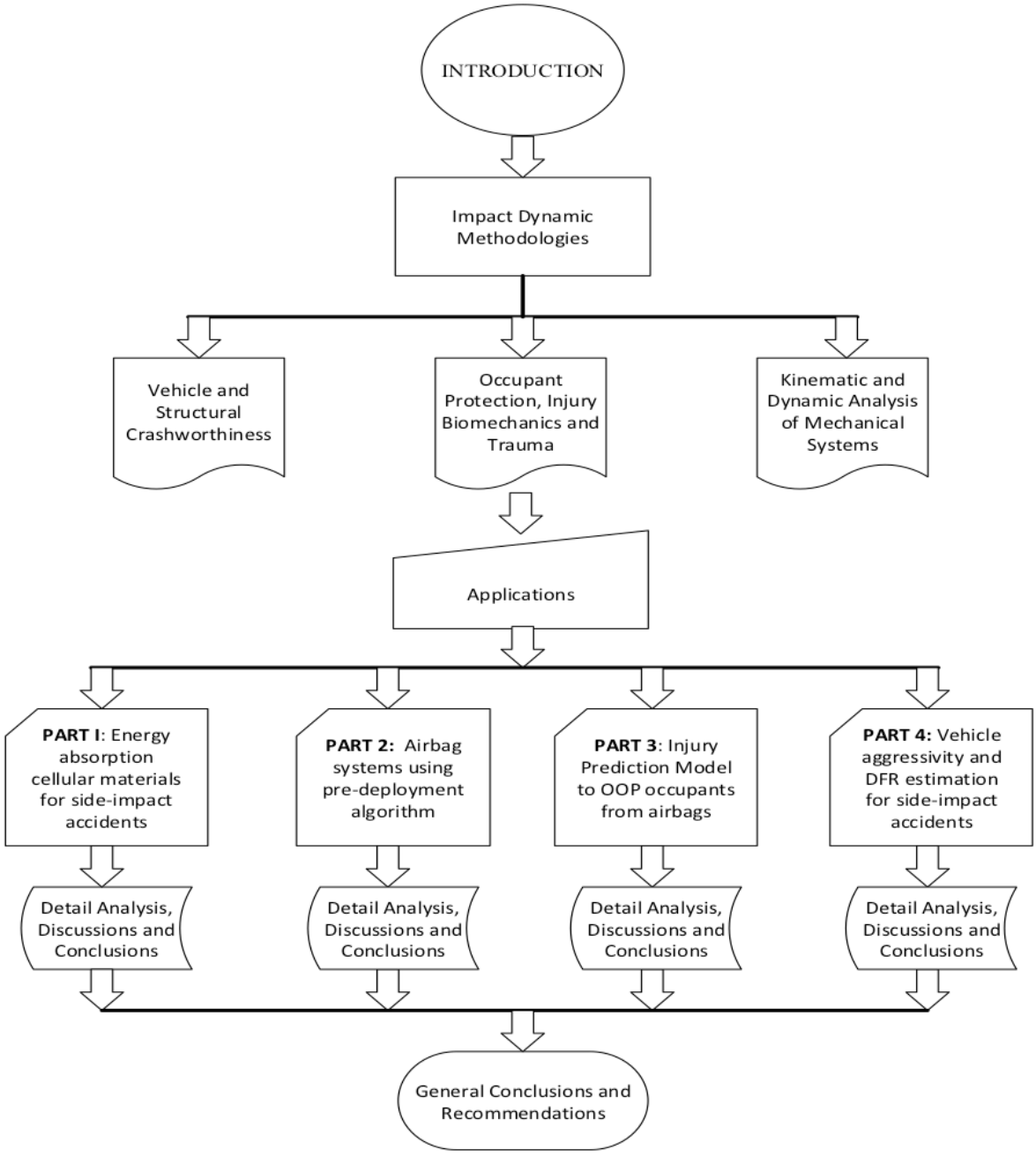

Figure 1.10. General Methodology for this thesis

The general approach to achieve the goal of this thesis is illustrated in Figure 1.10. The details of the methodology outlined in this thesis to reach the eventual objective of this thesis are as follows:

- First, a general overview on impact dynamic methodologies was discussed in this chapter. A detailed literature review on vehicle crashworthiness, occupant protection,

injury criteria and trauma, and kinematic and analysis of mechanical system were also presented. (chapter one).

- Second, the influence of impact dynamics on various crashworthiness subjects such as vehicle and structural strength, occupants' injury biomechanics and fatalities risks, and pre-crash sensing algorithm are discussed and its applications shall be investigated in four case studies. Due to very different engineering approach in approaching each case studies, an overall summary is provided in detail as the following:
    - **Part One (chapter two):** Application to energy-absorption of cellular paddings in side-impact accidents – "A Finite Element Analysis of High Energy Absorption Cellular Materials in Enhancing Passive Safety of Road Vehicles in Side-Impact Accidents." This study investigates the performance of high-energy absorption cellular material in enhancing vehicle structural strength in side-impact accidents. The structural performance of the side-structure with and without the installation of cellular materials in between the door panels is presented in this work.
    - **Part Two (chapter three):** Application to airbag system using pre-deployment algorithm – "A Numerical Analysis of Pre-Deploying Effect of Side-Impact Airbags in Reducing Occupant Injuries." The primary objective of this study is to investigate the benefits of pre-deploying side-impact airbags in reducing occupant injuries by using finite element analysis. This study has shown that the reduction in injury levels to the upper body regions is significant by incorporating the proposed methodology to existing airbag systems.
    - **Part Three (chapters four and five):** Application to injury prediction model to out-of-position occupants from side- and frontal- deploying airbags – "A Response Surface Methodology in Predicting Injuries to Out-of-Position

Occupants from Frontal Airbags." The primary objective of this study is to investigate the influence of various parameters on the injury levels of out-of-position children (Hybrid III 6-year old). The facet vehicle interior and airbag is constructed using the multi-body dynamic code, MADYMO 7.4.2. The response surface method is utilized to evaluate the relationship of various parameters on the injury responses of the 6-year old. It is shown that the regression model is quite sufficient in predicting the injury levels.

- **Part Four (chapter six):** Application to multi-vehicle crashes, aggressivity and occupants relative fatality risks - "Finite Element Approach in Estimating Driver Fatality Ratio of A Fleet of LTV Striking A Passenger Car Based on Various Objective Measurements in Side-Impact Accidents." This study investigates various mathematical models to evaluate a generic multi-vehicle crash. This study is extended to predict the relative injury risks of occupants in a side-impact accident using computational finite element method. The simulated results indicated the driver fatality ratio in a multi-vehicle crash can be estimated using intrusion and deceleration ratios.

- The final step in this thesis is to make a general conclusion on the different case studies utilized in contributing to the broad knowledge on vehicle crashworthiness. Additional, recommendations for future studies on various applications related to impact dynamics and crashworthiness is presented.

1.5 References

[1] Timoshenko, S. P., and Goodier, J. N., *Theory of Elasticity*, McGraw Hill, 1970

[2] Dubowsky, S., and Freudenstein, F., "Dynamic Analysis of Mechanical Systems with Clearances," *Journal of Engineering for Industry, Series B, Vol. 93(1), pp. 310-316.*

[3] Flores, P., Ambrosio, J., Claro, J. C. P., and Lankarani, H. M., "Influence of the contact-impact force model on the dynamic response of multi-body systems," *Journal of Multi-Body Dynamics,* 2005, DOI: 10.1243/146441906X77722.

[4] Lankarani, H. M., and Nikravesh, P. E., "A Contact Force Model with Hysteresis Damping for Impact Analysis of Mechanical Systems," *Journal of Mechanical Design, 112(3),* 1990, pp.369-376.

[5] Zhang, Z., Xu, L., Tay, Y.Y. and Lankarani H.M., "Multi-Objective Optimization of Mechanisms with Clearances in Revolute Joint," 5th European Conference of Mechanism Science, Guimarães, Portugal, 2014.

[6] Zhang, Z., Xu, L., Flores, P., and Lankarani H.M., "A DoE- and Kriging-based Model for Studying the Dynamics of Multibody Mechanical Systems with Revolute Clearance Joints," *ASME Journal of Computational and Nonlinear Dynamics, CND-13-1195,* pp.13, 2013, DOI:10.1115/1.4026233.

[7] Bengisu, M. T., Hidayetoglu, T., and Akay, A., "A theoretical and experimental investigation of contact loss in the clearances of a four-bar mechanism," *Journal of Mechanisms, Transsmissions, and Automation in Design, ASME 108,* 1986, pp. 237 - 224.

[8] Furuhashi, T., Morita, N., and Matsuura, M., "Dynamic Researches of Four-Bar Linkage with Clearance at Turning Pairs: 4th Report, Forces Acting at Joints of Crank-Lever Mechanism," *Transactions of the Japan Society of Mechanical Engineers, 43(376),* 1977, pp. 4644–4651.

[9] Deck, J. F., and Dubowsky, S., "On the limitations of predictions of the dynamic response of machines with clearance connections," *Flexible Mechanisms, Dynamics, and Analysis,* 1992, pp. 461-469.

[10] Haines, R. S., "Two-dimensional motion and impact at revolute joints," *Mechanism and Machine Theory,* 1980, pp. 361-370.

[11] Khulief, Y. A., and Shabana, A. A., "Dynamic analysis of constrained system of rigid and flexible bodies with intermittent motion," *Journal of Mech., Trans, and Automation 108(1),* 1986, pp. 38-45, DOI: 10. 1115/1.3260781.

[12] Moradi, R., "Impact Dynamics of Mechanical Systems and Structures, and Applications in Crash Energy Management, Impulse Mitigation, and Impact Injury Biomechanics," PhD Dissertation, Wichita State University, KS, USA, 2012.

[13] Canadarm, Canadian Space Agency. http://www.asc-csa.gc.ca/eng/default.asp (retrieved, January 2014)

[14] US. National Highway Traffic Safety Administration (NHTSA), 2013, "Fatality Analysis Reporting System (FARS)," http://www-fars.nhtsa.dot.gov/Main/index.aspx (retrieved, January 2014).

[15] Annonymous, "Traffic Safety Facts," National Highway Traffic Safety Administration, Traffic Safety Facts 2010, 2010.

[16] Summers, S. M., Hollowell, W. T., and Prasad, A., "NHTSA's research program for vehicle compatibility," National Highway Traffic Safety Administration, paper no. 307.

[17] Joksch, H., Massie, D., and Pichler, R., "Vehicle Aggressivity: Fleet Characterization Using Traffic Collision Data," National Highway Traffic Safety Administration DOT HS 808 679, 1998.

[18] Summers, S., Prasad, A., and Hollowell, W. T., "NHTSA's research program for vehicle aggressivity and fleet compatibility," National Highway Traffic Safety Administration, paper no. 249

[19] Gabler, H. C., Hollowell, W., "NHTSA's Vehicle Aggressivity and Compatibility Research Program," National Highway Traffic Safety Administration, paper no. 98-S3-O-01, 1998.

[20] Moradi, R., Setpally, R., and Lankarani, H. M., "Use of Finite Element Analysis for the Prediction of Driver Fatality Ratio Based on Vehicle Intrusion Ratio in Head-On Collisions," *Applied Mathematics,* 2013, pp. 56-63, DOI: 10.4236/am.2013.45A007.

[21] Annonymous, "IIHS Side Impact Test Program – Rating Guidelines," Insurance Insitute for Highway Safety, 2006.

[22] Hollowell, W. T., Gabler, H. C., Stucki, S. L., Summers, S., and Hackney, J. R., "Updated Review of Potential Test Procedures for FMVSS No. 208," Office of Vehicle Safety Research, National Highway Traffic Safety Administration, 1999.

[23] Annonymous, "Moderate Overlap Frontal Crashworthiness Evaluation Crash Test Protocol," Insurance Institute for Highway Safety, Version XIV, 2012.

[24] Annonymous, "Small Overlap Frontal Crashworthiness Evaluation Crash Test Protocol," Insurance Institute for Highway Safety, Version II, 2012.

[25] Annonymous, "Evaluation of FMVSS 214 Side Impact Protection Dynamic Performance Requirement," National Highway Traffic Safety Administration, DOT HS 809 004, 1999.

[26] Annonymous, "Side Impact Crashworthiness Evaluation Crash Test Protocol," Insurance Institute for Highway Safety, Version VI, 2012.

[27] Hinch, J., Hollowell W. T., Kanianthra, J., Evans, W. D., Klein, T., Longthorne, A., Ratchford, S., Morris, J., and Subramanian, R., "Air Bag Technology in Light Passenger Vehicles," Office of Research and Development, National Highway Traffic Safety Administration, Revision 2, 2001.

[28] Glassbrenner, D., "Estimating the Lives Saved by Safety Belts and Air Bags," National Highway Traffic Safety Administration, paper no. 500.

[29] Crandall, C. S., Olson, L. M., and Sklar, D. P., “Mortality Reduction with Air Bag and Seat Belt Use in Head-on Passenger Car Collisions,” *American Journal of Epidermiology* Vol. 153, No. 3., 2001. pp. 219 – 224.

[30] Bean, J. D., Kahane, C. J., Mynatt, M., Rodney, W. R., Carla, J. R., and Wiacek, C., “Fatalities in Frontal Crashes Despite Seat Belts and Air Bags,” National Highway Traffic Safety Adminstration, NHTSA DOT HS 811 202, 2009.

[31] Gurdjian, E. S, Lange, W. A., Patrick, L. M., Thomas, L. M., *Impact Injury and Crash Protection.* Springfield, Illinois: Thomas, 1970.

[32] Gadd, C. W., “Use of a weight-impulse criterion for estimating injury hazard,” Proceeding of 10th Stapp Car Crash Conference, Society of Automotive Engineers, 1966, pp. 164 – 174.

[33] Versace, J., “A review of the severity index,” Proceeding of 15th Stapp Car Crash Conference, Society of Autmotive Engineers, 1971, pp. 771 – 796.

[34] Title 49 Code of Federal Regulations, Part 571.208, “Occupant Crash Protection,” Federal Motor Vehicle Safety Standard 208.

[35] Lau, I. V., and Viano, D. C, "The Viscous Criterion - Bases and Applications of an Injury Severity Index for Soft Tissues," SAE Technical Paper 861882, 1986, DOI: 10.4271/861772.

[36] Pintar, F. A., Yoganandan, N., Hines, M. H, Maltese, M. R., McFadden, J., Saul, R., Eppinger, R., Khaewpong, N., and Kleinberger, M., "Chestband analysis of human tolerance to side impact," Stapp Car Crash Conference, 1997, pp. 63 - 74.

[37] Kuppa, S., Eppinger, R., Maltese, M., Naik, R., Pintar, F., Yoganandan, N., Saul, R., and McFadden, J., "Assessment of Thoracic Injury Criteria for Side Impact," International IRCOBI Conference on the Biomechanics of Impact, 2000, pp. 131-146.

[38] Wang, J. T., "Analytical Studies of Injury Criteria for the Thorax," *Journal of Biomechanical Engineering,* Vol. 111, 1989.

[39] Chung, J., Cavanaught, J., King, A., Koh, S., and Deng, Y., "Thoracic Injury Mechanisms and Biomechanical Responses in Lateral Velocity Pulse Impact," 43rd Stapp Car Crash Conference, 1999, pp. 39-54.

[40] Lau, I., Capp, J., and Obermeyer, J., “A Comparison of Frontal and Side Impact: Crash Dynamics, Countermeasures and Subsystem Tests,” SAE Technical Paper 912896, 1991, doi:10.4271/912896.

[41] Annonymous, "Guidelines for Rating Injury Measurements," Insurance Institute for Highway Safety, Version II, 2008.

[42] Ryan, J. J., "Human crash deceleration tests on seat-belts," *Aerospace Med, Vol. 3.,* 1961, pp. 167-174.

[43] Cheng, R., Mital, N. K., Levine, R. S., and King, A. I., "Biodynamics of the living human spine during -Gx impact acceleration," Proceedings of the 23rd Stapp Car Crash Conference, 1979, pp. 723 - 764.

[44] Mertz, H. J., and Patrick, L. M., "Strength and response of the human neck," Proceedings of the 15th Stapp Car Crash Conference, 1971, pp. 207 - 255.

[45] Eppinger R., Sun E. Kuppa S., Saul R., "Development of Improved Injury Criteria for the Assessment of Advanced Automotive Restraint Systems – II," NHTSA Report, 2000.

[46] Atkinson, T., "Injury Metrics in Automotive Safety System Design - A Short Course," Injury Analysis and Prevention LLC, 2001.

[47] Nikravesh, P. E., *Computer-Aided Analysis of Mechanical Systems*. Englewood Cliffs, New Jersey: Prentice Hall, 1988.

[48] Baumgarte, J., "Stabilization of constraints and integrals of motion in dynamical systems," *Computer Methods in Applied Mechanics and Engineering,* Vol. 1, 1972, pp 1-16.

[49] Flores, P., Machado, M., Seabra, E., Silva, M.T., "A Parametric Study on the Baumgarte Stabilization Method for Forward Dynamics of Constrained Multibody Systems," *Journal of Computational and Nonlinear Dynamics,* Vol. 6(1), 2011, pp. 0110191-0110199.

[50] Haug, E. J., Wehage, R. A., and Barman, N. C., "Dynamic Analysis and Design of Constrained Mechanical Systems," *Journal of Mechanical Design,* 104, 1982, pp.778-784.

[51] Flores, P., "Dynamic Analysis of Mechanical Systems with Imperfect Kinematic Joints," PhD Dissertation, University of Minho, Braga, Portugal, 2004.

[52] Baumgarte, J., "A New Method of Stabilization for Holonomic Constraints," *Journal of Applied Mechanics,* 1983, pp. 869-870

[53] MSC ADAMS user manual, MSC Software, 2013.

[54] MADYMO theory manual, Release 7.4.1, TNO Road-Vehicles Research Institute, 2013.

[55] Dye, J., "Development and application of computational dynamic and kinematic constrained multi-body simulations in MATLAB," M.S. Thesis, Wichita State University, KS, USA, 2011.

[56] Schiehlen, W., "Computational Dynamics: Theory and applications of multibody systems," *European Journal of Mechanics and Solids,* 2006, DOI:10.1016/j.euromechsol.2006.03.004.

[57] Huculak, R. D., Lankarani, H. M., "Use of Euler parameters for the evaluation of ATD head trajectory from angular rate sensor and accelerometer data in aircraft seat certification testing," *International Journal of Crashworthiness,* 18:2, pp. 174-182, 2013, DOI: 10.1080/13588265.2013.766404

[58] Moradi, R., Bromwell, T., Jategaonkar, R., and Lankarani, H., "Crash Energy Management of Rotorcraft Seat Based on Limit Load Curves and Corresponding Occupant Pelvic Load," 2013 ASME International Mechanical Engineering Congress and Exposition, 2013.

[59] Tay, Y.Y., Moradi, R., and Lankarani, H.M., "A DoE Method in Predicting Injuries to Out-of-Position Occupants from Torso-only Side-Impact Airbags," *Global Journal of Researches in Engineering (B),* Vol. 13, Issue 2, Ver. 1, 2013, 2013, pp. 1-14.

[60] Moradi, R., and Lankarani, H. M., "Evaluation of the kinematics and injury potential to different sizes of pedestrains impacted by a utility vehicle with a frontal guard," *International Journal of Crashworthiness,* 2011, DOI: 10.180/13588265.2011.616115, pp. 645-655.

[61] MADYMO coupling manual, release 7.2, TNO Road-Vehicles Research Institute, 2013.

[62] Campbell, B., and Cronin, D., "Coupled Human Body Side Impact Model to Predict Thoracic Injury," NHTSA Paper number 09-0255, 2009.

[63] Kral, J., Setru, P, and Rajeswaran, S., "IIHS Side Impact Analysis using LS-DYNA/MADYMO Coupling," 8th International LS-DYNA Users Conference, 2004.

CHAPTER TWO

A FINITE ELEMENT ANALYSIS OF HIGH-ENERGY ABSORPTION CELLULAR MATERIALS IN ENHANCING PASSIVE SAFETY OF ROAD VEHICLES IN SIDE-IMPACT ACCIDENTS

2.1 Abstract

In an effort to increase road vehicles' structural strength, cellular materials such as foam has been utilized and installed in vital parts of the vehicle. The limited structural crush zones in side-impact collisions, when compared to frontal-impacts, have shown to cause higher deformation to the passenger compartments that will lead to severe injury to the vehicle occupants. Therefore, the need to further enhance road vehicles' passive safety system to protect the occupants during side-impact collisions is necessary. In addition to many passive safety features, cellular materials have been installed in current vehicles to serve as structural reinforcement by absorbing impact energy from transferring to the occupants. This study is aimed at investigating the effect of various cellular materials in enhancing vehicle crashworthiness such as side door's intrusion, interior door's acceleration and the internal energy of the cellular materials. To fulfill the objective of this paper, an existing finite element model of a sedan vehicle is modified to include a cellular material sandwiched in between the door panels. The cellular materials used for this study are IMPAXX, PUF, MAC, DAX and CONFOR foams. The mechanical properties of the cellular materials utilized in the computational model are validated. Various dynamic responses of the vehicle structure with the inclusion of the five selected materials are numerically tested and compared against the vehicle structure without the cellular materials. Side-impact simulations in accordance to Federal Motor Vehicle Safety Standard (FMVSS) No. 214 standard are used to replicate side-impact collisions. This study quantifies the energy-absorption and side door intrusion with

[1] This entire chapter has been published in the following source:

- **Yi Yang, Tay**, Chee Sern, Lim, and Hamid M., Lankarani, "A Finite Element Analysis of High-Energy Absorption Cellular Materials in Enhancing Passive Safety of Road Vehicles in Side-Impact Accidents," *International Journal of Crashworthiness,* 19:3, 2014, pp. 288-300, DOI: 10.1080/13588265.2014.893789.

different cellular padding. It also shows that the inclusion of cellular materials significantly reduces occupant compartment's intrusion and deceleration of the vehicle by at least 30 percent. Therefore, the inclusion of cellular materials has shown promising results in improving the crashworthiness of road vehicles.

2.2 Introduction

The overall improvements in the crashworthiness of current road vehicles have improved remarkable over the past few decades. This is proven by a statistical study conducted by National Highway Traffic Safety Administration (NHTSA) showing that occupants' fatality rates in 2009 were 1.14 occupants per 100 million vehicle miles compared to 1.55 fatality ratio in 1999 [1]. In 2011, side-impact collisions account for 22 percent of the total accidents in passenger vehicles. In terms of fatal crashes, side-impact collisions account for 25 percent of all fatal crashes [2]. Although side-impact crashes account for a high percentage of fatal crashes, it is known that most of the safety improvements implemented were focused predominantly on frontal-crashes due to the higher closing speed of frontal crashes on impact. It is shown that from the early 1980's to 2000, vehicle occupants' fatality rate in frontal crashes decreased by 52 percent while the decreased in side crashes was only 24 percent [3]. Therefore, the safety performance in side impact collisions should be further improved.

Due to the limited space around a vehicle's side structure to absorb impact energy, protecting the occupants in an event of side collision has posted considerable challenges. Therefore, the construction of the vehicle's side structures becomes an important consideration for maximizing structural strength. One of the effective and feasible strategies in enhancing a vehicle's structural performance is to increase the energy absorption capability by incorporating high energy absorption materials such as cellular materials. Such materials possess the capability of undergoing a prolonged stress plateau over a large

percentage of total strain. To date, some of the most commonly used cellular materials in crashworthiness applications are IMPAXX foam, polyurethane foam (PUF) and micro-agglomerated cork (MAC). In addition, higher energy absorption aircraft seat cushions such as DAX and CONFOR foams may also be feasible for this study due to the materials' large plateau characteristics in the load-deflection curve [4-6].

Over the past decade, cellular materials have demonstrated to have significant impact in enhancing the energy absorption of vehicle structures as well as to serve as structural reinforcement [7- 9]. Some of the studies that inspired the use of cellular materials for vehicle applications are reported by Cernicchi et al.[10], Cazzola et al. [11] and Gupta [12]. Gupta [12] studied the performance of the B-pillar with foam application when subjected to an impact force onto the edge of the vehicle roof. It was concluded that the B-pillar with the inclusion of cellular paddings significantly reduces the bending and deformation of the B-pillar by at least 15 percent. In terms of improvement of vehicle structure in frontal crashes, Droste et al. [13] showed that buckling of the B-pillar can be improved by installing a foam filled tube in the B-pillar. In an interesting study by Paulino et al. [9], the effectiveness of cellular materials was demonstrated by incorporating a MAC padding in between the door panels. A side-impact simulation was performed to assess the dynamic responses of the vehicle door with and without the MAC padding. The results showed that the use of MAC padding effectively reduced the door's acceleration and intrusion by 54 percent and 10 percent respectively. However, because the study was conducted only using the door panels; it failed to address some major issues such as the effect of dynamic response of A and B-pillars reinforcements on the door structure. It is evident that the inclusion of cellular materials into vehicle's structure can reduce structural intrusion and increase the occupant's survival space. Currently, optimization of advanced airbag systems is an on-going research to increase efficiency and to reduce unintended injuries from deploying airbags [14, 15]. Hence,

the implementation of cellular materials in vehicle applications coupled with advanced airbag systems can further reduce occupants' fatality risks.

The main objective of this work is to investigate the dynamic responses of the vehicle by utilizing different types of high-energy absorption cellular materials. The cellular materials used in this study consist of IMPAXX, PUF, MAC, DAX foam and CONFOR foam. The cellular materials and vehicle model are validated to ensure proper finite element (FE) modeling. Next, the cellular materials are confined in between the door panels and the non-linear finite element analysis (FEA) software, LS-DYNA, is used to conduct the side-impact simulations on a full-sized 2001 Ford Taurus FE model. The dynamic responses of the vehicle such as the door's intrusions, lateral accelerations and energy absorption are then obtained and a comparative analysis is performed.

2.3 Methodology

This study involved modeling and analysis of the cellular materials and vehicle model using computer simulations and laboratory test data. In the first part of this study, the cellular materials' stress-strain curves and force-deflection curves is obtained and validated against various studies and laboratory test data. In addition, the Ford Taurus FE vehicle model is also validated against the National Crash Analysis Center (NCAC) side-impact simulation results. The second part of this study involves the inclusion of cellular paddings into the door panels and side-impact simulations are performed to evaluate the dynamic response of the vehicle with and without the cellular paddings. The side-impact simulations are conducted in accordance to FMVSS No. 214 side-impact protocol.

2.3.1 Cellular material model development and validation with experiments

A general overview of the mechanical properties and LS-DYNA material cards for the cellular material used in this study is provided in Table 2.1, where ρ, E and ν are the density, elastic modulus and Poisson coefficient of the cellular materials respectively and $\widehat{E}$ is

the elastic modulus of the cellular materials at full compressed or dense state. The different mechanical properties of these paddings ensure a complete analysis across a wide variety of high energy absorption materials. The cellular materials PUF, MAC and IMPAXX stress-strain curves are validated and compared to various studies by Slik et al. [16], Coelha et al. [17] and Shim et al. [18]. The DAX 55 and Confor Green foams' stress-strain curves are obtained through the quasi-static test performed at Wichita State University's Composite Laboratory. Similarly, the finite element (FE) simulations for DAX 55 and CONFOR green foams are also validated against the experimental data to ensure proper FE modeling before incorporating these materials in the vehicle model.

Table 2.1. Mechanical properties and LS-DYNA material cards of cellular materials

Cellular Materials	**ρ** (**kg/m^3**)	**E** (**MPa**)	**Ê** (**MPa**)	ν	**Stress-Strain Curve**	**Validation Method**	**LS-DYNA Material Card**
DAX 55	35.0	0.05	25	0.31	refer to Figure 4 (a)	Experimental	MAT 57
Confor Green	96.1	1.5	1200	0.33	refer to Figure 4 (b)	Experimental	MAT 57
IMPAXX	33.6	16.3	3400	0.40	refer to Figure 4 (c)	Slik et al. [16]	MAT 57
MAC	293.0	15.0	8700	0.30	refer to Figure 4 (d)	Coelha et al. [17]	MAT 26
PUF	25.6	2.9	1600	0.44	refer to Figure 4 (e)	Shim et al. [18]	MAT 57

The experimental load-deflection curve of the DAX 55 and CONFOR green foams, as shown in Figures 2.2(a) and (b), are tested using an MTS machine. The 978kN (220-kip) MTS machine, as shown in Figure 2.1, is equipped with two 667kN (150-kip) strain gage type and 44kN (10-kip) piezoelectric load cells and a 489kN (110-kip) servo hydraulic actuator. Each foam specimen is placed on flat rigid platform and a 50in^2 round rigid indenter is used to apply a vertical compression loading to the center of the foam specimen. Prior to the experimental test, the foam specimen is preflex twice to a total of 75 percent of its full thickness at a rate of 3.3mm/s and the specimen is allowed to rest for 360s after preflex. Next, the foam is indented at a loading rate of 0.762m/s using a triangular pulse to emulate a quasi-static test. The data acquisition is performed by using the load cells to measure the

compression loading applied to the foam and displacement transducer is used to measure the foam's vertical deformation. A pre-defined displacement threshold is set to release the compression load in order to protect the MTS load cell from overloading when the foam specimen bottoms out. The nominal stress-strain curve of each foam specimen is derived from the average load-deflection curve.

The FE quasi-static simulation setup can be seen in Figure 2.3. The cellular material is sandwiched in between a rigid base and a rigid impactor. Similar to the experimental setup, the rigid impactor has a constant downward velocity of 0.07m/s to replicate a quasi-static compression test. The material cards *MAT 057 – LOW DENSITY FOAM and *MAT 063 – CRUSHABLE FOAM can be used interchangeably to describe the low density and high compressible behavior of foams. However, it should be noted that the use of *MAT 063 – CRUSHABLE FOAM cannot properly define the unloading phase of the cellular materials. In terms of defining the low recovery rate of cellular materials, a low hysteric unloading factor of and high unloading shape factor are used. It is found that hysteric unloading factor of 0.01 and shape factor of 15 to 25 is sufficient in defining the unloading phase of the cellular materials. The material properties of the impactor is defined using *MAT 20 – RIGID to replicate a rigid impactor. The LS-DYNA material card used for the MAC is *MAT 026 – HONEYCOMB to adequately define the anisotropic behavior of MAC and the material cards used for the remaining cellular materials are *MAT 057 – LOW DENSITY FOAM. The material cards for each cellular material can be obtained from Table 3.1. The yield strength for MAC, which is an additional required input parameter for *MAT 026 – HONEYCOMB is set at $\sigma_y = 1.0$MPa, per [17]. Table 2.2 illustrates the additional input parameters used in this study for the MAT 57 in the modeling of foams. As discussed previously, these set of parameters are utilized for the modeling of DAX55, CONFOR green, PUF and IMPAXX foams. The stress-strain curve input for each material can be referred

from Figure 2.4. The tension cut-off stress, denoted as τ_i, is left at the default value since the cellular foam will not fail in tension for this application [23]. The parameters that control the shape of the unloading curve is governed by two non-dimensional parameters, the hysteric unloading factor and shape factor, which are set as 0.101 and 25 respectively. A maximum recommended value for damping coefficient of 0.5 is utilized to increase stability due to the relatively large difference in stiffness between the cellular foams and the rigid parts. For both the Young's relaxation modulus, E_d and the decay constant, β, the default value of 0.0 is utilized.

Table 2.2. Additional parameters for LS-DYNA MAT 57 material's card

MAT 57 Parameters	**Value**
Tension cut-off stress, τ_i	1.00E20 MPa
Hysteric unloading factor	0.101
Decay constant, β	0.0 s^{-1}
Viscous damping coefficient	0.50
Shape factor	25.0
Young's relaxation modulus, E_d	0.0 MPa

Figure 2.4 (a) – (e) represent the material model validation for CONFOR Green, DAX55, IMPAXX, MAC and PUF respectively. It can be seen that these materials' possess the desired plateau shapes and are in good agreement with simulation and experimental data from this study and various studies. It should be noted that the stress-strain curve for the CONFOR green simulation showed slightly higher load across the entire deflection range but the plateau shape, rise time and peak value is in good agreement with the experimental data. It can also be observed from the validation figures that only the loading phase of the cellular materials is included for comparison. In broad terms, the primary focus of this study is to investigate the foam when undergo loading or compression therefore it is not necessary to include the unloading phase. Overall, the cellular materials are considered validated and suitable to be included into the vehicle model for further analysis.

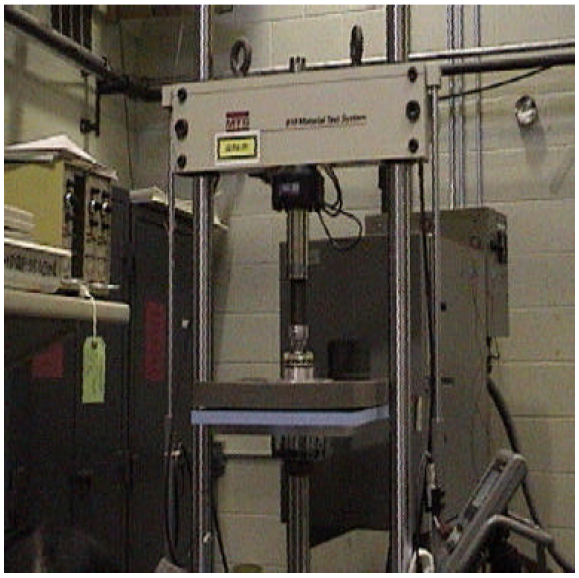

Figure 2.1. MTS machine test setup for the load-deflection test

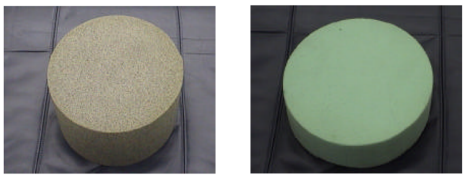

Figure 2.2. (a) DAX 55 foam ; (b) CONFOR green foam

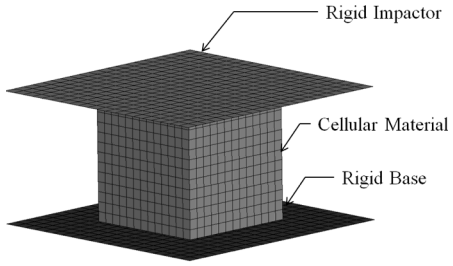

Figure 2.3. Finite element model for the quasi-static test

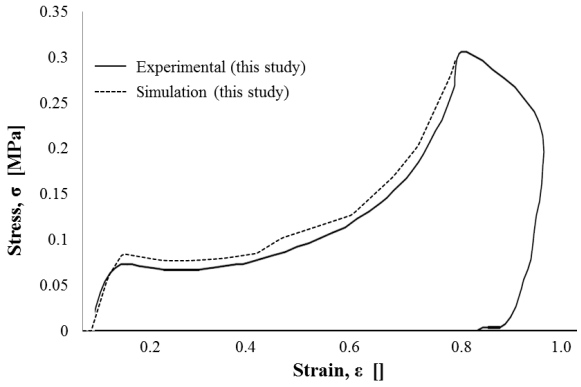

(a)

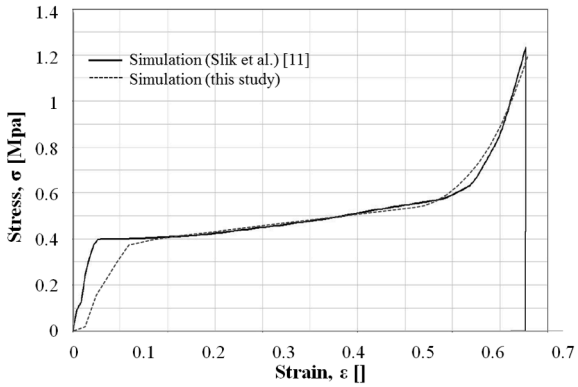

(c)

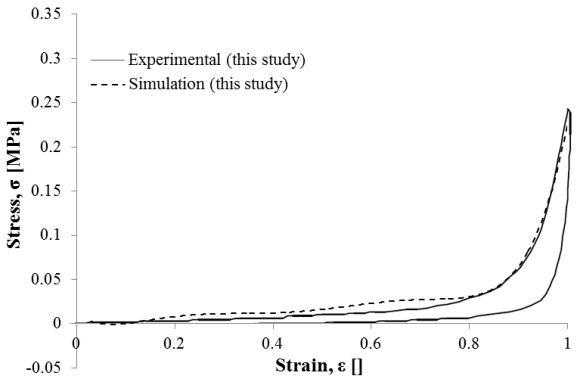

(b)

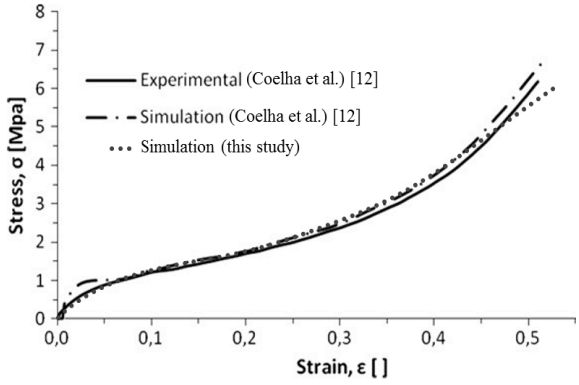

(d)

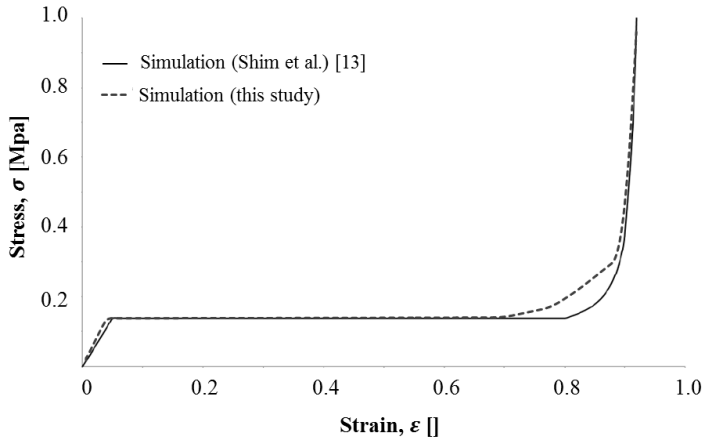

(e)

Figure 2.4. Comparison of stress-strain curve from numerical simulation and experimental data (a) CONFOR green from this study ; (b) DAX 55 from this study ; (c) IMPAXX from this study and from Slik et al. [16] ; (d) MAC comparison this study and from Coelha et al. [17] ; (e) PUF from this study and from Shim et al. [18]

2.3.2 Vehicle model

Once the cellular materials are validated, these materials can be incorporated into the vehicle side panels. The vehicle used in this study is a detailed FE full sized sedan model, Ford Taurus [19]. In order to evaluate the performance of the cellular materials, the FMVSS No. 214 side-impact standard test protocol is used to replicate a side-impact collision. The impactor or moving deformable barrier (MDB) used in this study is developed by LS-DYNA Cooperation [20]. According to FMVSS 214, the MDB impacts the vehicle at 14.98m/s, crabbing at 27-degrees angle. The point of impact is at the vehicle A-pillar. The side-impact simulation test setup is represented in Figure 2.5.

Due to the complexity of the side-impact setup, it is important to have the vehicle and MDB model validated first to ensure proper contacts between the vehicle and the MDB. The vehicle side-impact simulation is validated with a similar simulation conducted by NCAC [16].

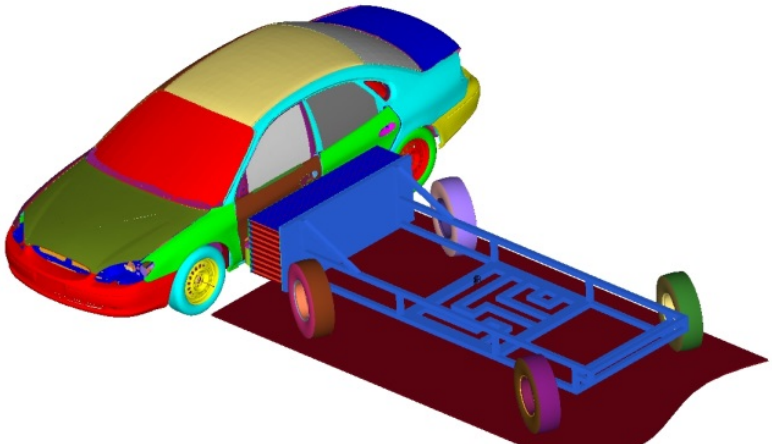

Figure 2.5. FMVSS 214 side-impact simulation setup

Figure 2.6 (a) and (b) represent the dynamic responses of the vehicle from this study and from NCAC's simulated results. It can be seen that the right sill – rear seat acceleration is in good agreement with both NHTSA and NCAC test. The peak y-acceleration at 0.08s is very similar for all three tests. It can be seen from approximately 0.35 to 0.055s, the NCAC's simulation shows a smoother curve while the simulation from this study presents a short but sharp decrease in acceleration at 0.4s. In addition to the right sill's acceleration, the right sill's y-velocity is also used for the vehicle model validation. It can be seen that the y-velocity from this study is slightly higher than the NHTSA and NCAC tests which otherwise are very similar the both tests in magnitude, shape and rise time. Based on these comparison graphs, it is conclusive that the validation for the vehicle model is successful.

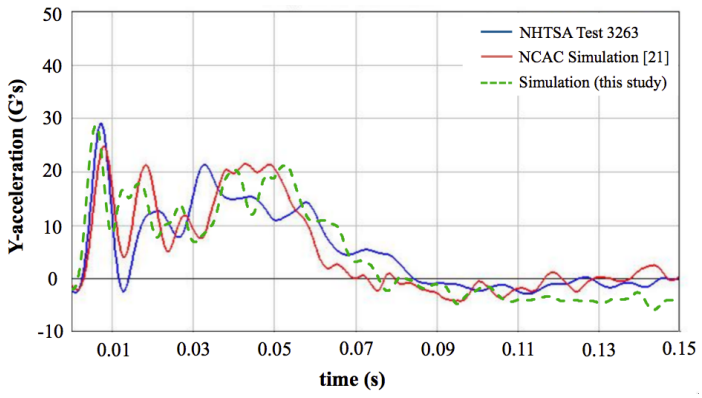

(a)

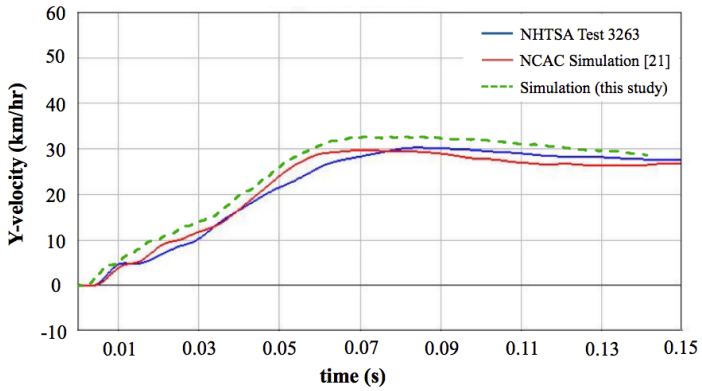

(b)

Figure 2.6. Dynamic response of the vehicle right sill from this study and from NCAC (a) rear seat y-acceleration; (b) rear seat y-velocity [21]

2.3.3 Inclusion of cellular materials into vehicle model

Once the validation of the cellular and vehicle model is completed, the cellular materials can be included into the vehicle panels. The modeling of the cellular materials is performed using a CAD program and meshed using Hypermesh. The finite element and the geometry of the foam are illustrated in Figure 2.7. The cellular padding is defined as a solid element using a quad-node tetrahedral element with an average element length of 15mm. Additionally, the cellular padding is discretized into 11,111 elements and 7,266 nodes. Due to the soft characteristics of these materials, negative volume instabilities is controlled with the use of LS-Dyna hourglass control card, *CONTROL_HOURGLASS. As mentioned previously, the material model used for PUF, IMPAXX, DAX and CONFOR Green are *MAT 057 – LOW DENSITY FOAM. However, the material behavior of MAC can be more accurately defined using *MAT 26 – HONEYCOMB.

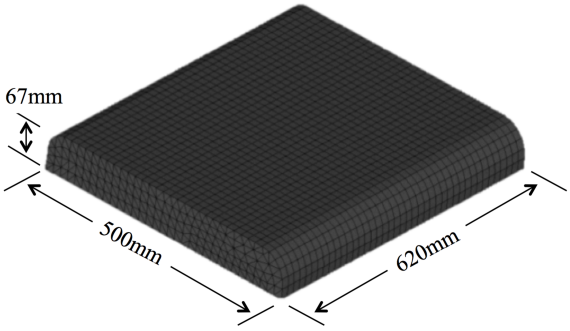

Figure 2.7. Finite element model of the cellular padding

The contact definition for the entire model is extremely important to ensure proper interaction between components. For example, although the vehicle model (joints, welds) is constrained properly, prior simulations showed that the absence of self-contact between the vehicle's components resulted in inter-penetration of the components hence rendering the results inaccurate. Therefore, the vehicle self-contact is defined using LS-DYNA card *CONTACT_AUTOMATIC_SINGLE_SURFACE and the contact between the cellular model and the vehicle is *CONTACT_AUTOMATIC_SURFACE_TO_SURFACE to eliminate penetration within the components. The same contact algorithm is employed to define the contact between between the vehicle and MDB. The static and dynamic coefficient of friction is set at 0.60 for the contact between the vehicle and MDB while the coefficient of friction of 0.20 is set for the contact between the door panels and the cellular materials. It is a common practice to set the dynamic and static friction equal to reduce noisy data. As such, the transition curve from the static to dynamic friction, which is governed by the friction decay coefficient, is set at zero. Due to the contact oscillation between the cellular material and the structure, a coefficient of viscous damping value of 50 is applied to the model to critically damp the oscillation and to improve stabilities. It is important to note that the contact behavior of the structure is highly dependent on the contact parameters, thus, it is important to determine the sensitivity of the contact parameters by making few runs with upper and lower boundary conditions.

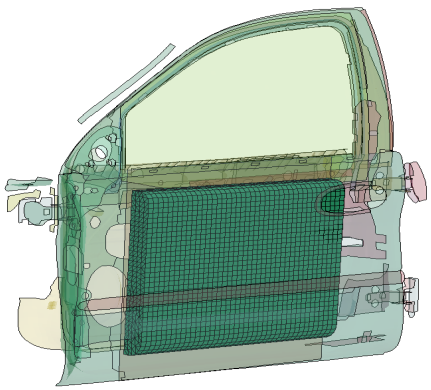

Figure 2.8. Inclusion of cellular material into the door panel

Figure 2.8 represents the inclusion of the cellular material into the door's panels. The position and the geometry of the cellular material are extremely relevant in this study. Firstly, preliminary simulations showed that the material must be in contact with the outer door panel to maximize energy absorption. Secondly, the thickness of the material must not affect other mechanisms in the door such as the window crank mechanism or the reinforced beams. Thus, in order to satisfy these criteria, the material is modeled according to the curvature of the outer door surface and has a thickness that spans across the depth of the outer door. Consequently, the cellular padding is located 285mm from the A-pillar, 100mm from the B-pillar and 63mm below the window-sill. The dynamic response of the vehicle by varying the placement or the geometry of the cellular padding is not discussed as it falls out of scope of this study.

Once the modeling of the vehicle and cellular materials are completed, the side-impact simulations in accordance to FMVSS 214 protocol are conducted to investigate and analyze the effect of these cellular materials on the dynamic responses of the vehicle.

2.4 Results and Discussions

For comparison purposes, the post-crash deformation of the vehicle with the cellular padding is compared to the post-crash without the padding. In terms of quantifying the vehicle's dynamic response, simulated results such as door panel intrusion level, door's interior lateral acceleration are obtained. Besides that, the vehicles' structural strength is analyzed in terms of total energy absorbed by the door's panels and the energy absorption of only the paddings is also analyzed for comparison.

2.4.1 Post-crash deformation of vehicle

The post-crash vehicle deformation with and without cellular padding is shown in Figure 2.9. By observing the deformation of the outer door more closely from both figures, it can be seen that the cellular padding reduced the deformation or the intrusion of the outer

padding compared to the vehicle without the padding. It is also shown that the outer door for the vehicle without the padding is completely crushed and is in contact with the inner door panel. Hence, without the padding, most of the kinetic energy is transferred from the outer door to the inner door.

To avoid repetitive kinematics figures, Figure 2.10 represents the kinematics of the Ford Taurus without the cellular padding at different instances of time while Figure 2.11 shows the kinematics with CONFOR Green padding. In terms of the side structure without cellular padding, it can be seen that the outer panel initiated contact with the inner and interior panels at 10ms. It can also be seen that from 0 – 10ms, the interior has not yet initiate contact with the cushion seat. At $t = 20ms$, once the outer panel is complete crushed and the intrusion of the inner panel reach the cushion seat. On the contrary, it is shown that the side structure with cellular padding reduces the crush force exerted by the side panel. Thus, the deformation rate of the seat is reduced and the seat maintains its initial shape. At $t = 50ms$, it can also be observed by comparing both kinematics that the width of the back seat for the simulation without cellular padding is more crushed than the simulation with CONFOR Green padding.

Although no occupant was included in this model, it can be predicted that the intrusions will affect the occupant after 20ms. From 30ms onwards, the kinematic diagrams showed that the rate of deformation of the side panels and the cushion seat are reduced. It can be concluded that the most important timeframe in side-impact collision for this study is from initial contact at 0ms to approximately 30ms. It is reasonable to expect high dynamic forces being exerted by the side structures on the seat cushions and the occupant within this timeframe. In addition, the slower rate of deformation of the seat with cellular paddings should reduce the impact force of the side panel on the occupants. Thus, the inclusion of cellular paddings in side-impact crashes could enhance occupant safety.

Although the post-crash result is a good indication in analyzing the intrusion, it fails to provide solid information on the dynamic response of the vehicle such as the intrusion velocity, interior acceleration and the energy absorbed by the side panels. The dynamic responses of the vehicle are provided in the following sections.

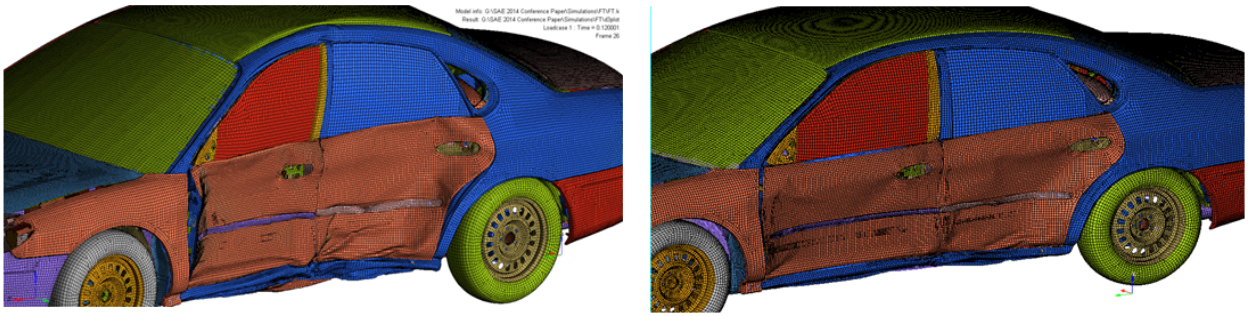

(a) (b)

Figure 2.9. (a) Post-crash deformation without cellular padding; (b) Post-crash deformation with cellular padding

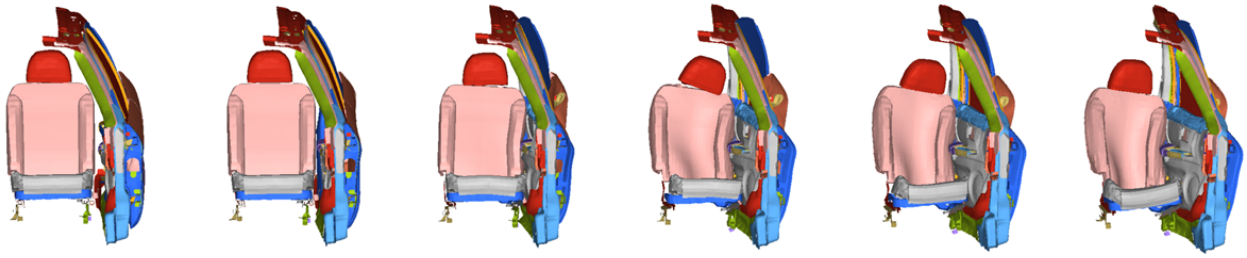

0ms 10ms 20ms 30ms 40ms 50ms

Figure 2.10. Simulated deformation of the Ford Taurus' seat and door panels without cellular padding

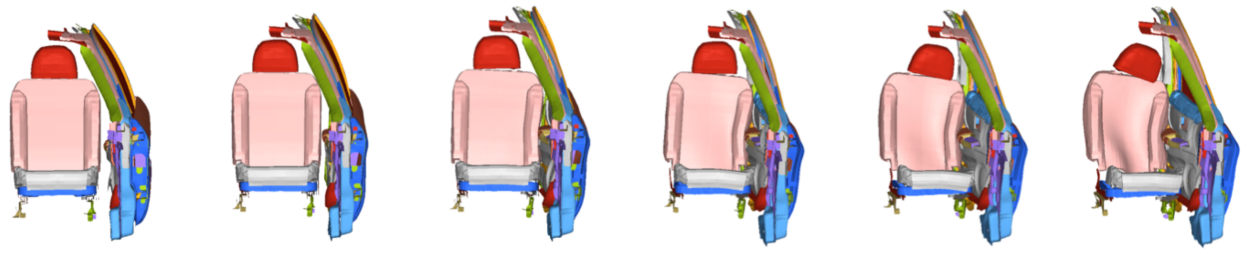

0ms 10ms 20ms 30ms 40ms 50ms

Figure 2.11. Simulated deformation of the Ford Taurus' seat and door panels with CONFOR Green padding

2.4.2 Door's panel intrusion

The vehicle door panels' intrusions were measured according to recommendation by NHTSA's new car assessment program [17]. The intrusion levels are divided from level one through five as seen in Figure 2.12. In this study, the intrusion level at the occupant H-point (level 2) and window-sill (level 4) are measured. The height of the H-point and window-sill

relative to ground is 524mm 902mm respectively. The purpose of selecting these points for measurement is that the H-point and window-sill intrusions correlate well with intrusion to the occupant's pelvic and thoracic body region.

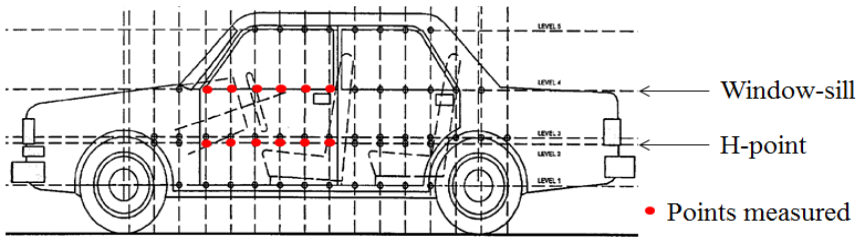

Figure 2.12. Ford Taurus side intrusion measurement levels [22]

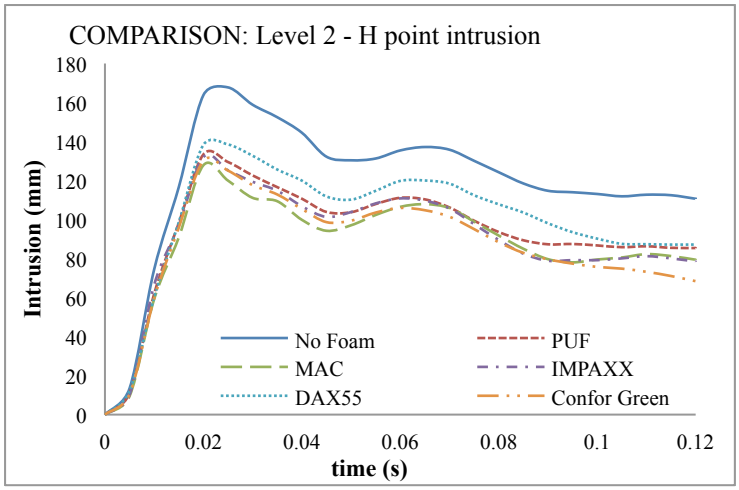

Figure 2.13. H-point intrusion

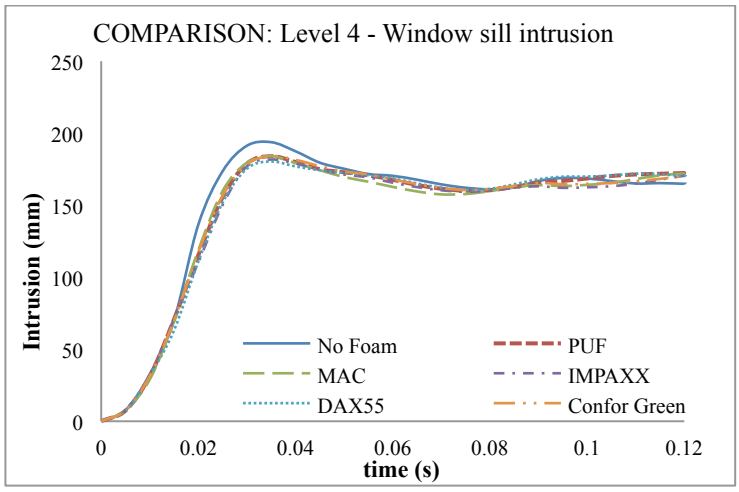

Figure 2.14. Window-sill intrusion

The intrusion levels as shown in Figures 2.13 and 2.14 are the average measurements of ten randomly selected points of the driver's door along the horizontal plane of the two selected intrusion levels. Figure 2.13 represents the door's intrusion at H-point. It is very

clear that the intrusion levels are significant reduced with the inclusion of cellular paddings. The maximum intrusion without padding is approximately 167mm while the maximum intrusion with the cellular padding is approximately 138mm. Hence, in terms of peak intrusion values, the intrusion at the H-point is decreased by at least 29 percent. By solely comparing the intrusion level of the cellular paddings (without the vehicle model), it can be seen that the door's panel with the inclusion DAX 55 yielded the highest intrusion level and the MAC padding yielded the lowest intrusion.

The intrusion measured at window-sill is slightly reduced with the inclusion of cellular paddings as shown in Figure 2.14. No significant change in intrusion in the window-sill is observed. This insignificant response is expected because no padding is installed in the window-sill. It can also be seen that the selection of paddings did not affect the window sill's intrusion level. Hence, based on the intrusions at H-point and window-sill, it is conclusive that the inclusions of cellular paddings on the door panels have greater effect on the intrusion at the H-point compared to the window-sill's intrusion. The intrusion of the B-pillar measured from the driver's seat centerline is shown in Figure 2.16. It can be seen that the lateral distance with and without CONFOR padding is measured at 11cm and 8cm. Both intrusion levels are "acceptable" according to IIHS intrusion rating. However, the intrusion with cellular padding is at the higher end of the "acceptable" profile while the intrusion without padding is at the lower end of the profile.

In vehicular accidents, deceleration and intrusion of the occupant cabin are two leading factors of occupant injuries. Unlike frontal accidents where deceleration is the dominant factor of occupant injuries, the limited crush space in side impact accidents makes the structural intrusion the dominant factor of injuries. The crush space for frontal accidents is typically in the range of 60 to 80 cm and 10 to 40 cm for side accidents [24]. Therefore, the reduction in intrusion levels with the inclusion of cellular materials will greatly benefit the

occupants by creating more survival occupant space. Although FMVSS 214 side-impact protocol is used in this study; there exists no detail guideline in quantifying structural rating based on intrusion level. The Insurance Highway for Highway Safety (IIHS) provides an excellent guideline in this matter by measuring contour line of the B-pillar at pre-crash and post-crash. As such, the IIHS intrusion profile is used as a guideline for this study. Due to the different implementation of side-impact protocols of both FMVSS and IIHS, it is important to note that the post-crash intrusion from this study may differ significantly from that of IIHS. Figure 2.15 represents the intrusion rating based on the contour line of the B-pillar.

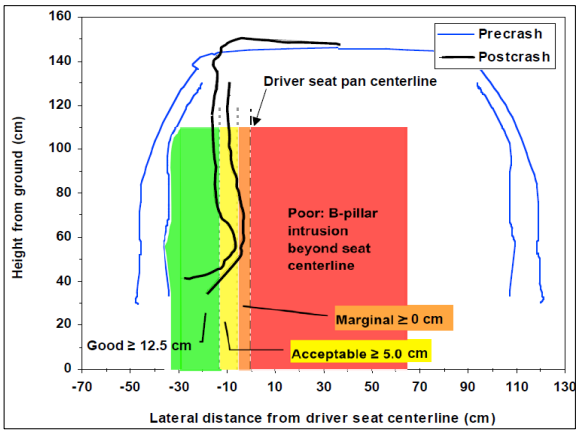

Figure 2.15. IIHS crush profile and compartment intrusion [25]

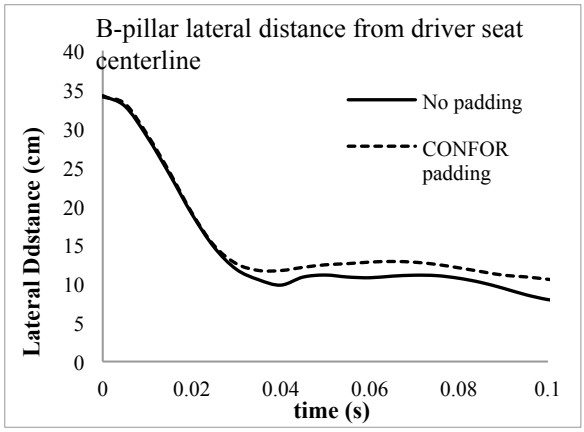

Figure 2.16. B-pillar intrusion relative to driver seat centerline according to IIHS structural rating

2.4.3 Energy absorption

The energy absorption or internal energy of the vehicle side doors can be seen in Figure 2.17. In an effort to increase clarity, only the side structures such as side door's

panels, side interiors and side reinforcement beams are selected for the energy absorption analysis. The reason for selecting only these components for analysis is that the total internal energy of the vehicle with the cellular padding is insignificant when compared to the total internal energy without the padding. The overall result indicated that the total energy absorbed by the side structures increased with the inclusion of cellular padding. It can be seen that the energy absorbed is the highest with PUF padding follow by CONFOR green, DAX55, IMPAXX and MAC. In the previous discussion, it was shown that the vehicle side structure with the PUF padding yielded the highest energy absorption capability. However, by comparing only the cellular paddings as shown in Figure 2.18, it is shown that the internal energy with the inclusion of CONFOR foam is the highest followed by PUF and IMPAXX. The MAC and DAX 55 internal energies are the lowest but share similar shape and magnitude. According to these comparisons, PUF and CONFOR foams are highly efficient in absorbing impact energy.

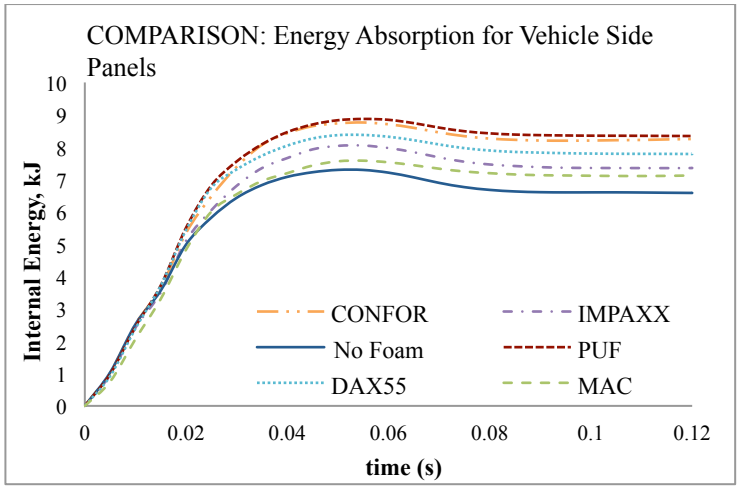

Figure 2.17. Vehicle side structure energy absorption

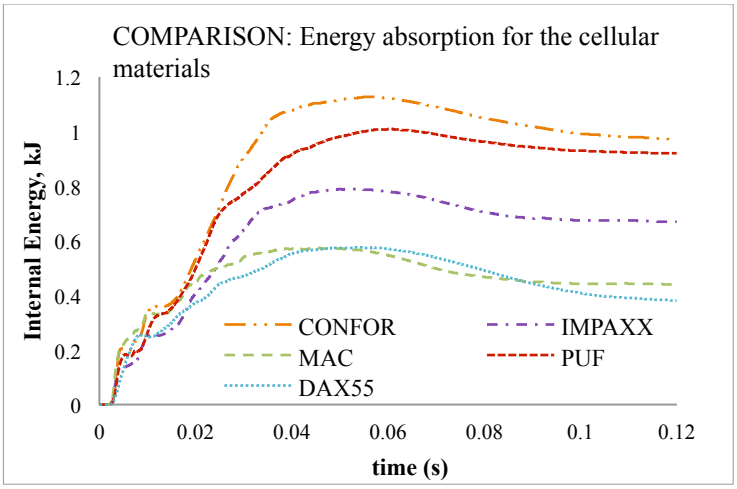

Figure 2.18. Cellular materials energy absorption

The analysis of energy absorption does not present any meaningful results without analyzing its effect on the vehicle's deceleration. The increase in energy absorption of the side panels can reduce the deceleration of the vehicle by damping the impact energy, which in turn can reduce the impact force of the interior on the occupants. The deceleration of the vehicle is illustrated in the subsequent section.

2.4.4 Interior door panel lateral acceleration

The results in Figure 2.19 illustrate the lateral or y-acceleration of the vehicle interior that is measured at the occupant H-point. By analyzing the lateral acceleration and kinematic graphs simultaneously, it can be concluded that the first peak in acceleration at $t \approx 6ms$ can be neglected as this corresponds to the instant at which the MDB initiates contact with the outer panel. In addition to the first peak, the second peak at $t \approx 14ms$ represents the contact initiated by the outer panel to the inner and interior panel. In the case of an in-position occupant, the second peak should not pose any immediate injuries to the occupant because the interior panel is not yet in contact with the occupant. However, in the case of an out-of-position occupant, this second peak in acceleration will cause injuries to the occupant.

The third peak in acceleration is at approximately $t \approx 20ms$ after the initial impact. This peak is the most relevant to this study because it represents the contact between the interior panel and cushion seat. It can clearly be seen that the peak acceleration without the

cellular padding is approximately 147G's and the cellular padding reduced the peak acceleration to approximately 100G's. This translates to approximately 30 percent reductions in peak acceleration. By solely comparing peak acceleration of the panel with cellular padding at $t = 15 - 20ms$, it can be seen that the lateral acceleration with MAC padding is the highest followed by PUF and DAX55. CONFOR green and IMPAXX scored the lowest acceleration.

The lateral acceleration analysis for $t > 40ms$ is not important in this study because it is relatively small in magnitude compared to acceleration in the $t = 0 - 30ms$ timeframe. In addition, the acceleration after $50ms$ is not shown in Figure 2.19 as the accelerations basically oscillates between zero magnitude. The kinematic analysis previously also shows that the deformation of the seat cushion stops after $t = 30ms$. In conclusion, the study on the lateral acceleration of the inner panel shows that the peak acceleration with the inclusion of cellular paddings is significantly reduced by at least 30 percent.

In addition, it is relevant to note that the 30 percent reduction in the interior's lateral acceleration may not translate to similar percentage reduction in occupant injury. Pelvic lateral acceleration is the standard injury measurements using anthropomorphic test dummies (ATD). Therefore, the accuracy of the pelvic injury level reduction with the cellular paddings cannot be determined without including the ATD into the simulation.

To summarize the overall findings, the cellular paddings' performance ratings are categorized as shown in Table 2.3. The CONFOR green padding is constantly ranked the highest in all performance categories. On the other hand, MAC and DAX55 paddings scored the lowest in performance in most categories. Finally, IMPAXX padding ranked average in terms of H-point intrusion and energy absorption.

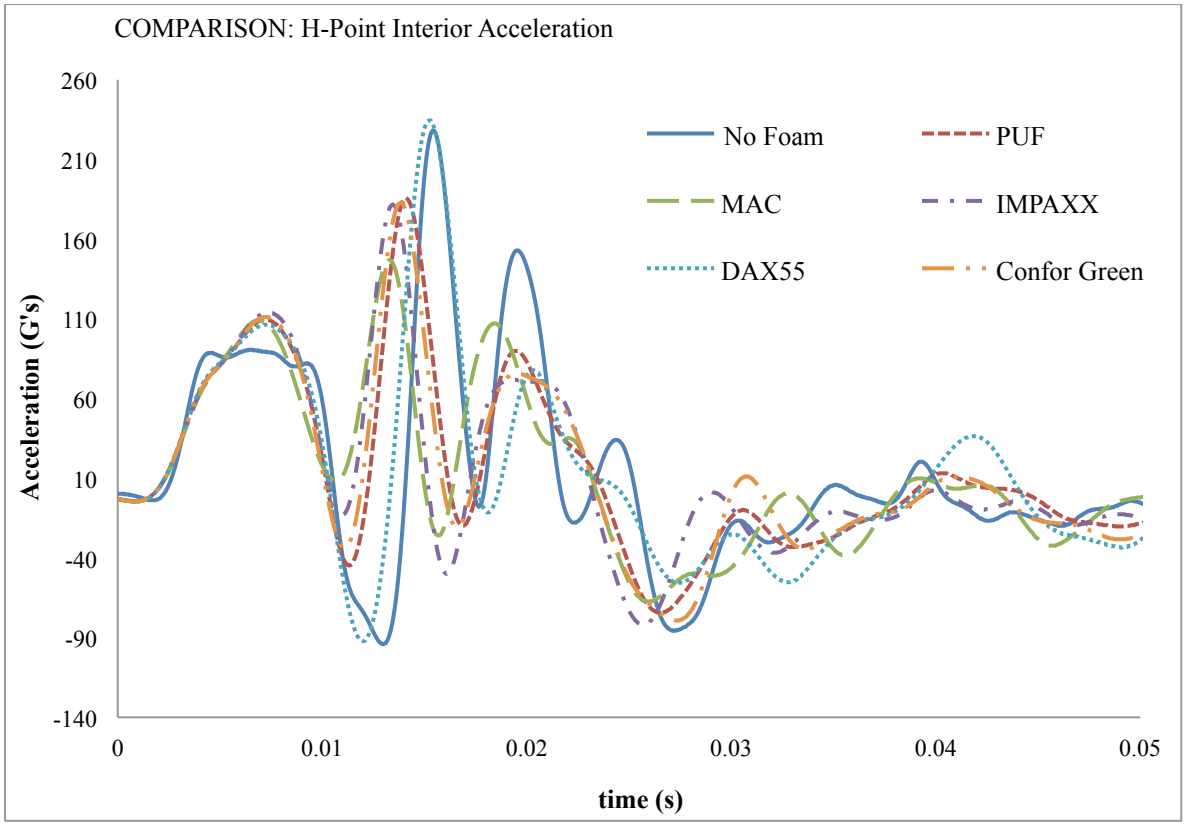

Figure 2.19. Interior H-point lateral acceleration

Table 2.3. Performance rating summary

Performance Category		**Performance Rating** (Worst → Best)					
H-Point Intrusion		No padding	DAX 55	PUF	IMPAXX	Confor green	MAC
Energy Absorption:	*Entire Side Panels*	MAC	No padding	IMPAXX	DAX55	Confor green	PUF
	Cellular Materials Only	-	DAX55	MAC	IMPAXX	PUF	Confor green
Lateral-acceleration		No padding	MAC	PUF	DAX55	IMPAXX	Confor green

2.5 Conclusions

The performance of high-energy absorption cellular materials was presented in this paper. The method of investigation was to analyze the structural dynamic and kinematic responses of the vehicle with and without the cellular padding in side-impact crashes. The numerical models for cellular materials PUF, MAC and IMPAXX were validated with similar studies reported in the literature. In addition, the DAX 55 foam and CONFOR green

foams' mechanical properties such as load-deflection curve were obtained from experimental data and then validated using computer simulations. Similarly, the vehicle model was also validated to ensure proper contact definitions were assigned. The cellular padding model was modeled using quad-node tetrahedral solid element and was discretized into 11,111 element and 7,266 nodes. The cellular materials were included in between the vehicle side panels, and side-impact simulations in accordance to FMVSS 214 side-impact protocol were performed using the non-linear FEA software, LS-DYNA. The following conclusions can be made from this study:

- The inclusion of cellular padding in the door panels reduced the door's intrusion by at least 29 percent. The simulation result with MAC padding resulted in the highest reduction in intrusion while DAX55 was the lowest.
- The energy absorption capability of the entire side door structure with cellular padding, except for MAC, was increased with the inclusion of cellular paddings. PUF and CONFOR green paddings resulted in the largest increment in energy absorbed. In order to properly compare the energy absorption capability of the cellular paddings, the internal energy of only the paddings (not inclusive of the door structure) was measured. Similar to the energy absorbed analysis on the entire door structure, PUF and CONFOR green paddings were the highest among these materials. Lastly, IMPAXX foam's energy absorbed was average in both cases.
- The interior's peak acceleration with cellular paddings at $t \approx 20ms$, where the interior panel initiated contact with the cushion seat was significantly reduced compared to without padding. These cellular paddings reduced the peak acceleration by at least 30 percent.

Overall, the objective of this paper to evaluate the performance of various cellular materials on the response of the vehicle was achieved. The simulated results showed that the

crashworthiness of the vehicle would benefit from the inclusion of high-energy absorption cellular materials. It was also evident that CONFOR green and polyurethane foam were most suitable to be used for vehicle crash applications. Future works may include analyzing the injury biomechanics of an occupant or dummy model by utilizing the best cellular paddings from this study, namely, either the PUF, CONFOR Green or IMPAXX paddings. Moreover, the contact force between the vehicle interior and the ATD can be analyzed to investigate the reduction in impact force with the inclusion of cellular padding. The dynamic responses with the inclusion of cellular paddings in all of the vital parts of the vehicles are also unknown but should further improve the overall crashworthiness of road vehicles.

2.6 References

[1] Annonymous, 2007, "An Evaluation of Side Impact Protection," US. National Highway Traffic Safety Administration (NHTSA), DOT HS 810 748.

[2] Annonymous, 2011, "Traffic Safety Facts 2011", U.S. Department of Transportation NHTSA DOT HS 811 754.

[3] Jayasuriya, M. M, and Saha, N. K. , 2005, "Local structural force evaluation of a vehicle in side barrier impacts," *International Journal of Crashworthiness, 10:5, 451-461, DOI: 10.1533/ijcr.2005.0359.*

[4] Bhonge, P. S., Thorbole, K. C. and Lankarani, H. M., 2010, "Computational Modeling and Performance Evaluation of a DAX-Foam Aircraft Seat Cushion Utilizing High Loading Rate Dynamic Characteristics," 2010 ASME International Mechanical Engineering Congress and Exposition.

[5] Behesti, HKH and Lankarani, H. M., 2005, "A simplified test methodology for crashworthiness evaluation of aircraft seat cushions," *International Journal of Crashworthiness, Vol. 11, No. 1, pp. 27-35.*

[6] Adams, A., Lankarani, H. M., and Safi, N. M., 2003, "Aircraft Seat Cushion Performance Evaluation and Replacement Implementation," Proceedings of the 2003 ASEE Conference and Exposition.

[7] Gupta, S., 2011, 2011, "Using CAE to Evaluate Structural Foam Design For Increasing Roof Strength" 8th European LS-DYNA Users Conference.

[8] Mkrtchyan, L., Maier, M. and Huber, U., 2008, "Structural polyurethane foam: testing and modelling for automotive applications," *International Journal of Crashworthiness, 13:5, 523-532, DOI: 10.1080/13588260802221310.*

[9] Paulino, M. and Teixeira-Dias, F., 2011, "An energy absorption performance index for cellular materials – development of a side-impact cork padding," *International Journal of Crashworthiness, 16:2, 135-153, DOI: 10.1080/13588265.2010.536688.*

[10] Cernicchi, A., Galvanetto, U., and, Lannucci, L., 2008, "Virtual modeling of safety helmets: practical problems," *International Journal of Crashworthiness*, 13:4, 451 – 467, DOI: 10.180/13588260802055460.

[11] Cazzola, G. J., Fazio, E. A., and, Aparicio Izquierdo, F., 2013, "Study of the bending response of metal foam-filled beams applied to enhance the rolloever beahavior of coach structures," *International Journal of Crashworthiness, 18:6, 620-632, DOI: 10.1080/13588265,2013.831516.*

[12] Gupta, S., 2011, "Using CAE to Evaluate a Structural Foam Design for Increasing Roof Strength," 8th European LS-DYNA Users Conference, Strasbourg.

[13] Droste, A., and Rottger, J., 2007, "Crash Performance Increase with Structural BETAFOAM," LS-DYNA Anwenderforum, Frankenthal.

[14] Tay, Y. Y., Moradi, R., and Lankarani, H. M., 2013, "A Numerical Analysis of Pre-Deployment Effect of Side-Impact Airbags in Reducing Occupant Injuries," IMECE 2013, Proceedings of ASME 2013 International Mechanical Engineering Congress & Exposition.

[15] Tay, Y. Y., Moradi, R., and Lankarani, H. M., 2013, "A DoE Method in Predicting Injuries to Out-of-Position Occupants from Torso-only Side-Impact Airbags," *Global Journal of Researches in Engineering (B) Volume XIII Issue II Version 1, pp. 1-14.*

[16] Slik, G., Vogel, G. and Chawda, V., 2006, "Material Model Validation of a High Efficient Energy Absorbing Foam" 5th LS-Dyna Forum.

[17] Coelha, R. M., Alves de Sousa, R. J., Fernandes, F.A.O. and Teixeira-Dias, F., 2012, "New Composite Liners for Energy Absorption Purposes", *Materials & Design, Vol. 43, pp. 384-392.*

[18] Shim, V., Tu, Z. and Lim, C., 2002, "Two-dimensional response of crushable polyurethane foam to low velocity impact" *International Journal of Impact Engineering 24(6-7): 703–731.*

[19] Annonymous, 2013, National Crash Analysis Center, ncac.gwu.edu (retrieved: August, 2013).

[20] Annonymous, 2013, Livermore Software Technology Corporation, www.lstc.com (retrieved: Oct, 2013).

[21] Marzougui, D., Samaha, R., Cui, C. and Kan, C., 2012, “Extended Validation of the Finite Element Model for the 2001 Ford Taurus Passenger Sedan,” The National Crash Analysis Center and The George Washington University, NCAC 2012-W-004.

[22] Annonymous, 2000, “New Car Assessment Program Side Impact Test – 2000 Ford Taurus 4 Door Sedan,” NHTSA No: MY0211, Report No: 214D-MGA-2000-04.

[23] Olivares, G., Acosta, J. F., and Yadav, V., 2010, "Certification by Analysis I and II," Computational Mechanics Laboratory, National Institute for Aviation Research, Wichita State University.

[24] Chan, C. Y., 2000, *Fundamentals of Crash Sensing in Automotive in Air Bag Systems*, Warrendale, Pennsylvania: Society of Automotive Engineers, Inc.

[25] Annonymous, 2012, “Side Impact Crashworthiness Evaluation Crash Test Protocol (Version VI),” Insurance Highway Institute for Highway Safety.

CHAPTER THREE

A NUMERICAL ANALYSIS OF PRE-DEPLOYMENT EFFECT OF SIDE-IMPACT AIRBAGS IN REDUCING OCCUPANT INJURIES

3.1 Abstract

Side impact collisions represent the second greatest cause of fatality in motor vehicle accidents. Side-impact airbags (SABs), though not mandated by NHTSA, have been installed in recent model year vehicle due to its effectiveness in reducing passengers' injuries and fatality rates. However, the increase in number of frontal and side airbags installed in modern vehicles has concomitantly led to the rise of airbag related injuries. A typical side-impact mechanical or electronic sensor require much higher sensitivity due to the limited crush zones making SABs deployment more lethal to out-of-position passengers and children. Appropriate pre-crash sensing needs to be utilized in order to properly restraint passengers and reduce passengers' injuries in a vehicle collision. A typical passenger vehicle utilizes sensors to activate airbag deployment when certain crush displacement, velocity and or acceleration threshold are met. In this study, it is assumed that an ideal pre-crash sensing system such as a combination of proximity and velocity and acceleration sensors is used to govern the SAB pre-deployment algorithm. The main focus of this paper is to provide a numerical analysis of the benefit of pre-deploying SAB in lateral crashes in reducing occupant injuries. The effectiveness of SABs at low and high speed side-impact collisions are examined using numerical Anthropomorphic Test Dummy (ATD) model. Finite Element Analysis (FEA) is primarily used to evaluate this concept. Velocities ranging from 33.5mph to 50mph are used in the FEA simulations. The ATD used in this test is the ES-2re 50th percentile side-impact dummy (SID). Crucial injury criteria such as Head Injury Criteria

[1]This entire chapter has been presented at and published in the following source:

- **Yi Yang Tay**, Rasoul Moradi, Hamid M. Lankarani, "A Numerical Analysis of Pre-Deployment Effect of Side-Impact Airbags in Reducing Occupant Injuries," Proceedings of ASME 2013 International Mechanical Engineering Congress & Exposition, San Diego, USA, DOI: 10.1115/IMECE2013-63234, November 2013.

(HIC), Thoracic Trauma Index (TTI), and thorax deflection are computed for the ATD and compared against those from a typical airbag system without pre-crash sensing. It is shown that the pre-deployment of SABs has the potential of reducing airbag parameters such as deployment velocity and rise rate that will directly contribute to reducing airbag related injuries.

3.2 Introduction

Side-impact airbags (SABs) are used in lateral collisions to reduce occupant injuries from impacting vehicle interior by properly restraining the occupant. Unlike frontal airbags, side airbags are currently not mandated by the US standard [1]. However, the crashworthiness advantage of utilizing SABs has seen a rise in SABs installation as standard safety equipment in current passenger vehicles. Side-impact airbags are categorized into thorax or torso-only airbags, pelvis-torso (combo) airbags or separate head and torso airbags. Torso-only SABs are typically deployed from the seats that extend upward and outward to provide cushioning to the chest and pelvic area. Alternatively, the head and shoulder can be protected by utilizing curtain airbag [2].

In 2007, NHTSA estimated that side-impact airbags reduced fatality risks by at least 12% [2]. In lateral collisions, the occupant's chest and pelvic body regions are the most susceptible body parts to get injured. Side impact airbags can cause serious and fatal injuries on out-of-position (OOP) occupants. An occupant is categorized as an OOP occupant if the occupant is in the path of the deploying airbag prior to collision by seating, leaning or sleeping in close proximity to the airbag or that the occupant is displaced closer to the airbag by a pre-impact or at-impact event [3].

A study conducted by NHTSA estimated that chest and pelvic injuries accounts for 46% of fatalities and 66% of injuries in lateral collisions [4]. In another studies conducted by NHTSA, the SCI database shows that a total of 242 cases of fatalities involving airbag

deployment as of year 2003. Out of this 242 cases, 84 cases involved adult drivers and passengers and the remaining 158 cases involved children fatalities [3]. Hence, it is shown that airbags technology can be improved to further reduce injuries caused by airbags.

Federal Motor Vehicle Safety Standards (FMVSS) are safety regulations provided to govern the minimum standard requirements for all passenger vehicles. FMVSS No. 214 established standard testing configuration for side-impact protection. The setup involves positioning a FMVSS moving deformable barrier (MDB) velocity vectors at 27^0 relative to the vertical-axis and impacting the A-pillar of the vehicle at closing speed of 33.5mph. Table 3.1 summarizes FMVSS No. 214 test configurations.

Table 3.1. FMVSS 214 Test Configuration [5]

Impact Angle	27^0 crab angle	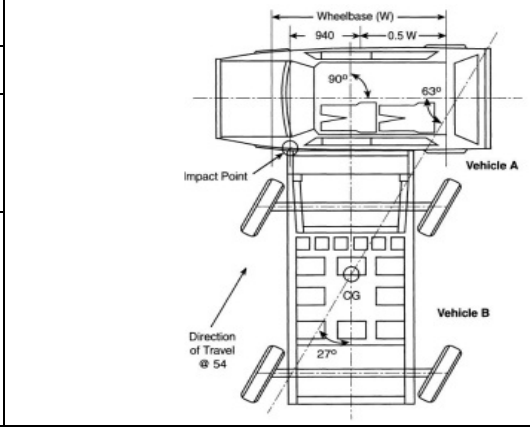
Impact Velocity	33.5mph	
Barrier	1369kg; 279mm above ground; 1676mm width	
MBD Velocity Vectors	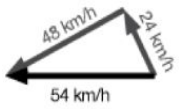	

In most cases, lateral collisions require higher sensitivity of mechanical or electronic crash sensors due to the limited crush zones compared to frontal collisions. A typical 30-40mph vehicle-to-vehicle frontal collision sensor triggering time is approximately 30 to 50ms [6,7]. Contrary, lateral crashes have only a third of airbag triggering time compared to frontal impact counterparts [7]. This means that at a typical 33.5mph lateral crash, regardless of the vehicle geometry and types of SABs used, the crush zones of the vehicle will most likely come in contact with the occupant before the full deployment of SAB.

Vehicle safety features are mainly categorized into active and passive safety that plays vital roles in compensating human reaction deficit. Passive safety includes features such as seatbelt pre-tensioning, emergency brake assistant and airbag pre-arming prior to

collision [8]. The study on the pre-deployment of SABs by utilizing pre-crash sensing concept falls under the passive safety category. The technology on pre-crash sensing is not new. For example, adaptive cruise control uses sensor to ensure proper distance between two vehicles and ultrasonic sensors are used as parking aid.

The pre-deployment of airbags is not possible by utilizing conventional mechanical and electronic crush sensors because physical contact between the vehicle and any incoming objects are required. Currently, researchers are beginning to harvest the benefit of pre-deploying of airbags by developing many mathematical algorithm and model for airbag deployment [9]. Some of the factors that govern the effectiveness of pre-crash sensors are sensor robustness, accurate object detection, and response time. Ultrasonic, radar and lidar sensors are the current sensors used by many for this type of applications. For example, BMW 5 series uses a combination of radar and ultrasonic sensor for application of HADAS [10]. The sensors architecture used for BMW HADAS application can also be made applicable for the pre-deployment of SAB by analyzing the surrounding environment in real time and decide whether to deploy the SAB should collision becomes inevitable. Lastly, quicker sensing time allows automotive manufacturers to tweak airbag characteristics such as reducing airbag deployment velocity, rise time, permeability and etc. to reduce injuries mitigated by airbag deployment.

The purpose of this study is to provide a fundamental numerical analysis of the benefit of pre-deploying an in-position SAB in reducing occupant injuries across a wide range of impact velocities. As such, this paper will not discuss the pre-crash sensing system but it is assumed that an ideal, robust and reliable pre-crash algorithm is used to correctly and accurately pre-deploy the SAB. The LS-Dyna finite element analysis (FEA) software was used exclusively to evaluate and compare occupants' dynamic and kinematic responses. A systematic approach to determine the advantage of pre-crash sensing concept is to measure,

analyze and compare injury criteria against each test conditions. The FEA simulations takes the form of 3 main test conditions, namely, FMVSS 214 standard test simulation, group test simulations with standard SAB at various MDB closing velocities and group test with pre-crash sensing in the pre-deployment of SAB at various MDB closing velocity. Ultimately, the effectiveness of utilizing pre-crash sensing in the pre-deployment SAB at low and high speed lateral collision shall be computed, analyzed and compared against test conditions without pre-crash sensing.

3.3 Computational FEA Methodology

The FEA has been utilized to analyze different test conditions. The software used to solve non-linear dynamic systems was LS-Dyna by Livermore Software Technology Corporation (LSTC). LSTC also provided FEA model of the US-SID computational Anthropomorphic Test Dummies (ATD) and the FMVSS 214 moveable deformable barrier [11]. The SAB is modeled and then augmented into the design. The SAB is of hybrid type airbag and is constrained to the seat to ensure proper constrains during simulation. A typical sedan car, namely Ford Taurus year model 1993, is obtained from National Crash Analysis Center (NCAC) [12]. The vehicle model used is a modified model (28,400 elements) instead of a detailed model (1,057,113 elements) to save computational time.

The US-SID is currently not regulated by FMVSS 214 due to its limitation in mechanical design. The existing US standard calls for the use of ES-2re 50^{th} Percentile ATD due to its enhanced bio-fidelity, reproducibility and durability compared to US-SID [13]. Some of the significant differences in the design of these two dummies are the present of two arms with ES-2re while the US-SID's arm is modeled with a reversible foam block [14]. Furthermore, the US-SID is designed with 5 ribs covered in solid viscous damping material that connects to a spring/damper system. Alternatively, ES-2re is designed with 3 ribs with 3

separate independent spring/damper systems. Hence, it allows ES-2re the ability to extract rib deformation at 3 points.

3.3.1 Vehicle model

As mentioned before, to save the computation time, the modified model of Ford Taurus is utilized in this study. To ensure acceptable agreement with the detailed model, a simple side impact simulation according to FMVSS 214 is performed and the results are compared with the detailed model of the same car in the same crash scenario, conducted by NCAC [15].

NCAC conducted the side-impact test with a MDB at an initial velocity of 38.2mph and crabbing at 27 degrees angle, approximately 5mph above the standard requirement of FMVSS 214. Hence, the MDB velocity has been altered in accordance to NCAC simulation to correctly validate the structure integrity of the modified model. Figure 1(a) shows the FMVSS 214 38.2mph side-impact. The post-crash deformation of the detailed model of Ford Taurus can be seen in Figure 3.1(b) while the modified model can be seen in Figure 3.1(c). It can be seen from Figure 3.1(c) that that the post-crash deformation and structure response of the modified model are in good agreement with the detailed model as seen in Figure 1(b). The lateral acceleration and velocity of the modified model rear seat right sill was obtained and compared against the detailed model and NHTSA Test 3263 [16].

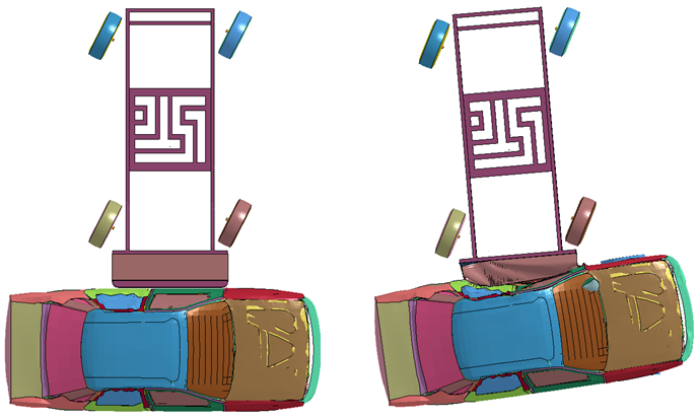

(a)

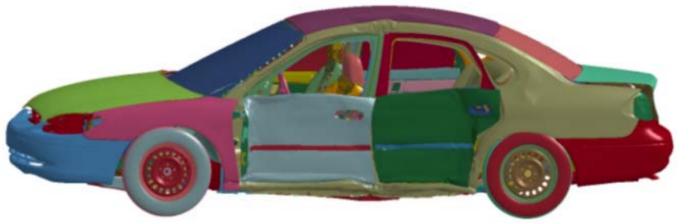

(b)

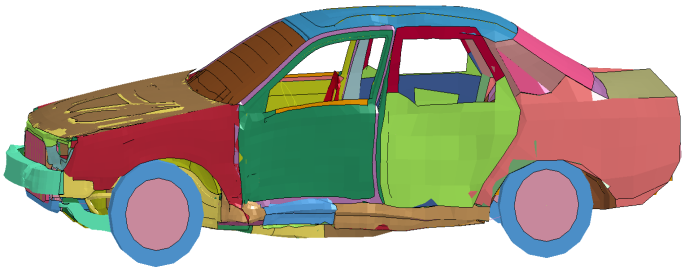

(c)

Figure 3.1 (a) Side-impact configurations for Ford Taurus FE model; (b) NCAC Ford Taurus post-crash deformation [15]; (c) Ford Taurus post-crash deformation from this study

Figures 3.2 and 3.3 represent the right sill, rear seat y-acceleration and y-velocity respectively. It can be seen that the velocity and acceleration of the right sill is in close proximity with the detailed FEA model and NHTSA Test 3263 test.

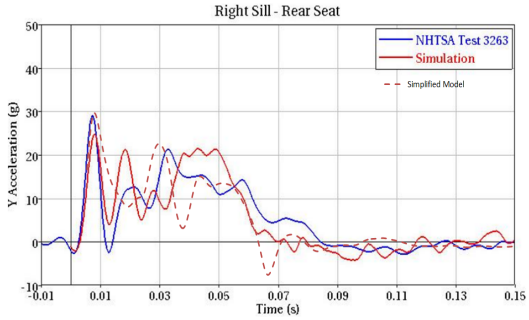

Figure 3.2: Right Sill – Rear Seat Y-Acceleration

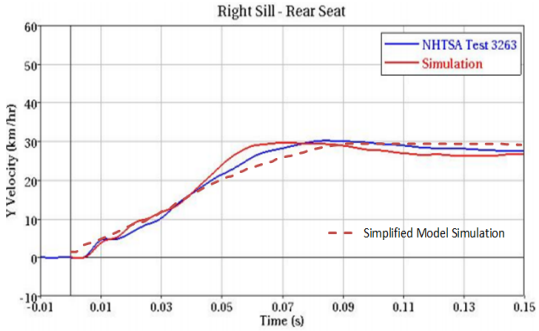

Figure 3.3: Right Sill - Rear Seat Y Velocity

It can be concluded that the modified model can be used with the same level of accuracy as the detailed model in this study.

3.3.2 Airbag and ATD models

Once good correlation between the modified and detailed model has been reached, an in-position side-impact airbag is modeled as shell and given fabric material property of *MAT_FABRIC (34) in LS-Dyna [17]. The airbag model is a single-chamber with one inflator type thorax-pelvic airbag. The airbag is assumed by a uniform pressure change which was represented by mass flow rate. A constant airbag load curve representing airbag mass flow rate, as shown in Figure 3.4, is applied to the airbag to ensure proper inflation. Airbag inflator gas temperature is held constant at 427^{o}C. Figure 3.5 shows the SAB reaching full inflation state at 20ms. The in-position of the SAB allows the ATD to be in full and optimal contact with the airbag. By incorporating an in-position airbag, other factors that are not of interest such as airbag unfolding can be eliminated.

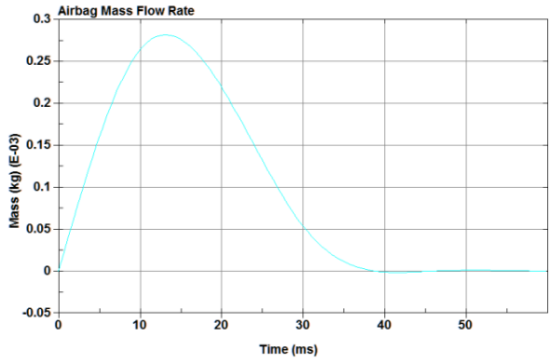

Figure 3.4: FEA Simulations Airbag Mass Flow Rate

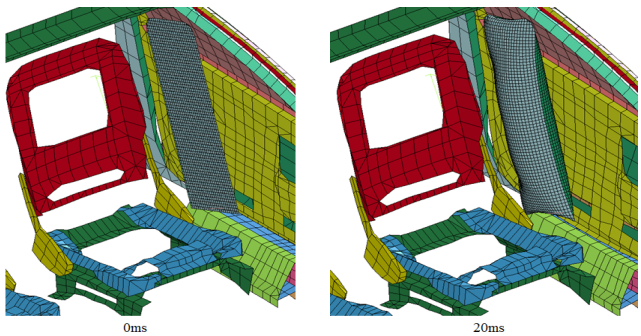

Figure 3.5: Single-Chamber SAB Inflation Process

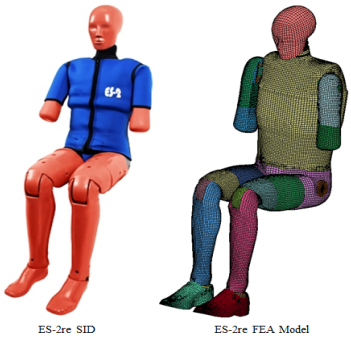

Figure 3.6: ES-2re Side Impact Dummy

Figure 3.6 shows the ES-2re ATD used for the simulation. The ATD was positioned to the seat and constrained to the driver seat once the airbag modeling is completed. The *CONTACT_SURFACE_TO_SURFACE card are primarily used for surface contact between the ATD and vehicle interior. Once satisfactory correlation is reached, trial FEA simulation runs are conducted to ensure proper contact between all parts.

3.4 Parametric Study with and without Pre-Deployment of SAB at Different Crash Speeds

Table 3.2 shows the outline for the test simulations matrix for three different test scenarios. The standard test is performed in accordance to standard set forth by FMVSS No. 214. The moving deformable barrier impact velocity is 33.5mph at crab angle 27^0. This test was used as a standard comparison for group test #1 and group test #2. Group test #1 consists of lateral collision FEA simulation with the sensor trigger time offset of 5ms after initial contact between the vehicle and MDB. Group test #2 is FEA simulations with airbag pre-deployment with similar test setup as group test #1. SABs deployment elapse time for both group tests was set at 20ms and shared similar mechanical and material properties. Group test #2 simulations were then directly compared against group test #1 for occupant injury ratings.

The total LS-Dyna simulation time is set at 120ms for simulation with airbag pre-deployment and 100ms for simulation without airbag pre-deployment. Additional 20ms

termination time for simulations with airbag pre-deployment was necessary to allow a fully inflated SAB prior to actual collision.

Table 3.2. LS-Dyna Test Simulations Run Matrix

FMVSS 214 Standard Test. Without SAB and without Pre-Deployment of SAB		
MDB Velocity: 33.5mph		
Group Test #1: Side-Impact Test. SAB Constrained to Seat without Pre-Deployment of SAB		
MDB Velocity	Airbag Initial Conditions	
	Triggering Time (ms)	Fully Inflated Elapse Time (ms)
33.5mph	5	15
40.0mph		
45.0mph		
50.0mph		
Group Test #2: Side-Impact Test. SAB Constrained to Seat with Pre-Deployment of SAB		
MDB Velocity	Airbag latest pre-deployment time based on proximity of the MDB relative to A-pillar	
33.5mph	x-position (mm)	y-position (mm)
40.0mph	101.98	200.15
45.0mph	121.77	268.86
50.0mph	152.21	298.74

3.5 Evaluation of Proximity Sensor for LS-DYNA Simulation

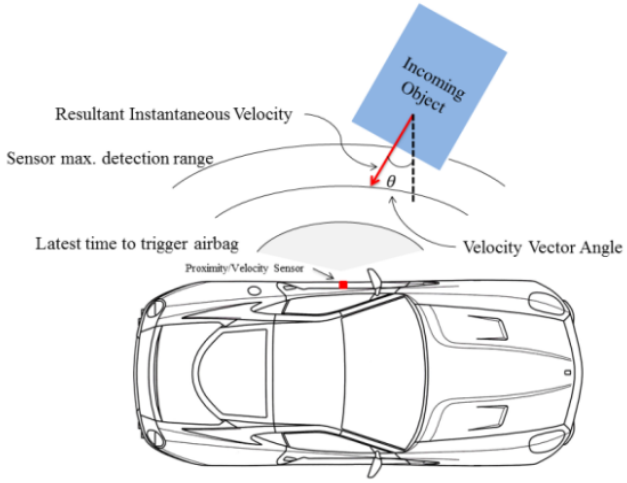

Figure 3.7: Illustration of Pre-Crash Sensor Concept

Figure 3.7 illustrates the graphical concept developed for the purpose of this paper. In an ideal situation, the proximity based pre-crash sensor evaluates the instantaneous position and velocity of the MDB and decides the latest sensor triggering threshold. The latest triggering time is tabulated in Table 3.2, Group test #2. The distance of MDB relative to

vehicle A-pillar at which the sensor must initiate the inflation of the airbag can be calculated using simple trigonometry formula as shown in Equation (3.1).

$$\begin{bmatrix} x \\ y \end{bmatrix} = \begin{bmatrix} V_{resultant} \cos(\theta)\, t \\ (V_{resultant} \sin(\theta)\, t \end{bmatrix} \tag{3.1}$$

where, $V_{resultant}$ is the MDB resultant velocity; θ is the angle of the MDB velocity vector; t is the total airbag inflation period.

For conceptual purposes, there are simply too many variables involved to realize this concept without holding some variables constant. The airbag fully inflated elapse time was held constant at 15ms. Besides that, a typical sensor triggering time of 5ms was also held constant. Hence, the total elapse time for fully inflated SAB was set constant at 20ms. It simply means regardless of the proximity, velocity or acceleration of an incoming object, the total integration of the entire system must take place 20ms prior to actual collision between vehicle and MDB.

Figure 3.8 represents the vehicle A-pillar, MDB and SABs volume curve for the group test #2 33.5mph FEA simulation. The initial impact was at 18ms as shown in curve B which is the resultant displacement of A-pillar. The airbag was ignited at time 0ms and reached designated peak volume denoted by curve C by time 20ms.

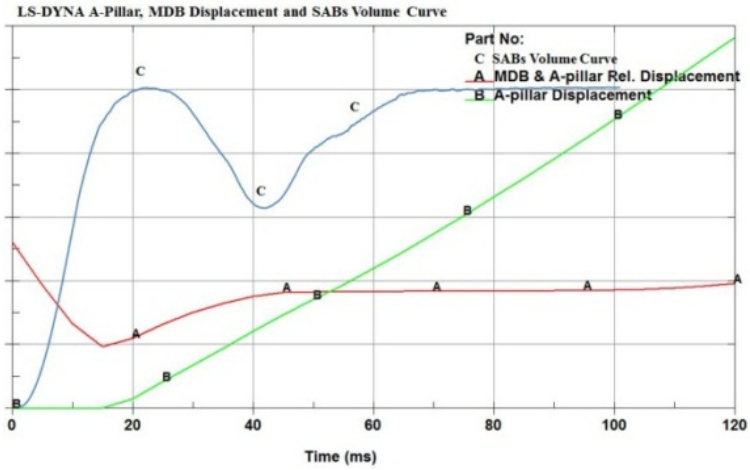

Figure 3.8: MDB and A-pillar Displacement at 33.5 MDB Velocity

3.6 Injury Criteria

The injury criterion of this study was categorized into 2 body regions, namely, thorax and pelvis. Neck injuries were omitted due to the limitations of ES-2re in measuring neck injuries. Pelvis injury limit of 130G's in lateral acceleration is based on Haffner's cadaver test results. [18] The thoracic trauma index (TTI) is an important injury measurement in lateral collisions. US regulations of SID TTI(d) is based on the mean of the upper rib and lower rib lateral acceleration in G's. It is governed by Equation (3.2).

$$TTI(d) = \frac{1}{2}[G_R + G_{LS}] \tag{3.2}$$

The standard limit for TTI(d) is 85G's for 2-door sedans and 90G's for 4-door sedans. Viscous Criteria (VC) is the product of instantaneous chest velocity, V(t) and instantaneous chest compression ratio, C(t). [19] VC is currently not validated by US standards due to current limitation in measuring devices. However, VC can be computed for research purposes in comparing FEA crash simulations [20]. Lastly, the US standard limits HIC at 1000, 36ms window, based on Mertz analysis of cadaver test data [21].

Table 3.3: FMVSS No. 214 Standard Injury Criteria

Requirement	**FMVSS 214 Old Regulation**	**FMVSS 214 New Regulation**
ATD	US-SID	Front Seat: ES-2re Back Seat: SID IIs
Protection Criteria	Chest TTI < 85G's (4-doors) Chest TTI < 90G's (2-doors) Pelvic Acceleration < 130 G's	Sid II: HIC36<1000 Chest Acceleration<82G's Pelvic Force<5.525kN ES-2re: HIC36<1000 Chest Deflection<44mm Abdominal force<2.5kN Pelvic force<6kN

Table 3.4: ES-2re Injury Criteria

Injury Criteria	Threshold Limit
Thoracic Trauma Index (TTI)	<90G's for 4 doors
Viscous Criteria (VC)	<1.0
Pelvis Force	<6kN
Pelvis Acceleration	<130G's

The old and current FMVSS 214 injury criterion can be referred from Table 3.3. Thoracic and pelvis injury rating were given higher consideration due to the involvement of these body regions in primary impact with the vehicle interior. The HIC value will not be included in this study due to the absent of curtain airbag. Although pelvic acceleration and viscous criterion is no longer mandated in the current FMVSS 214 regulations, these injury values can provide useful information for future research. Table 3.4 summarizes the injury criterion of interest for this study.

3.7 Results and Discussions

This section discusses the results from the FEA simulations. The results take the form of sample LS-DYNA screenshots of different tests conditions, tabulation of the results and graphical comparisons of the injury ratings. Figures 3.9 to 3.11 are sample FEA simulation figures for 3 test conditions, namely FMVSS 214 standard test, group test #1 and group test #2. FMVSS 214 33.5mph standard test at different time can be seen from Figure 3.9. Similarly, FEA simulations with SABs and without pre-crash sensing at 40mph MDB closing velocity, denoted as group test #1, are shown in Figure 3.10. Lastly, Figure 3.11 is the FEA simulations with SABs and pre-crash sensing at 40mph MDB closing velocity, denoted as group test #2. It is important to note that in group test #3, the initial impact between the MDB and vehicle is offset at 20ms to allow sufficient time for the pre-deployment of SAB.

Figures 3.9 represent the standard FMVSS 214 test without SABs. This test serves as a benchmark and foundation in emphasizing the effect of SAB in reducing injury criteria rating. It is shown at 40ms that the vehicle side interior comes in contact with the chest and pelvis area. It can also be seen that the head experienced secondary impact on the vehicle

window at a much later time at 70ms. This FEA simulation represents the response of an occupant without side-impact protection.

Figures 3.10 represents sample FEA simulations for the 50mph MDB side-impact test from group test #1. As shown in these figures, SAB provided sufficient cushioning to the dummy from primary impact to the chest and pelvis compared to the simulation without side-impact protection. However, the simulation at 40ms highlights the inability of the SAB to reach optimal surface area before reaching the dummy. It simply means that the clearance distance between the dummy and the vehicle side frame is reduced significantly as observed at 50ms. In addition, it can be seen that the airbag is crushed between the dummy and the vehicle side frame at 50ms.

Similarly, the 50mph MDB sample FEA simulation from group test #2 can be seen in Figure 3.11. This test calls for the repositioning of the MDB to allow the pre-deployment of SAB as shown at 0ms. The dummy is observed to be better cushioned at 40ms compared to FEA simulation without pre-crash sensing. At 50ms, the clearance distance between the vehicle side frame and the ATD can be seen to be clearly higher compared to simulation without pre-deploying the SAB. Besides that, the kinematics show that the neck rotation is lesser compared to group test #1. These FEA sample simulations indicated reasonable improvement in utilizing pre-crash sensing in pre-deployment of SAB by allowing sufficient time to fully deploy SAB in higher velocity side-impact crashes.

Table 3.5 shows the summary for all 15 FEA simulations. The injury limit is at the top row of the table for ease of comparison between injury limits and results from FEA simulations. Figures 3.12 to 3.18 represent the graphical comparisons for group test #1 and group test #2.

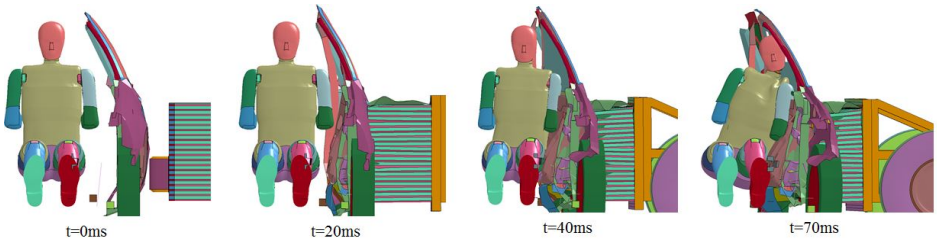

Figure 3.9: ATD Kinematics *without* SAB and *without* Pre-Deployment of SAB for FMVSS 214 Test Benchmark

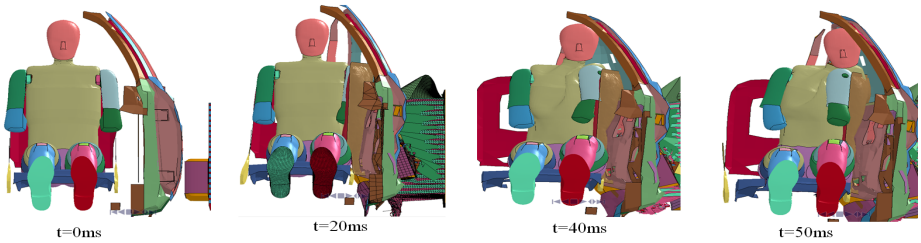

Figure 3.10: ATD Kinematics *without* Pre-Deployment of SAB at 50mph FMVSS 214 Test

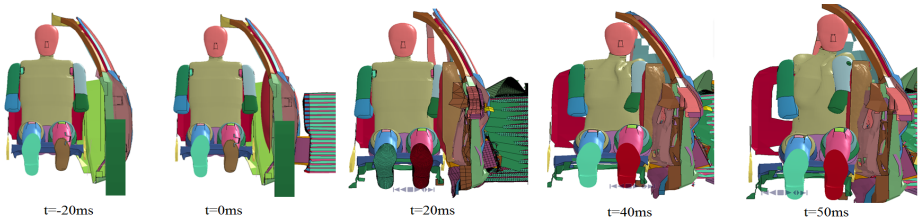

Figure 3.11: ATD Kinematics *with* Pre-Deployment of SAB at 50mph FMVSS 214 Test

Table 3.5: Tabulation of LS-Dyna Simulation Results on All Tests Conditions

Injury Limit				***43mm***			***6kN***	***130G's***	***85G's***	***1.0***
Sim. #	**DMB Velocity (mph)**	**SAB**	**SAB Pre-Deployment**	**Max Up. Rib Deflection (mm)**	**Max. Mid Rib Deflection (mm)**	**Max. Low. Rib Deflection (mm)**	**Max. Pelvic Force (kN)**	**Max. Pelvic Accel. (G's)**	**Max. TTI (G's)**	**Max. V*C**
FMVSS 214 Test Benchmark. *Without* SAB and *without* Pre-Deployment of SAB										
1	33.5	No	No	43	36	20	2.33	54	70	0.78
Group Test #1: Side-Impact Test. SAB Constrained to Seat *without* Pre-Deployment of SAB										
2	33.5	Yes	No	40	33	24	2.07	37.8	72	0.52
3	40	Yes	No	46	38	28	3.23	54.5	84	0.59
4	45	Yes	No	48	47	34	4.02	65.8	110	0.63
5	50	Yes	No	50	48	48	4.39	98.0	133	0.71
Group Test #2: Side-Impact Test. SAB Constrained to Seat *with* Pre-Deployment of SAB										
6	33.5	Yes	Yes	36	30	20	2.11	34.5	61	0.44
7	40	Yes	Yes	42	36	27	2.78	35.9	79	0.46
8	45	Yes	Yes	44	42	31	3.21	50.8	87	0.54
9	50	Yes	Yes	48	44	45	3.27	69.7	109	0.68

The cells shaded in red as shown in Table 3.5 represent the injury values that were above the injury threshold. At 40mph crash, it can be seen that the occupant injury ratings

were below the threshold limit with the pre-deployment of SAB while the occupant's upper rib cannot be safely protected without the pre-deployment of SAB. Similarly, at higher impact velocities of 45mph crash, the occupant injury rating for the upper, middle rib and the TTI(d) were significantly above the proposed threshold limit without pre-deploying the SAB. While the occupant upper rib and TTI(d) values were also above the limit with the pre-deployment of SAB, it can be seen that the values were much lower and closer to the proposed limit. Hence, based on the injury criteria of the occupant, the occupant injuries were significantly reduced at higher side-impact crashes.

Figures 3.12 to 3.14 represents the ATD upper, middle and lower rib deflection. The limit of the maximum rib deformation is 44mm. It can be seen that the upper, middle and lower rib deflections with the pre-deployment of airbag, denoted as group test 2, were constantly below that of group test 1. It is shown that without the pre-deployment of SAB, the upper rib deforms above the limit at 40mph. With the pre-deployment of SAB, the upper rib only deforms above the limit at 50mph. The analysis also shows that group test 1 deforms above the limit at 45mph while the group test 2 is in close proximity and within the limit at 50mph. At 50mph, the lower rib for both group tests failed to deform within the limit.

Figures 3.15 and 3.16 represents the pelvic force and acceleration. It can be seen that both group test results were constantly below the respective limit of 6kN and 130G's. The pelvic force and acceleration on both cases was found to be quite similar at impact speed at 33.5mph. However, the injury ratings on both cases were significantly reduced with increasing impact speed.

Figure 3.17 shows the TTI(d) comparisons for both group tests. Similarly, it can be seen that with the pre-deployment of SAB, the TTI(d) for group test 2 was constantly below that of group test 1. At 45mph, it can be seen that TTI(d) for group test 1 was much higher compared to group test 2 at velocities above 40mph. At 50mph, both group tests were above

the threshold. The viscous criteria comparison can be referred from Figure 3.18. It can be seen that both group test was below the VC limit of 1.0.

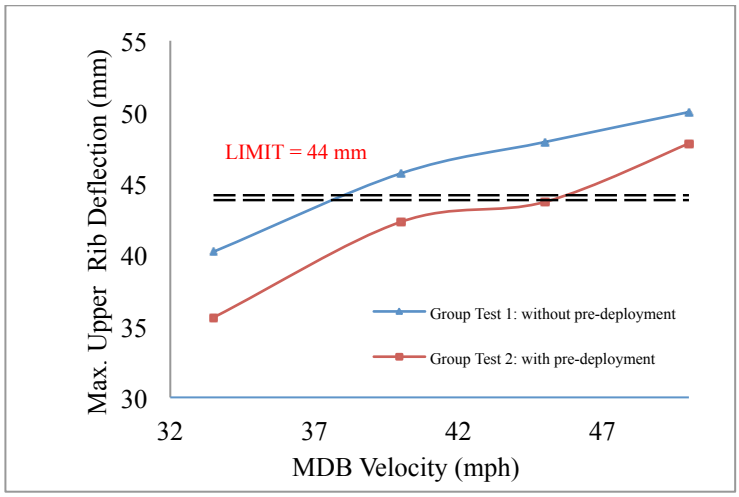

Figure 3.12: Max. Upper Rib Deflection Comparison of Group Test #1 and Group Test #2

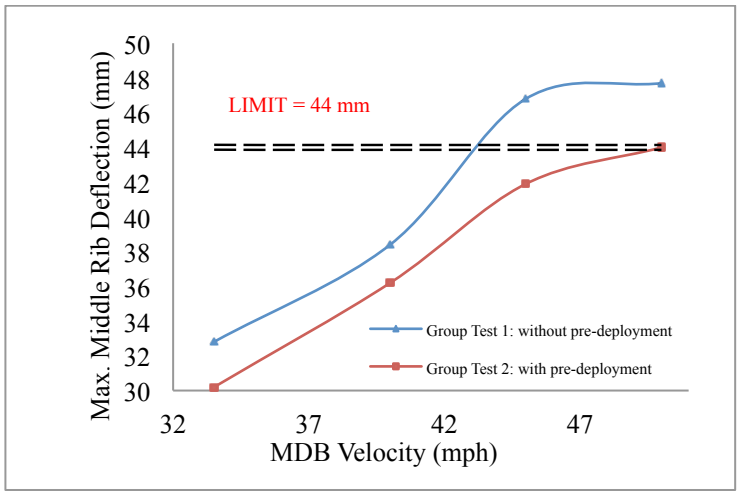

Figure 3.13: Max. Middle Rib Deflection Comparison of Group Test #1 and Group Test #2

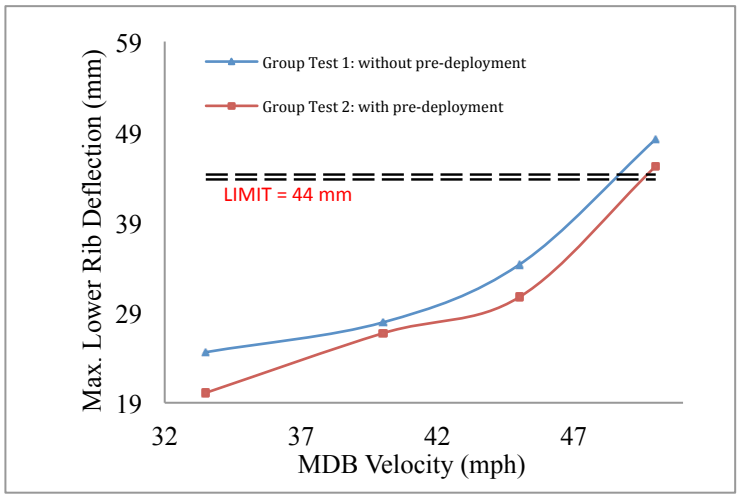

Figure 3.14: Max. Lower Rib Deflection Comparison of Group Test #1 and Group Test #2

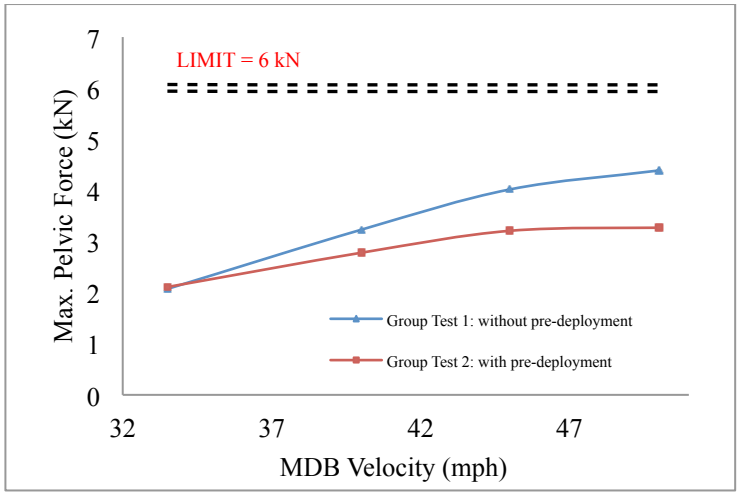

Figure 3.15: Max. Pelvic Force Comparison of Group Test #1 and Group Test #2

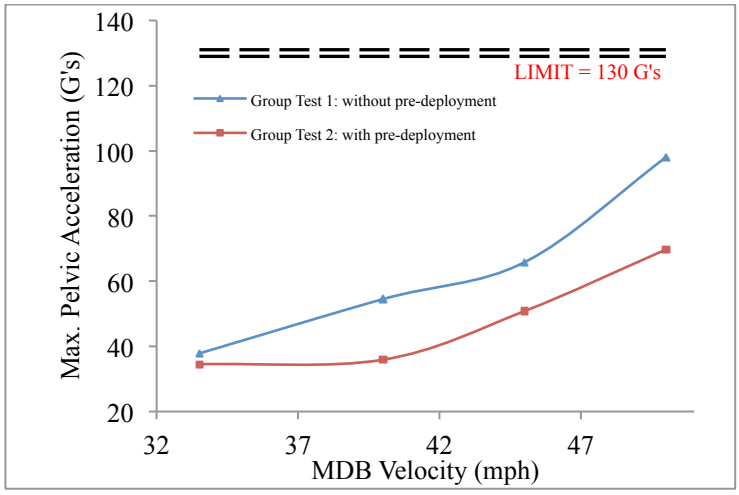

Figure 3.16: Max. Pelvic Acceleration Comparison of Group Test #1 and Group Test #2

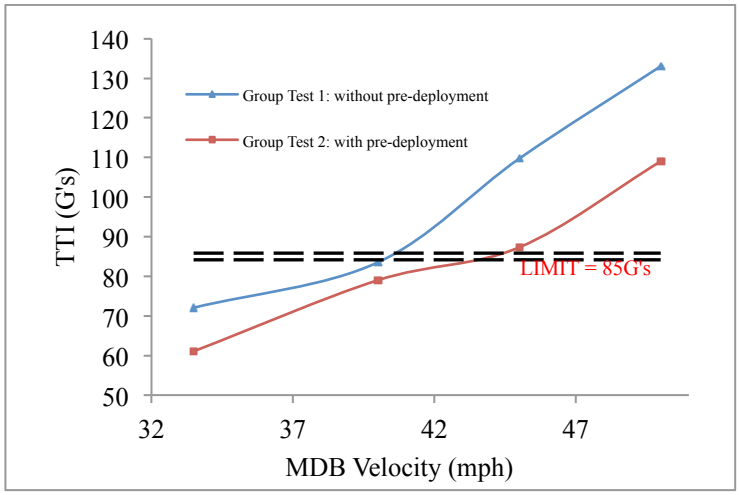

Figure 3.17: TTI(d) Comparison of Group Test #1 and Group Test #2

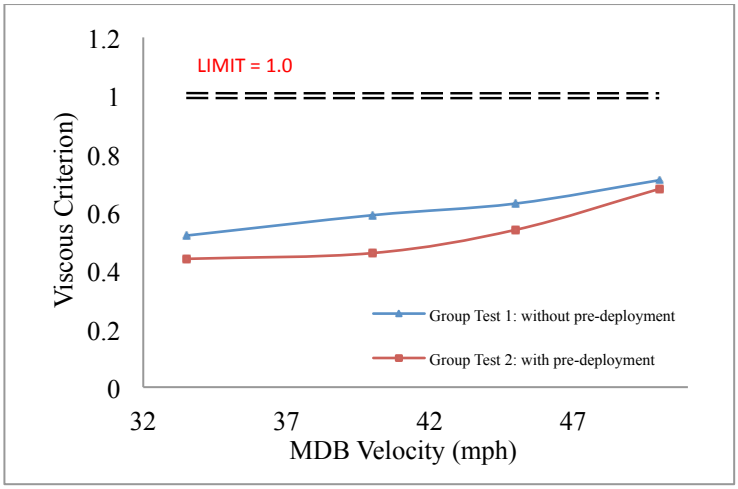

Figure 3.18: Viscous Criteria Comparison of Group Test #1 and Group Test

3.8 Conclusions

The main objective of this paper was to provide a simplified computational methodology of the side impact scenario with the pre-deployment algorithm of the SAB based on an ideal proximity and velocity sensing system to show the benefits of such systems in reducing occupant injury. The concept of pre-crash sensing algorithm was not discussed in this paper. However, it was assumed that reliable and accurate sensor system was used to always pre-deploy the SAB 20ms prior to actual side impact. The methodology was proven with the aid of LS-Dyna FEA simulation software. These simulations setup were conducted in accordance to FMVSS 214 standards except for the closing speed of the MDB which were increased gradually from 33.5mph to 50mph.

The vehicle model was augmented with a single chamber thorax-pelvic airbag. The ES-2re ATD developed by LSTC was then included into the model.

The post-crash results was analyzed in terms of injury criteria such as TTI(d), the upper, middle and lower rib deformations, VC and pelvic force and acceleration. However, the injury to the head or HIC values was not necessary in this study due to the lack of curtain airbags. The effect of pre-deploying the SAB prior to impact showed a significant and constant reduction of injury across all impact velocities as discussed in Section 3.

Most importantly, all injury ratings show significant reduction in occupant injuries at higher speed impact crashes. This study showed that occupant can benefit significantly from pre-deploying the SAB prior to actual collision.

Overall, it can be concluded that pre-deployment of SAB benefit occupant safety by reducing injury especially in the thorax and pelvic body regions. More research needs to be done to determine the effect of the modifying the SAB parameters and characteristics on affecting occupant safety.

3.9 References

[1] Anonymous, 2012, "Status Report, Family Cars," Vol. 47, No. 10, Insurance Institute for Highway Safety, Highway Loss Data Institute, pp. 7.

[2] Kahane, C. J., 2007, "AN EVALUATION OF SIDE IMPACT PROTECTION FMVSS 214 TTI(d) Improvements and Side Airbags," NHTSA Technical Report, DOT HS 810 748, Department of Transportation NHTSA, Washington, DC.

[3] Kindelberger, J., Chidester, A., Ferguson, E, "Air Bag Crash Investigations," NHTSA Paper No. 299.

[4] Watson, B., Cronin, D., and Campbell, B., 2009, "Study of Vehicle Dynamics and Occupant Response in Side Impact Crash Tests," NHTSA No. 09-0016.

[5] Title 49 Code of Federal Regulations (CFR), 49 CFR 572, 2011, Ch. V.

[6] Pack, R., Koopmann, J., Yu, H., and Najm, W.G., 2005, "Pre-Crash Sensing Countermeasures and Benefits," NHTSA No. 05-0202.

[7] Chan, C.Y., 2000, "Fundamentals of Crash Sensing in Automotive Air Bag Systems," SAE International.

[8] Hinch, J. and et al., 2001, "Air Bag Technology In Light Passenger Vehicles", Office of Research and Development, National Highway Traffic Safety Administration, Revision 2.

[9] Cho, K., Choi, S., Wee, S., Shin, K., 2010, "Design of an Airbag Deployment Algorithm Using a Radar Sensor,"

[10] Aeberhard, M. and Kaempchen, N., "High-Level Sensor Data Fusion Architecture for Vehicle Surround Environment Perception," BMW Group Research and Technology

[11] LS-DYNA. 2013, Livermore Software Technology Corporation. http://lstc.com

[12] NCAC. 2013, National Crash Analysis Center. http://ncac.gwu.edu

[13] Federal Register, 2006, "Anthropomorphic Test Devices; ES-2re Side Impact Crash Test Dummy (ES-2 With Rib Extensions); 50th Percentile Adult Male," 49 CFR Part 572, Vol. 71, No. 240.

[14] Schuster, P., et al., 2004, "Considerations for ES-2re Model in FMVSS Tests." LS-DYNA Forum 2004 Proceedings, DYNAmore GmbH.

[15] Marzougui, D., Samaha, R., Cui, C., Kan, C., 2012, "Extended Validation of the Finite Element Model for the Ford Taurus Passenger Sedan," NCAC 2012-W-004

[16] Strassburg, G. 2000, "New Car Assessment Program Side Impact Test," U.S. Department of Transportation National Highway Traffic Safety Administration, NHTSA No: MY0211

[17] *LS-DYNA Keyword User's Manual, Volume II Material Models*, 2012, Version 971. Livermore Software Technology Corporation.

[18] Haffner, J. H., Marcus, J. H., and Eppinger, R. H., 1985, *Synthesis of Pelvic Fracture Criteria for Lateral Impact Loading*, Enhanced Safety Vehicles, 10th ESV Conference.

[19] Lau, I.V., and Viano D.C., 1986, "The Viscous Criterion - Bases and Applications of an Injury Severity Index for Soft Tissues," SAE Technical Paper 861882, doi: 10.4271/861882.

[20] Digges, K. H., 1998, "Injury Measurements and Criteria," Proceedings of 1998 AGARD Conference on Biomechanics, Dayton.

[21] Mertz, H., Prasad, and P., Nusholtz, G., 1996, "Head Injury Risk Assessment for Forehead Impacts," SAE Technical Paper No. 960099, doi:10.4271/960099.

CHAPTER FOUR

A DOE METHOD IN PREDICTING INJURIES TO OUT-OF-POSITION OCCUPANTS FROM TORSO-ONLY SIDE-IMPACT AIRBAGS

4.1 Abstract

Airbag systems such as frontal and side-impact airbags are developed to reduce occupant injuries during vehicle collisions. Yet, such systems have caused serious injuries to out-of-position occupants especially to smaller females and children. The primary objective of this study is to examine the different influential factors such as mass flow rate, fabric permeability ratio, fabric maximum inflated depth that contribute to OOP occupant injuries in airbag-related accidents. A mathematical model of Heidelberg stationary test, vehicle interior and seat mounted side-airbag is developed using the MADYMO code 7.4.2. The mathematical model of the airbag used in this study is a torso-only seat-mounted side-impact airbag (SAB). The airbag model is validated against similar study conducted by Hallman et al. and the results are found to be in good agreement. Once the airbag model is validated, the airbag and the anthropomorphic test dummy are positioned in a vehicle environment to better predict the occupant injuries in a static environment. The ATD test configurations are performed in accordance to the recommendations by The Side Airbag Out-Of-Position Injury Technical Working Group. Lastly, a set of parametric equations to predict the OOP occupants' injuries are developed using the full factorial design.

4.2 Introduction

The safety of road vehicle has improved remarkably in recent years. A study conducted by the National Highway Traffic Safety Administration (NHTSA) shows that in year 2009, the fatality rate has been reduced to 1.14 people per 100 million vehicle miles travel as opposed to 1.55 fatalities 10 years ago [1]. Even with this promising result, the

[1] This entire chapter has been published in the following source:

- **Yi Yang Tay**, Rasoul Moradi, Hamid M. Lankarani, "A DoE Method in Predicting Injuries to Out-of-Position Occupants from Torso-only Side-Impact Airbags," *Global Journal of Researches in Engineering (B),* Vol. 13, Issue 2, Ver. 1, 2013, pp. 1 – 14.

ultimate common goal in the automotive industry and government regulations is to reduce occupant injuries and fatalities to nearly zero in all crash scenarios. The vastly improved occupant safety rating cannot be made possible without the technology enhancement in vehicle safety. One of the widely used safety features which have shown to have the highest effect in reducing occupant injuries in recent vehicles are the frontal and side-impact airbags. A study published in 2007 by NHTSA shows that torso only side-airbag reduced fatality by approximately 17% compared to vehicle without side airbags, while the combination of torso and head side airbag further reduce fatality by approximately 35% [2]. Hence, it is evident that airbags provide tremendous amount of occupant safety in vehicle side collisions.

The increasing utilization of airbags on vehicles has also seen a rise in injuries caused by deploying airbags on out-of-position (OOP) and in-position occupants. The earliest recorded airbag related injuries dated back to early 1990, some of the most common injuries or fatalities caused by airbag are rib fractures, fractured sternum, head injuries, minor bruises, abrasions to the upper limbs and face and eyes injuries from chemical keratitis [3, 4]. OOP occupants are considered more prone to injuries from deploying airbags compared to in-position occupants due to the fact OOP occupants can be exposed to significant amount of force imposed by a deploying airbag. An occupant is considered as an OOP occupant if the occupant is in the path of a deploying airbag by either leaning or seating too close to the side structure or front panel that houses the airbag mechanism. If the occupant is initially positioned correctly but displaced closer to the airbag during the course of a collision, the occupant is also considered as an OOP occupant [5].

In 2003, NHTSA's Special Crash Investigation (SCI) conducted a study on 242 cases of airbag related injuries; it was shown that out of the 242 cases considered, 227 occupants were fatally injured by airbags. Besides that, out of the 242 cases, approximately 60% comprised of children fatalities [5]. Although NHTSA has amended its regulations to allow

automotive makers to reduce airbag deploying force in 1997, the study conducted by NHTSA's SCI showed that children are more vulnerable to airbag related injuries and fatalities. In 2002, NHTSA Transportation Research Center conducted a set of experiments on airbag aggressivity using static side impact seat-mounted and door mounted airbags on 3 year-old, 6 year-old and 12 month CRABI dummy using a fleet of model years 1999 to 2001 sedan cars. It was observed from the test results that 80% of the seat mounted and all door-mounted airbag for 3-year old dummy exceeded the injury reference values (IARV) [6]. For the 6 year-old dummy, 60% of all seat mounted and door mounted airbags conducted exceeded the IARV. This shows that advance airbags installed in recent vehicles can still, albeit lower risks, cause serious injuries to OOP occupants.

In order to successfully minimize the injuries mitigated by deploying airbag on various occupants on future vehicles, a systematic and wide used experimental procedure has been developed by *The Side Airbag Out-Of-Position Injury Technical Working Group* (TWG) to evaluate airbag aggressivity [7]. The purpose of TWG is to recommend a standard procedure and injury assessment for testing the aggressivity of deploying airbag on various test configurations and occupants. Therefore, the TWG recommendations and test configurations are used as a guideline in this study.

The main objective of this paper is to present a set of prediction model in predicting injuries to OOP occupants from a deploying airbag. The multi-body dynamic software, MADYMO 7.4.2 is used exclusively to evaluate the occupant's injury response and the Design-of-Experiment's (DoE) full factorial design is used to develop the injury prediction model. To achieve this objective, three main influential parameters or factors on affecting OOP occupant injuries have been identified and categorized into factorial design's high and low levels. Next, three OOP test configurations which comprised of TWG's testing configurations for the Hybrid III 3-year old, Hybrid III 6-year old and SID IIs are selected.

Finally, a set of prediction equations for each OOP test configurations is obtained using the DoE regression model to represent the occupant injury level. This computational and DoE study can provide future researcher with a new dimension in designing and analyzing newer airbags by providing a platform for estimating the injury response of OOP occupants from future airbags design.

4.3 Mathematical Evaluation of Airbag Model

The mathematical approach used in determining the governing factors that define the characteristics of the airbag model is presented in this section. In the design of airbag system, the occupant injury is significantly affected by many governing factors. As such, it is important to develop the airbag model based on accurate mathematical model that represents the dynamics of the airbag.

The airbag chamber(s) temperature, T can be formulated based on the constant pressure heat capacity, c_p parameter. According to the entropy of gases, for monatomic gases such as Helium (He) and Argon (Ar), the c_p is nearly equal to $\frac{5}{2}R$ while the c_p for diatomic gases such as Hydrogen (H_2) and Oxygen (O_2) is equals to $\frac{7}{2}R$ [8]. R is the universal gas constant or 8.3145 $Jk^{-1}mol^{-1}$. The National Institute of Standards and Technology (NIST) model and Poling model can be used to formulate the temperature dependency on the c_p. The NIST model is recommended for gases with relatively high temperatures, while the Poling model is applicable to low temperature gases [9]. Both NIST and Poling equation is described as Equation (4.1) and Equation (4.2) respectively:

$$c_p = a_0 + a_1T + a_2T^2 + a_3T^3 + \frac{1}{T^2}a_4 \tag{4.1}$$

$$c_p = b_0 + b_1T + b_2T^2 + b_3T^3 + b_4T^4 \tag{4.2}$$

where the T for both model is the absolute temperature of the gases, and the a_0 - a_4 and b_0 - b_4 is the heat capacity coefficients for the NIST and Poling model respectively. Both models

can only be used to accurately represent the c_p if the inflated gas consists of only one type gas. In order to properly predict the c_p of a mixture of gas, the Amagat's law of the partial volumes can be used to describe the $c_{p,mixture}$ and the NIST model can be further modified to Equation (3):

$$c_{p,mixture} = \sum a_0 x_i + T \sum a_{1_i} x_i + T^2 \sum a_{2_i} x_i + T^3 \sum a_{3_i} x_i + T^4 \sum a_{4_i} x_i \quad (4.3)$$

The relationship between the constant volume heat capacity, c_v and c_p is $R = c_v - c_p$. Similarly, the ratio of heat capacity is governed by $k = \frac{c_p}{c_v}$. Hence, the c_v can be calculated by knowing the value of c_p. Also, the temperature in the chamber can be formulated by solving the quartic equation, Equation (4.3).

The airbag can be considered as a closed system in which the bag is inflated by a uniform internal pressure. Once the temperature of the chamber is determined from Equation (4.3), the internal pressure acting on the membrane of the airbag can be formulated using the ideal gas law:

$$p = \frac{nRT}{\forall} \quad (4.4)$$

where n is the amount of moles; p is the airbag internal pressure; and $\forall$ is the airbag instantaneous volume. The ideal gas law can also be represented based on mass:

$$p = \frac{m\underline{R}T}{\forall} \quad (4.5)$$

with $\underline{R} = \frac{R}{MW}$; MW is the molar weight of the gases.

The airbag inflation process can be modeled as the instantaneous gas mass available in the airbag system. The available mass is influenced by the mass flow rate injected to the system by the inflator minus the gas flowing out of the airbag system through holes and permeable surfaces. Hence, the gas mass of the system can be formulated as:

$$\dot{m} = \dot{m}_{in,flow} - \dot{m}_{out,flow} \quad (4.6)$$

The $\dot{m}_{out,flow}$ can be calculated in terms of fabric permeability as shown in Equation (4.7):

$$\dot{m}_{out,flow} = A_{pores}\sqrt{2\rho\Delta p} \tag{4.7}$$

where ρ is gas density in the airbag chamber, Δp is the pressure difference between the airbag chamber and the ambient environment and A_{pores} is the total area of pores.

The A_{pores} can be formulated by multiplying the free area coefficient and the total airbag area, A_{total} :

$$\eta = \frac{A_{pores}}{A_{total}} \tag{4.8}$$

and, the Δp can be calculated as shown in Equation (4.9):

$$\Delta p = \frac{1}{2(\eta^2)}\,\rho v^2 \tag{4.9}$$

In order to accurately estimate the mass flow rate supply into the airbag chamber, the gas jet model must be calculated. By considering the inlet flow to be adiabatic flow, the inlet velocity can be calculated as:

$$v_0 = \sqrt{c_p(T_{exit})(k-1)} \tag{4.10}$$

where, c_p is the constant pressure heat capacity, T_{exit} is the constant temperature of the exit gas and k is the heat capacity ratio. The estimated mass flow rate supply to the gas chamber can then be formulated as:

$$\dot{m}_{in,flow} = A_i v_0 \rho_0 \tag{4.11}$$

where, the area of the inlet jet is represented as A_i and the gas density in the inlet represented by ρ_0. By combining Equations (4.6), (4.10) and (4.11), the mass flow rate in the system is formulated as:

$$\dot{m} = A_i\rho_0\sqrt{c_p(T_{exit})(k-1)} - A_{pores}\sqrt{2\rho.\Delta p} \tag{4.12}$$

It is known that the ambient pressure is 101.3kPa, Equation (4.12) can then be further expanded by combining Equations (4.5) and (4.12) as:

$$\dot{m} = A_i\rho_0\sqrt{c_p(T_{exit})(k-1)} - A_{pores}\sqrt{2\rho.(\frac{m\bar{R}T}{V} - 101.3)} \tag{4.13}$$

The preceding formulations can be used to accurately represent the airbag model. It can be seen that these equations must be solve simultaneously and no factors can be used to independently define the airbag mathematical model.

4.4 Computational Methodology

This study is conducted using multi-body software, MADYMO 7.4.2 and the results is analyzed using Design-of-Experiment software, Design Expert 7. To achieve the objective of developing a prediction model, this study consists of two parts. First, the testing scenario consisting of a Heidelberg stationary test is presented. The ATD used for the Heidelberg stationary test is a MADYMO 50^{th} percentile facet dummy model. The purpose of the Heidelberg stationary simulation is to validate the airbag model against the simulations by Hallman et al. [10] and to provide a foundation to test the linearity of the selected factors on occupants' injuries. The linearity of the factors will then be used to provide high and low values for the DoE factorial test. The Heidelberg test is extremely useful in providing high/low values for the DoE factorial design, because it isolates the effect of each factor on occupant injuries. The DoE test methodology is further explained later.

Second, due to the inability of the Heidelberg test to properly predict occupant injury in a vehicle environment, a Ford Taurus interior is modeled to represent a generic vehicle environment. By utilizing a vehicle environment in the static airbag test, occupant injuries can be better predicted by factoring in the effect of the airbag, vehicle geometry and placement of the ATD. As mentioned in the introduction section, The Side Airbag Out-of-Position Injury Technical Working Group suggested a list of recommended OOP test configurations for evaluating ATD's injuries from deploying side airbags as well as the optimal placement of ATD with respect to the vehicle geometry. The vehicle test procedures used in this study are in accordance with the TWG's test sections, namely, TWG's section 3.3.3.2, TWG's section 3.3.3.5 and TWG's sections 3.3.3.6 [7]. The test procedures are

carefully selected to represent a wide variety of occupants in terms of age, size and position. Figure 4.1 represents the selected TWG test procedures and Figure 4.1(a) – (c) are the graphical representation of the TWG's recommended test configurations.

The TWG 3.3.3.2 procedure places the Hybrid III 3-year old (3yo) in a rearward facing kneeling position is a procedure to measure injuries to the chest of a 3-year old OOP occupant. The TWG 3.3.3.5 where the Hybrid III 6-year old (6yo) is forward facing and seated on a booster cushion is a procedure to measure the loads on the head and neck region of a 6 year old due to the direct load acting on the back and shoulder. Lastly, the TWG 3.3.3.6 is a procedure to measure injuries to the SID-IIs or small females in which the dummy is positioned inboard facing with its ribs fully exposed to the deploying airbag. In order to fulfill the TWG recommended procedures, the ATD used for these test procedures are MADYMO validated ellipsoid models. For comparison purposes, Figure 4.2(a) – (c) represent the Humanetics Crash Dummies and Figure 4.3(a) – (c) represent the MADYMO dummies.

(a) (b) (c)

Figures 4.1. OOP test configurations [7].
(a) 3-year old dummy rearward facing and leaning on back seat; (b) 6-year old dummy forward facing and leaning on door panel; (c) small females inboard facing

Table 4.1. TWG selected test procedures

ATD	TWG Section	Test Position	Body Region of Interest
Hybrid III 3-Year Old	3.3.3.2	Rearward Facing	Head, Neck, Thorax
Hybrid III 6-Year Old	3.3.3.5	Forward facing on booster seat	Head, Neck
SID-IIs	3.3.3.6	Inboard facing	Head, Neck, Thorax, Abdomen, Pelvis

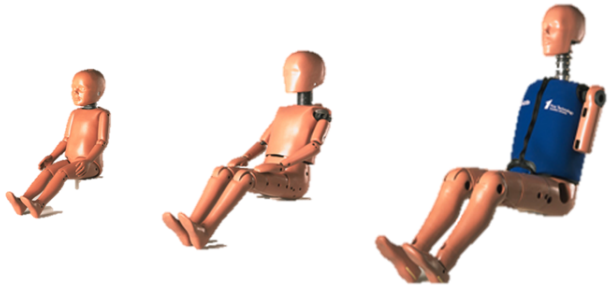

(a) (b) (c)

Figure 4.2. Humanetics crash dummies [11].
(a) Hybrid III 3yo; (b) Hybrid III 6yo; (c) SID-IIs

(a) (b) (c)

Figure 4.3. MADYMO ellipsoid ATD.
(a) Hybrid III 3yo; (b) Hybrid III 6yo; (c) SID-IIs

4.4.1 Airbag model

Due to the complexity of the airbag system in affecting the occupant's injury, the airbag model must be validated to ensure good accuracy in the airbag model. The ATD's viscous criterion and rib deflection is validated against study conducted by Hallman et al. [10].

Since the airbag governing parameters or factors such as the mass flow rate, the volume, the allowable fully inflated depth, and fabric permeability of the airbag are of great important in influencing occupant injuries. The airbag is modeled and fine-tuned in close relationship with the airbag model by Hallman et. al. [10] to ensure an accurate validation. The membrane of the airbag is of 0.5mm thickness. The inflator gases used in terms of molar fraction are 0.4% Nitrogen, 0.3% Carbon Dioxide, 0.3% Water Vapor to approximate atmosphere air mixture. The fully inflated depth of the airbag is constrained by twelve 18cm

elastic straps. The 3.44L airbag requires 20ms to reach fully inflated state and the maximum pressure is 168kPa. The gas exits the inflator jet at 508.8m/s^2 and the inflator temperature is 7280^{0}K. The mass flow rate necessary to properly inflate the bag, as shown in Figure 4.4, is determined by performing a tank test analysis.

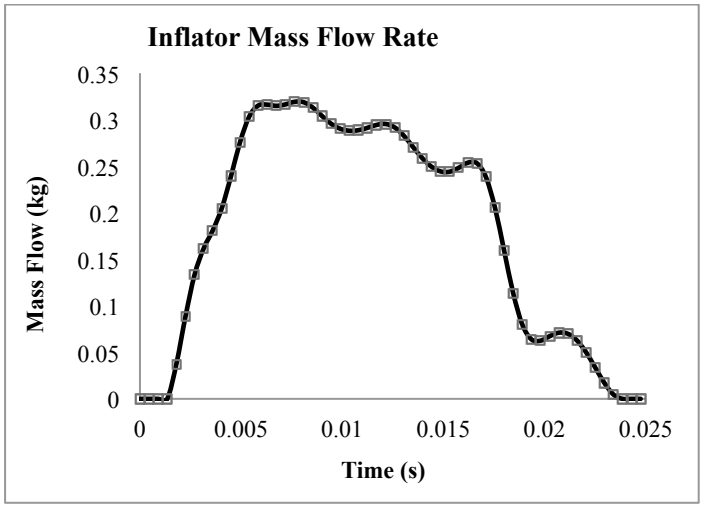

Figure 4.4. Inflator mass flow rate

In the preceding formulations in Section 4.3, it is shown that inlet mass flow rate is influenced by many parameters such as inlet velocities, geometry and inlet density. Besides that, the mass flow rate curve is also influenced by the selection of chemical compositions. Therefore, it is important to note that the mass flow rate shown in Figure 4.4 is based on a mixture of chemical composition as well as other parameters. The inflator model and the chemical compositions are held constant in this study will not be discussed as it is not within the scope of this study.

4.4.2 Airbag model validation

A study conducted by Hallman et al analyzed the effect of deploying a torso-only side impact airbags on out-of-position occupant's torso injury by utilizing MADYMO facet human model [10]. The torso injury evaluated in the study was occupant chest compression ratio and the viscous criteria. The method of evaluation was performed using Heidelberg stationary setup in which the ATD is placed in close proximity to the rigid impact wall.

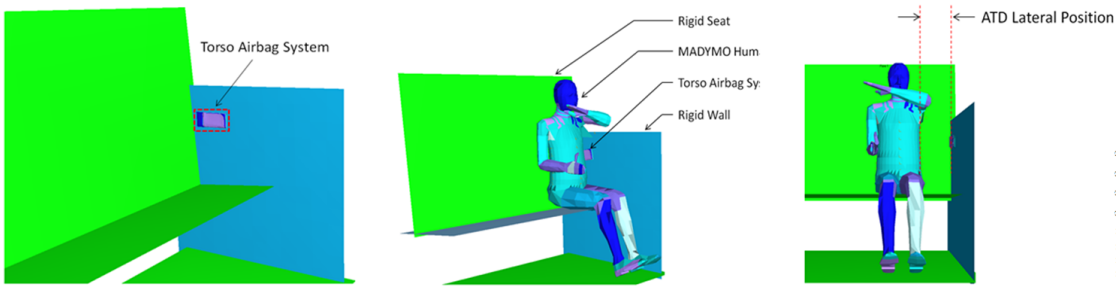

(a) (b) (c)

Figure 4.5. (a) Heidelberg stationary setup showing torso airbag model; (b) 3D view of Heidelberg stationary setup; (c) ATD lateral position

Figure 4.5(a) – (c) show the Heidelberg stationary setup. The ATD is seated on a frictionless rigid seat fixed to the platform of the setup. A rigid wall is to provide surface support for the airbag and to simulate a vehicle side frame. The ATD's arms are raised to allow the thorax region to be fully exposed to the airbag and the rigid wall; the shoulder body region does not contact the rigid wall. The ATD initial position is 2cm relative to the rigid wall and displaced in an increment of 2cm until the airbag does not contact the ATD during inflation process. The chest % compression and viscous criteria are obtained and compared to the simulation results by Hallman et al. [10]. Figure 4.6 shows the MADYMO human ATD's rib placement in which level 4 represents the upper rib, level 2 and 3 represent the middle rib and level 1 represent the lower rib.

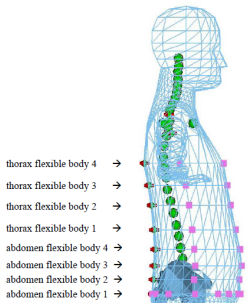

Figure 4.6. MADYMO human ATD rib levels [12]

Figure 4.5 shows the ATD and airbag kinematics at different instances of time at 2cm from the rigid wall. It is shown that at 0-20ms, the ATD is in the path of the deploying airbag and the 1st to 4th ribs are fully exposed to the deploying airbag. The comparison graphs for the simulations and results from Hallman et al. [10] are shown in Figure 4.8 and Figure 4.9.

The comparison results for the thorax viscous criteria and peak rib compression showed reasonable agreement. Once the airbag model is validated, the airbag model can then be used for the TWG's OOP simulations.

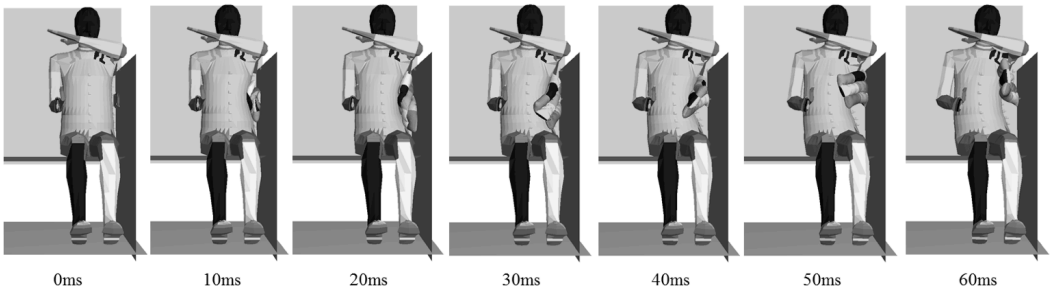

Figure 4.7. Simulated kinematics of ATD and torso-only airbag at 2cm relative to rigid wall for stationary test

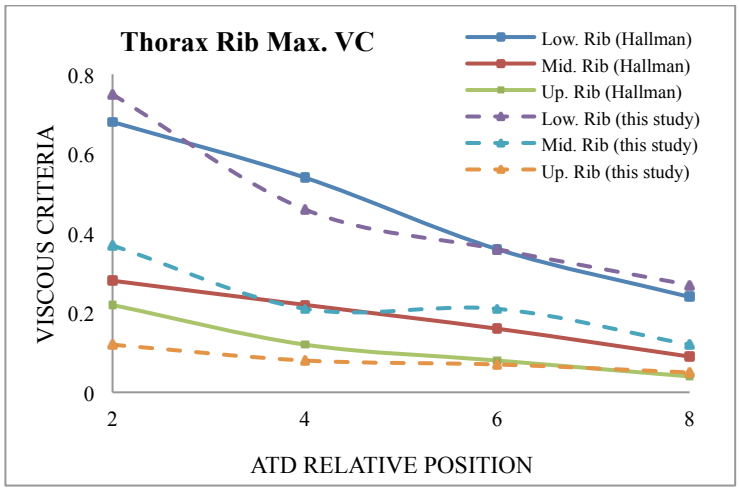

Figure 4.8. Comparison of ATD viscous criteria against results by Hallman et al.

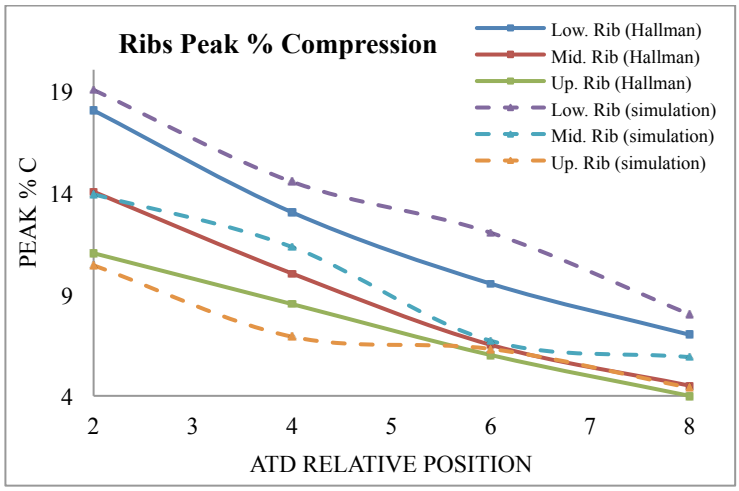

Figure 4.9. Comparison of ATD ribs maximum % compression against results by Hallman et al.

4.4.3 Vehicle model

A generic vehicle interior is modeled as shown in Figure 4.10. The vehicle model is a partial model of the Ford Taurus FE model. The vehicle's side-panels and cushion seats are selected to be included in this study because these parts are of great importance in influencing the occupant placement and the path of the deploying airbag.

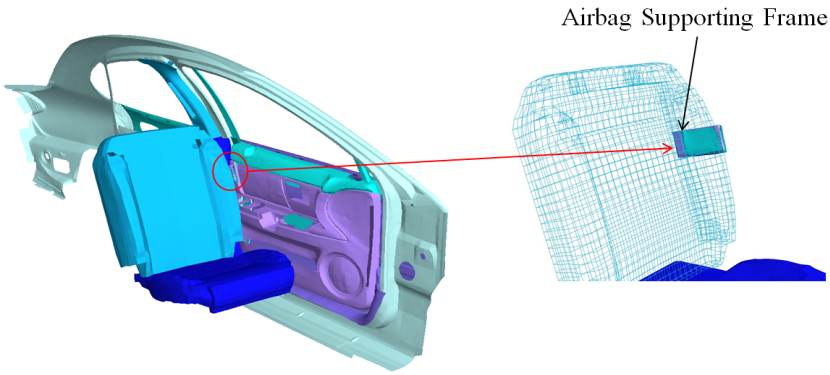

Figure 4.10. Partial Ford Taurus interior showing seat mounted side-impact airbag

Once the vehicle interior is successfully modeled and constrained properly, a torso-only side airbag (SAB) is mounted onto the back seat as shown in Figure 4.10. The airbag supporting frame is constrained to the back seat. The position of the supporting frame with respect to the back cushion is important to ensure proper airbag inflation. Figure 4.11 shows the SAB frame-by-frame deployment. It can be seen that the side airbag reaches fully deployed state in between 20ms to 35ms and extends outward to provide protection to the torso body region.

With the SAB positioning and the vehicle interior defined, the ATD is incorporated into the model in accordance to the TWG test procedures as shown in Figure 4.12. The surface contacts used between the ATD (multi-body), vehicle interior (FE) and SAB (FE) are *Contact.MB_FE* for multi-body to FE surfaces and *Contact.FE_FE* for FE-to-FE surfaces.

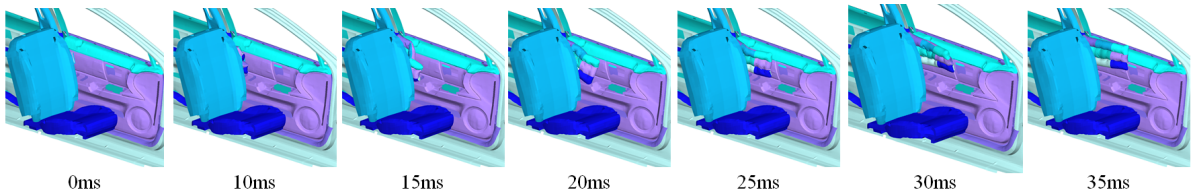

Figure 4.11. SAB frame-by-frame deployment process

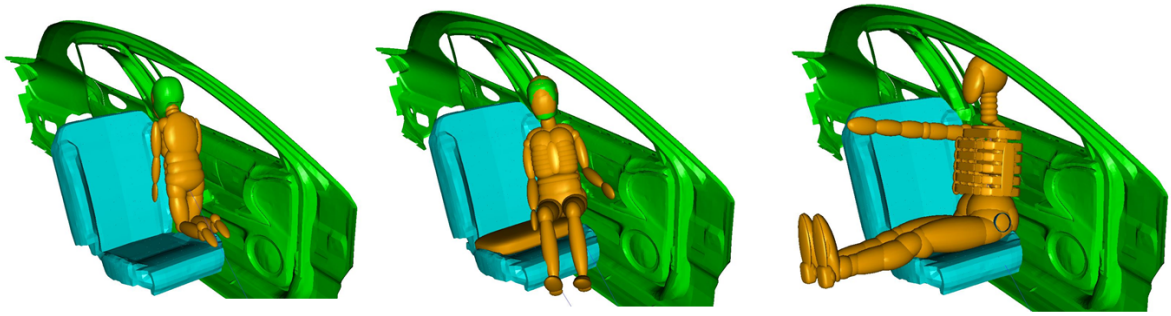

Figure 4.12. OOP test configurations. (a) 3yo dummy rearward facing; (b) 6yo dummy forward facing; (c) small female inboard facing

4.4.4 Parametric dtudy using Design-of-Experiment

The full factorial design is conducted to investigate the joint effect of the three factors on the injury criteria denoted as the output responses. This design also provides the relevant information such as interactions between factors. Once the factor's interaction is determined to be significant, design optimization may be conducted but it is not within the scope of this study to optimize the airbag design. Subsequently, a set of parametric equations can be obtained through the factorial's regression analysis to predict to occupant's injury levels. The DoE used is a single-replicate 2^3 factorial design, the 3 factors of interests are airbag mass flow rate, allowable inflated depth and fabric permeability. The design matrix for a 2^k factorial experiment can be seen in Table 4.2. The "+" and "-" geometric coding represents the high and low levels of the factors. The high and low factors used are quantitative values and because the factors are of only two levels, therefore, the response must be assumed to be linear over the range of the selected factor range.

Table 4.2. 2^3 Design matrix

Run	Factor: A (Mass Flow Rate)	Factor: B (Allowable Depth)	Factor: C (Fabric Permeability)	Labels	Responses
1	-	-	-	(1)	
2	+	-	-	a	
3	-	+	-	b	
4	+	+	-	ab	
5	-	-	+	c	
6	+	-	+	ac	
7	-	+	+	bc	
8	+	+	+	abc	

The high and low levels of each factors are determined using the Heidelberg stationary model in which the model is subjected to various level of parameters and the coefficient of determinant is used to indicate the linearity of the injury level. To avoid repetitive R^2 figures, only the R^2 for injury levels based on increasing mass flow rate are shown. The R^2 for the peak VC and rib % compression, as shown in Figure 4.13 and Figure 4.14, are all above 0.80.

The R^2 tabulation for all three factors can be seen in Table 4.3. It is shown that the R^2 for factors A, B and C are good with factor B peak VC yielded the lowest R^2. It can be concluded from this linearity test, represented by R^2, that the data are linearly distributed and it can be safely assumed that further studies on injuries to the thoracic body region are approximately linear over the range of high/low factor levels.

By performing DoE, a regression model or the fitted model can be determined to estimate occupant's injury from the governing factors. The generalized regression model for this design is represented as:

$$\hat{y} = \hat{\beta}_0 + \hat{\beta}_1 x_1 + \hat{\beta}_2 x_2 + \hat{\beta}_3 x_3 + \hat{\beta}_{12} x_1 x_2 + \hat{\beta}_{13} x_1 x_3 + \hat{\beta}_{23} x_2 x_3 + \hat{\beta}_{123} x_1 x_2 x_3 \quad (4.14)$$

where the coded x_1, x_2, x_3 represent factors A, B and C respectively and x_1x_2, x_1x_3, x_2x_3 and $x_1x_2x_3$ represent the interaction between factors.

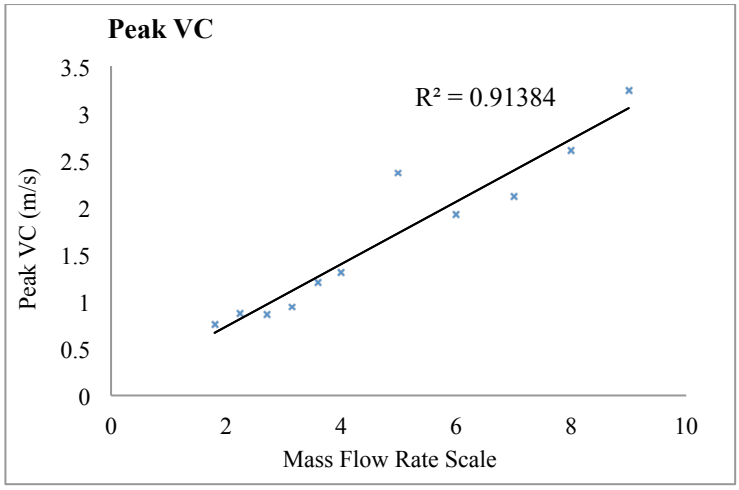

Figure 4.13. R-square for peak VC based on increasing mass flow rate

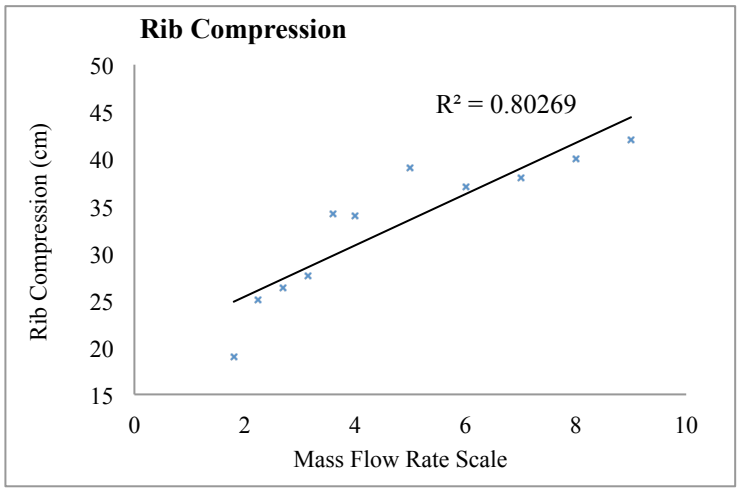

Figure 4.14. R-square for rib % compression based on increasing mass flow rate

Table 4.3. R^2 for all three factors determined by Heidelberg stationary simulation

Factors	Injury Parameters	R^2 Coefficient
Mass Flow Rate Scale (Factor A)	Peak VC	0.91
	Rib % Compression	0.80
Strap Length (Factor B)	Peak VC	0.67
	Rib % Compression	0.60
Fabric Permeability (Factor C)	Peak VC	0.75
	Rib % Compression	0.77

4.4.5 Injury criteria

The injury criteria mainly describe the effect of dynamic forces acting on a particular body region. A threshold limit is assigned to each injury criteria and the occupant is considered severely injured if the injury values exceed the injury limit. The threshold injury limits can be referred to the dummy Injury Assessment Reference Values (IARV) for OOP

occupants as shown in Table 4. The occupant injury caused by deploying airbag is monitored in three body regions, namely, the head, neck and thorax.

The head injury criteria (HIC) value is a measurement standard for measuring the injury to the head. The HIC_{36} threshold used for this study is 570. TWG predicts that the neck injuries will be the most important injury ratings for OOP test from deploying airbag. Based on TWG frontal airbag data, the cause of fatalities among children is the rupture of the connecting tissues at the occipital condoyle [7]. In order to properly predict the neck injury, two models of neck injuries can be utilized, namely, the N_{ij} index value or imposing limits threshold on neck forces and bending moments. The first model, the N_{ij} value, is used based on the linear combination of neck loads and moments. A N_{ij} value of above 1 indicates 30% risk of AIS 3+ injury to the cervical spine [13]. The second approach is to impose a limit threshold to the neck loadings. The lower neck forces were selected as the primary loadings to the neck. Recent research suggested that measuring the upper neck forces may not be adequate in determining the neck injuries due to the fact that OOP occupants' back may be exposed to the deploying side airbags [7]. The complete neck loadings can be found in NHTSA final ruling for neck injury criteria [14].

According to IIHS injury measurements, rib deflection equal to or less than 34mm is the border between good and acceptable rating [15]. Based on Viano injury curves for smaller size females, a 34mm deflection rating corresponds to 21 to 27 percent of severe thoracic injury [16]. An average rib deflection for SID-IIs of above 50mm is susceptible to an 80% chance of rib fracture.

The suggested rib deflection rate of 8.20m/s by IIHS marks the border between good and acceptable rating [15]. A deflection rate of 8.20m/s also correlates to an approximately 5% risk of AIS 4 thoracic injury. Based on research by Mertz et al [17], the lateral rib deflection rate is the same to the frontal deflection.

Table 4.4. ATD Injury Reference Value (IARV) for OOP Occupants

Body Region	Injury Parameters	Hybrid III 3-yo	Hybrid III 6-yo	SID-II
Head	HIC, 15ms window	570	723	779
Upper Neck	N_{ij}	1.0	1.0	1.0
N_{ij} Intercepts Values	Tension Force (N)	2120	2800	3880
	Compression Force (N)	2120	2800	3880
	Flexion Moment (N.m)	68	93	155
	Extension Moment (N.m)	27	37	61
Lower Neck Forces	Tension Force (N)	1130	1490	2070
	Compression Force (N)	1380	1820	2520
Thorax	Deflection (mm)	36	40	34
	Deflection rate (m/s)	8.0	8.5	8.2

4.5 Results and Discussions

A parametric study was conducted to investigate the OOP occupant injuries from a deploying side airbag. Three governing factors for the airbag model such as fabric permeability (factor C), inlet jet mass flow rate (factor B) and maximum allowable airbag depth (factor A) were analyzed and considered. As discussed in the methodology section, the airbag aggressively test was conducted on three scenario, namely, TWG 3.3.3.2, TWG 3.3.3.5 and TWG 3.3.3.6 OOP test configurations.

4.5.1 TWG 3.3.3.6 - small female inboard facing

The kinematics for SID-IIs simulation can be seen in Figure 4.15. The kinematics shown is simulation with A, B and C factors set at high level. It can be seen that the ATD is positioned inboard facing with arm stretched outward. The pelvic region was aligned to contact the door trim panel. The ATD first thoracic rib was aligned with the top edge of the airbag module to allow maximum contact force between the airbag and the thoracic region. The injury level measured were injuries to the thorax body regions such as the lower, middle and upper rib deflection as well as the thorax deflection rate.

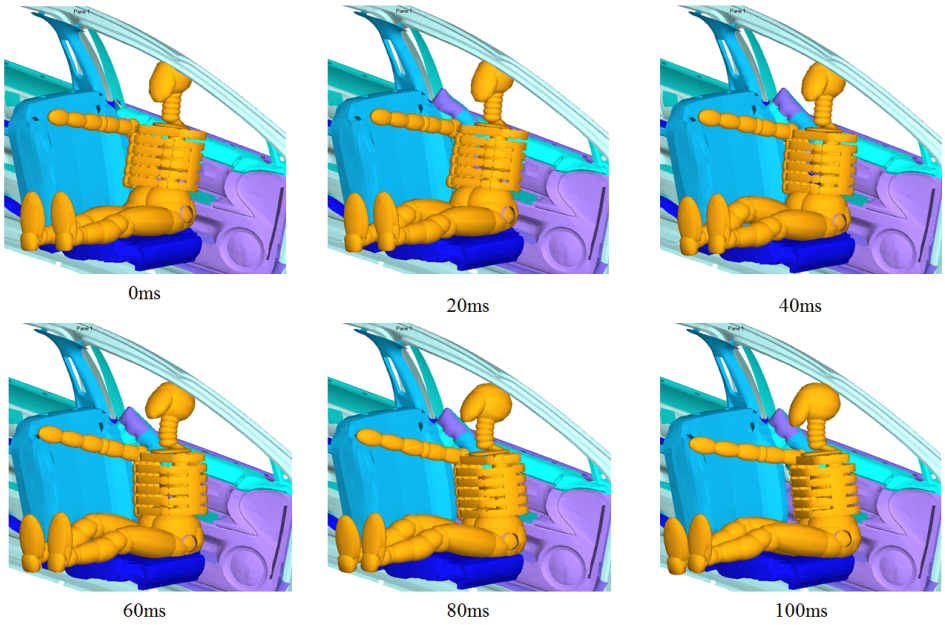

Figure 4.15. Simulated kinematics for SID-IIs with factor levels A, B and C set at high

Table 4.5. SID-IIs DoE Injuries Responses at Different Factors Levels

Run Order	Factors			Labels	Responses				
					Rib Lateral Deflections (mm)				Thorax Deflection Rate (m/s)
	A	B	C		Low	Mid	Up	Peak Rib Deflection (mm)	
1	-	-	-	(1)	21.12	16.65	14.48	21.12	7.07
2	+	-	-	a	29.90	24.43	25.10	29.90	6.72
3	-	+	-	b	9.60	12.51	10.86	12.51	4.44
4	+	+	-	ab	7.67	9.48	12.97	12.97	4.44
5	-	-	+	c	13.78	11.38	0.76	13.78	3.82
6	+	-	+	ac	59.14	39.76	31.63	59.14	7.00
7	-	+	+	bc	20.52	18.27	14.59	20.52	6.90
8	+	+	+	abc	17.98	12.35	19.18	19.18	7.20

Table 4.6. SID-IIs Simulation DoE Parametric Equation

DoE Responses	DoE Regression Model Equation
Lower Rib Deflection	$23.40 + 0.76A - 0.21B - 2238.89C - 0.023AB + 472.94AC + 57.3626BC - 10.22ABC$
Middle Rib Deflection	$16.05 + 1.58A - 0.060B - 1503.69C - 0.040AB + 391.25AC + 42.66BC - 8.59ABC$
Upper Rib Deflection	$13.32 + 1.83A - 0.057B - 2550.94C - 0.031AB + 357.38AC + 57.57BC - 6.50ABC$
Peak Rib Deflection	$22.26 + 1.58A - 0.20B - 2279.73C - 0.030AB + 677.71AC + 62.28BC - 14.03ABC$
Thorax Deflection Rate	$8.18 - 0.064A - 0.075B - 635.22C + 0.0013AB + 62.98AC + 17.51BC - 1.18ABC$

To complete the DoE design matrix, 8 simulations were performed as shown in Table 4.5. Table 4.6 represents the complete injuries responses at different combination of levels. It is shown that the rib deflection is above the IARV values for simulations #6. 5 out of 8 simulations also yielded at least one response is 80% or above the suggested IARV threshold. The regression model equations seen in Table 4.6 are calculated using Equation (4.14). These parametric equations can be used to generate model graphs that present a prediction model of OOP injury level based on any combinations of factors. Table 6 is a complete regression model that can be used to predict OOP SID-II injury risks from deploying airbag.

To avoid repetitive graph, only the DoE model graphs for selected injury level for SID-IIs simulation are shown. Figure 4.16 and Figure 4.17 represent the fitted model for SID-II peak rib deflection and Figure 4.18 and Figure 4.19 shows the fitted model for SID-II thorax deflection rate. The fitted model as shown in Figure 4.16 and Figure 4.17 is a good tool to measure the SID-II's peak rib deflection. It is shown that the maximum rib deflection can be obtained by using a high mass flow rate, low strap length and low fabric permeability. Similarly, Figure 4.17 suggests that the lowest rib deflection can be obtained by utilizing combination of high fabric permeability, high strap length and the combination of any level of mass flow rate. The thorax deflection rate as shown in fitted models Figure 4.18 and Figure 4.19 can be interpreted in two scenarios. The thorax deflection rate values are generally high with high mass flow rate, high strap length and low fabric permeability or low strap length, high fabric permeability and any level of mass flow rate. The blue region as seen in Figure 4.19 suggests that the lowest deflection rate can be achieved with the combination of low fabric permeability, low strap length and mass flow rate.

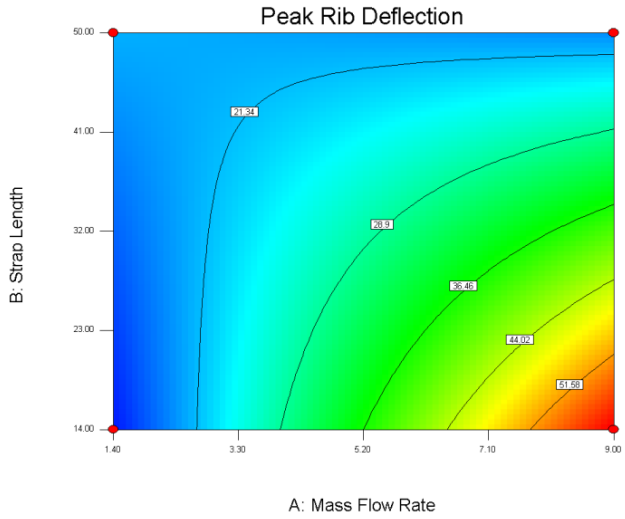

Figure 4.16. Peak Rib Deflection DoE Model Graph with C Level: Low

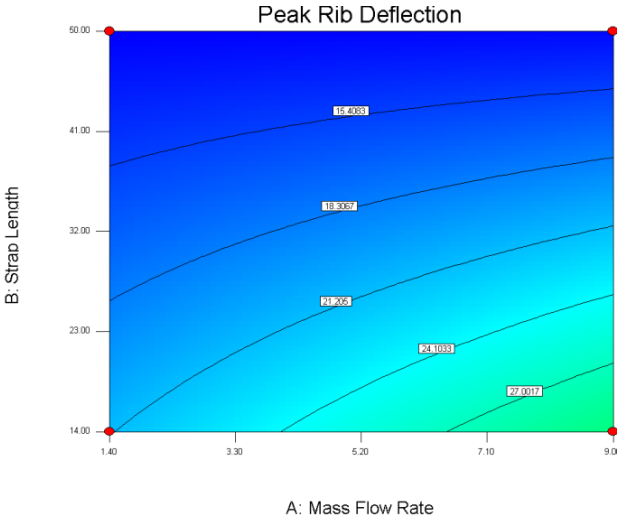

Figure 4.17. Peak Rib Deflection DoE Model Graph with C Level: High

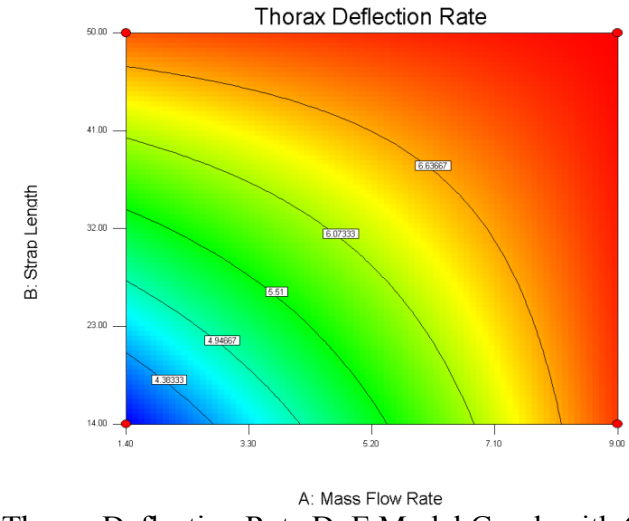

Figure 4.18. Thorax Deflection Rate DoE Model Graph with C Level: Low

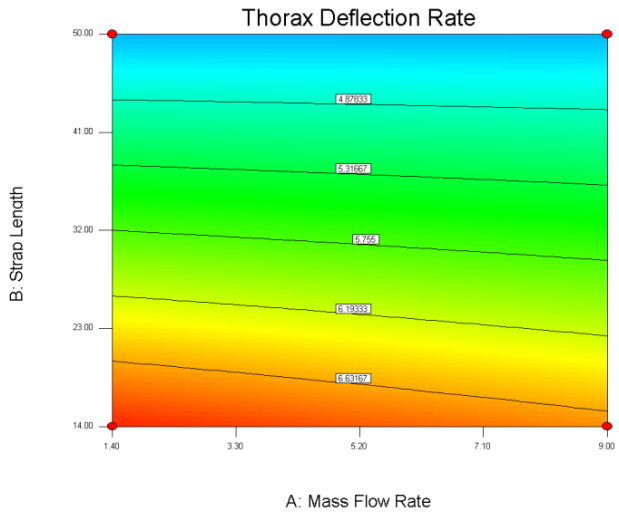

Figure 4.19. Thorax Deflection Rate DoE Model Graph with C Level: High

4.5.2 TWG 3.3.3.2 - 3-year old dummy rearward facing

In order to fully present the findings of injuries caused by deploying airbag on Hybrid III 3-Year Old, the ATD was positioned in accordance to TWG recommendation. According the TWG recommendation, the ATD was positioned kneeling and facing backwards along the outer-line of the bottom cushion. The sternum must be placed as close as possible to the leading edge of the back cushion and in contact with the back seat. Finally, the head must be in between the back cushion and the vehicle side trim to allow maximum contact. The ATD injury ratings of interest are the Neck N_{ij}, neck vertical loading values, rib deflection and rib deflection rate. The kinematics of the ATD at all factors set to high can be seen in Figure 4.20. It can be seen in the kinematic figures that the placement of the ATD completely blocked the path of the deploying airbag. As such, the airbag needed much longer time to reach fully deployed state. It is shown in 60 – 80ms that the airbag compressed the rib in order to reach full deployment. Table 4.7 shows the DoE tabulation of the simulation results.

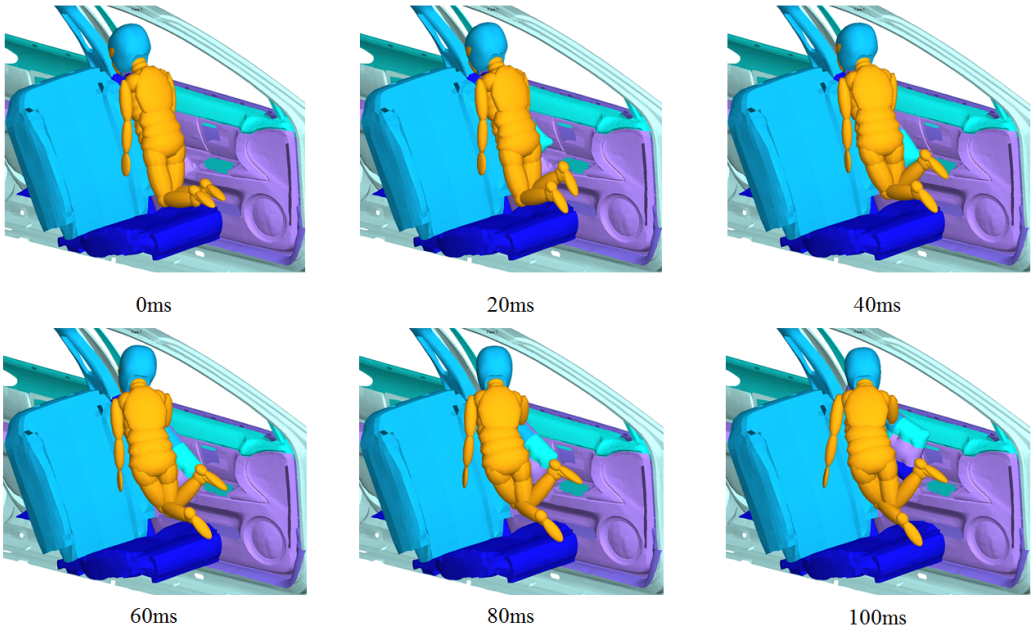

Figure 4.20. Simulated kinematics for Hybrid III 3yo with factor levels A, B and C set at high

Table 4.7. Hybrid III 3-Year Old DoE Injuries Responses at Different Factors Levels

Run Order	Factors			Labels	Responses				
	A	B	C		N_{ij}	Thorax Deflection (mm)	Thorax Deflection Rate (m/s)	Lower Neck Tension (+Fz)	Lower Neck Compression (-Fz)
1	-	-	-	(1)	0.19	3.0	1.27	123	178
2	+	-	-	a	0.57	12.5	5.33	152	549
3	-	+	-	b	0.20	5.6	2.12	119	160
4	+	+	-	ab	0.60	15.2	4.79	121	613
5	-	-	+	c	0.20	3.2	1.37	134	161
6	+	-	+	ac	0.57	18.9	6.55	197	609
7	-	+	+	bc	0.21	4.9	1.66	94	168
8	+	+	+	abc	0.60	15.7	5.19	107	578

The DoE results shown in Table 4.7 suggested that the thorax deflection rate for simulation number 6 is 80% that of the IARV threshold. Other responses are well below IARV threshold. These results suggest that the Hybrid III 3-year old for this particular configuration do not risk injuries from deploying airbag. Based on the ATD's kinematic responses, the airbag mainly contacted the front sternum of the ATD instead of the side thorax, this explains the low thorax deflection values. As shown in Table 4.8, the regression model obtained from DoE analysis can be used to predict the Hybrid-III 3-Year Old injuries risks from deploying airbag in the case of OOP.

Table 4.8. Hybrid III 3-Year Old Simulation DoE Parametric Equation

DoE Responses	DoE Regression Model Equation
Rib Deflection	$0.25 + 1.24A + 0.072B - 95.03C + 0.00037AB + 107.16AC + 0.058BC - 1.83ABC$
Thorax Deflection Rate	$0.32 + 0.62A + 0.024B - 36.24C - 0.0056AB + 13.03AC - 1.92BC$
N_{ij}	$0.12 + 0.049A + 0.00018B + 1.18C - 0.000073AB - 0.13AC$
Neck Peak Tension	$110.29 + 6.54A + 0.25B + 3107.75C - 0.14AB + 296.05AC$
Neck Peak Compression	$122.53 + 44.62A - 0.92B - 4950.29C + 0.30AB + 1627.19AC + 130.85BC - 43.86ABC$

4.5.3 TWG 3.3.3.2 - 6-year old dummy forward facing

The OOP test objective for the Hybrid III 6yo is to measure the injuries to the neck. The ATD's pelvis and thorax is positioned close to the leading edge of the back seat and the booster block. The left arm is positioned to rest of the side panel. The ATD's torso is placed directly in the path of the deploying airbag.

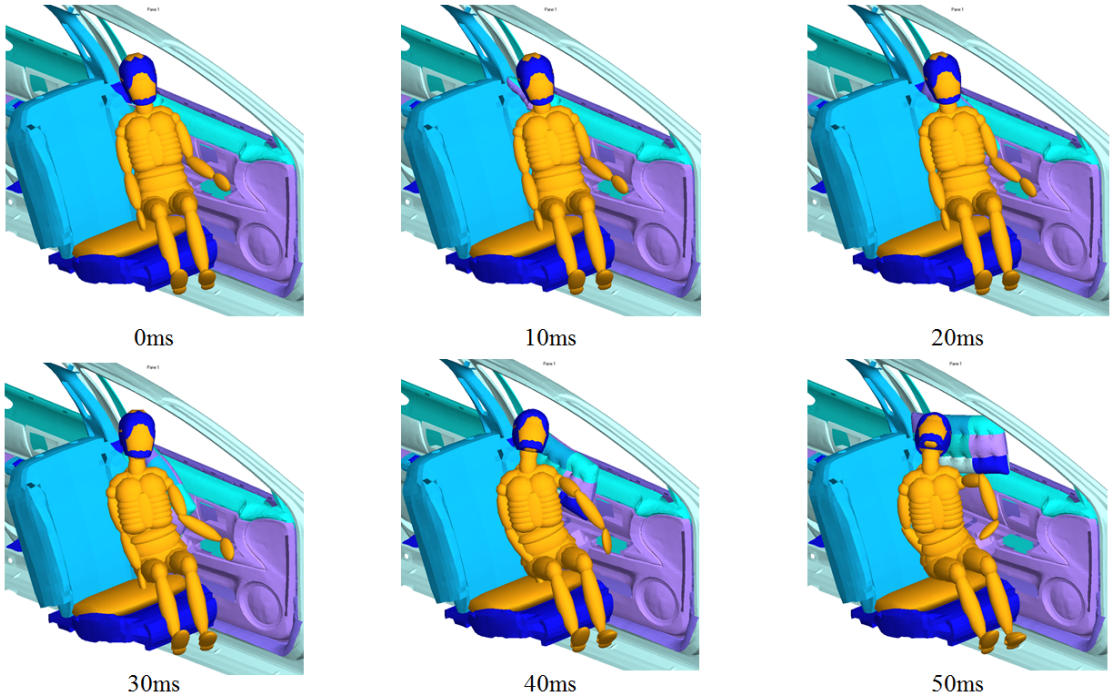

Figure 4.21. Simulated kinematics for Hybrid III 6yo with factor levels A, B and C set at high

Table 4.9. Hybrid III 6-Year Old DoE Injuries Responses at Different Factors Levels

Run Order	Factors			Labels	Responses		
	A	B	C		N_{ij}	Lower Neck Tension (+Fz)	Lower Neck Compression (-Fz)
1	-	-	-	(1)	0.16	114	295
2	+	-	-	a	0.33	315	440
3	-	+	-	b	0.20	139	229
4	+	+	-	ab	0.55	669	708
5	-	-	+	c	0.15	119	300
6	+	-	+	ac	0.33	301	431
7	-	+	+	bc	0.19	154	289
8	+	+	+	abc	0.62	729	688

Table 4.10. Hybrid III 6-Year Old Simulation DoE Parametric Equation

DoE Responses	DoE Regression Model Equation
N_{ij}	$0.13 + 0.0091A + 0.000011B - 1.83C + 0.00079AB + 0.59AC$
Neck Peak Tension	$105.83 + 6.73A - 1.60B - 2083.33C + 1.32AB + 116.67BC$
Neck Peak Compression	$288.04 + 5.85A - 2.61B + 4115.79C + 1.10AB - 618.42AC$

The complete DoE run matrix can be seen in Table 9. All the injury values are below the suggested IARV. The simulation kinematics in Figure 4.21 shows that the ATD's neck experienced large amount of rotation and compression to the occipital condoyle over a short period of time. It can also be seen that the neck is the only body region experienced large forces and deformation compared to the thorax body region. Besides that, it can be seen that the left arm may have sustain serious injuries. The IARV do not have a guideline for measuring injuries to the extremities. As such, injury assessment cannot be done on extremities. The results show that 6 year old at this test configurations do not risk any injuries to the neck region from deploying airbags. Table 4.10 represents the regression model equations for selected injuries response. It can also be seen that the 3 factors interaction, ABC, is not significant in affecting the injuries response.

4.6 Conclusions

The purpose of this study was to develop a set of parametric equations to predict injuries from a deploying airbag using computer simulations. The prediction model was developed through the use of DoE regression model and model graphs. The simulations were

conducted using MADYMO 7.4.2 and DoE results were evaluated using Design Expert 7. The selected three main influential factors that have major effect on OOP injuries were fabric permeability, airbag fully inflated depth and inflator mass flow rate. In order to accurately utilize the DoE factorial design, linear injury response between high and low factors have been verified using Heidelberg stationary.

The test scenarios selected for this study comprised of wide range of ATD in accordance to the recommendation by TWG. These scenarios were carefully selected to measure various injuries and to represent a whole spectrum of OOP occupants that are susceptible to deploying side airbags. DoE results from this study indicated that parametric equations were successfully obtained to determine the occupant injuries. The DoE results also suggested that two or higher interactions between factors governs the regression model. Therefore, it was conclusive that no single factor can be altered without affecting the injury response.

This study has shown that a set of equations can be generated using DoE's full factorial design. Full factorial design proved to be a useful statistical tool in evaluating the interactions between factors. Similarly, the injury prediction model was performed successfully by using the regression model. The results showed that the test configurations for SID-IIs had the highest injuries values that exceeded the IARV. This is mainly due to the seating position in which the thoracic body region was fully exposed to the deploying airbag. The low injury values for 3-year old and 6-year old suggest that the occupant was not susceptible to any risk of injury for these particular configurations. It is also important to conclude that the interest of this study is not to evaluate whether the injury level exceed certain injury threshold but rather to present systematic approach in developing a set of injury prediction model to evaluate injuries to OOP occupants from deploying airbag.

The methodology and mathematical models developed in this study can be utilized in the design stage of future airbags by using the prediction model to approximate injuries without the need to perform experimental testing. This study, however, did not verify the reliability of these set of equations on the recent model year vehicles. As such, further study needs to be conducted to verify this concept. Future works may also include optimizing the airbag model in reducing injuries to OOP occupants through the use of DoE's response surface methodology.

4.7 References

[1] US. National Highway Traffic Safety Administration (NHTSA), 2012, "An Analysis of Recent Improvement to Vehicle Safety," DOT HS 811 572.

[2] US. National Highway Traffic Safety Administration (NHTSA), 2007, "An Evaluation of Side Impact Protection," DOT HS 810 748.

[3] Cunningham, K., Brown, T. D., Gradwell, E., and Nee P. A., 2000, "Airbag Associated Fatal Head Injury: Case Report and Review of The Literature on Airbag Injuries," *J Accid Emerg Med 2000*, 17:139-142 doi:10.1136/emj. 17.2.139.

[4] Mohamed A. A., Banerjee A., 1998, "Patterns of Injury Associated with Automobile Airbag Use," *Medical Emergencies* 74:455-458.

[5] Kindelberger, J., Chidester, A., Ferguson, E, "Air Bag Crash Investigations," NHTSA Paper No. 299.

[6] Prasad, A. K., Samaha R. R., Louden, A., 2002, "Side Air Bag Research: Static Testing of Side Impact Air Bags Using Three and Six Year Old Hybrid III Dummies and the 12 Month CRABI Dummy," NHTSA and TRC, Inc.

[7] Lund, A., July, 2003, "Recommended Procedures for Evaluating Occupant Injury Risk From Deploying Side Airbags,"The side airbag out-of-position injury technical working group. Alliance, AIAM, AORC and IIHS.

[8] Tolman, C. R., 1921, "The Principle of Similitude and The Entropy of Polyatomic Gases," *Journal of the American Chemical Society 1921 43(4), 866-875*.

[9] Annonymous, 2003, "NIST Chemistry WebBook – NIST Standard Reference Database Number 69," WebBook.nist.gov/chemistry (Retrieved: Oct, 2013).

[10] Hallman, J., Yoganandan, N., Pintar, F., 2008, "Torso Side Airbag Out-Of-Position Evaluation using Stationary and Dynamic Occupants", *Biomed Sci Instrum, 44:123-128.*

[11] Humanetics Innovative Solutions Crash Test Dummies. www.humaneticsatd.com (Retrieved: Oct, 2013).

[12] MADYMO Human Body Models Manual, 2012, TNO TASS, www.tassinternational.com (Retrieved: June, 2013).

[13] Duma, S. M, et al, 1998, "Dynamic Response of the Hybrid III 3 Year Old Dummy Head and Neck During Side Airbag Loading", 42nd Annual Proceedings Association for the Advancement of Automotive Medicine.

[14] Eppinger R., Sun E. Kuppa S., Saul R., 2000, "Development of Improved Injury Criteria for the Assessment of Advanced Automotive Restraint Systems – II," NHTSA Report.

[15] Annonymous, 2008, "Side Impact Crash Worthiness Evaluation, Guidelines for Rating Injury Measures V2,"Insurance Institute For Highway Safety.

[16] Lau, I.V., and Viano D.C., 1986, "The Viscous Criterion - Bases and Applications of an Injury Severity Index for Soft Tissues," SAE Technical Paper 861882, doi: 10.4271/861882.

[17] Mertz, H. J. and Weber, D. A. 1982, "Interpretations of the Impact Responses of A Three-Year Old Child Dummy Relative to Child Injury Potential," Preceedings of the 9th International Technical Conference on Experimental Safety Vehicle. NHTSA.

CHAPTER FIVE

A RESPONSE SURFACE METHODOLOGY IN PREDICTING INJURIES TO OUT-OF-POSITION OCCUPANTS FROM FRONTAL-AIRBAGS

5.1 Abstract

Out-of-position (OOP) occupants, especially smaller females and children, are quite vulnerable to injuries caused by deploying airbags. This study is aimed at investigating the effects of various design parameters of a frontal airbag on OOP occupants' resulting injury levels. The study also investigates the predictive capability of the occupant's injury potential using a regression model developed from the response surface methodology. For this, the OOP occupant is represented using a MADYMO 3-year old child dummy. The objective measurements identified as the main injury causation parameters include the fabric permeability, friction coefficient between the occupant and the airbag, and the occupant's initial position. Due to the complexity of the airbag model, small iterations are done until the numerical model is found to be in reasonable agreement with another study available in the literature. The first part of the work is focused on analyzing the effect of a single parameter on the injury responses of the 3-year old child. The second part of the work covers the development of a set of regression model to predict the combined effects of various parameters on the injury responses of the occupant. It is shown that the regression model is fairly accurate and sufficient in predicting various injury levels to OOP occupants from a deploying airbag.

5.2 Introduction and Background

Research in occupant protection and vehicle crashworthiness continues to save lives. In general, the fatality risks of road vehicle occupants have been reduced by approximately 26% over the past 10 years [1]. During an accident, safety belts are used to restraint the

[1] This entire chapter will be presented at and published in the following source:

- Y.Y. Tay, R. Moradi, and H.M. Lankarani, "A Response Surface Methodology in Predicting Injuries to Out-of-Position Occupants from Frontal Airbags," IMECE 2014 International Mechanical Engineering Congress and Exposition, Montreal, Canada, November, 2014.

occupants from uncontrolled free-flying motion, and under certain conditions, airbags are deployed to provide cushion to the occupants from secondary impacts with the interior of a vehicle. The effectiveness of these two safety devices are demonstrated from a statistical study by NHTSA indicating that seat belts and airbags saved 15,147 and 2,788 lives respectively in 2007, and should the use of seat belts was increased to 100 percent, then additional 5,024 lives would have been saved. In more recent years, the National Highway Traffic Safety Administration (NHTSA) estimated that the use of frontal airbags saved approximately 15,000 lives [2, 3].

Despite the overall effectiveness of frontal airbag, the increasing utilization of airbags has also seen a rise in injuries caused by deploying airbags on out-of-position (OOP) and in-position occupants. OOP occupants are considered more prone to injuries from deploying airbags compared to in-position occupants due to the fact OOP occupants can be exposed to significant amount of force imposed by a deploying airbag. During the deployment of airbags, an occupant is considered in an OOP scenario if the occupant's initial position is in the path of the deploying airbag. Alternatively, the passenger can also be considered as an OOP occupant if he or she is displaced closer to the airbag system during the course of a collision [4].

In 2003, NHTSA's Special Crash Investigation (SCI) conducted a study on 242 cases of airbag related injuries, and it was shown that 90% of these cases considered sustained fatal injuries and approximately 60% comprised of children fatalities [4]. In 2002, NHTSA Transportation Research Center (TRC) conducted a set of experiments on airbag aggressivity in a static environment on various children dummies using a fleet of sedan cars. It was observed that 80% and 60% of 3- and 6-year old OOP tests exceeded the Injury Assessment Reference Values (IARV) respectively [5]. Rains et al. [6] conducted a performance testing to evaluate the injury sustain by OOP 3- and 6-year old dummies from a top-mounted frontal

airbag. At extreme proximity, they demonstrated that the neck loading for the 3-year old is twice as high as that of a 6-year old. Bass et al. [7] shows that OOP passenger occupants are likely to sustain thoracic injuries. Likewise, their study has shown that the distance of the occupant from the airbag module can substantially increase the chest's acceleration. Although NHTSA has amended its regulations to allow the automotive industry to reduce airbag deploying force in late 90's; these studies show that advance airbags installed in recent vehicles can still, albeit lower probability, cause serious injuries to OOP occupants.

Some of the most influential factors in airbag related injuries reported in various studies are airbag fabric materials, friction between the occupant and airbag fabric, inflator parameters and occupants initial position. Since the introduction of depowered airbag, several studies were conducted to evaluate the influence of airbag aggressiveness and parameters on various occupants' positions and sizes [8, 9, 10]. According to test procedures for evaluating OOP scenarios, the likelihood of an OOP occupant's position and its interaction with the airbag module are shown in Figure 5.1(a) and (b) [10]. Positions 1 and 2 are designed primarily to evaluate the potential injury levels to the head and neck body regions. The effect of occupant's position relative to the airbag module is well reported in an experimental study conducted by Prasad et al. [12,13]. Their study has shown that the occupant's head injuries levels are directly influenced by its positions. In another study by Watson and Cronin [13], they evaluated the effect of occupants' positions on thoracic injury potential and concluded that OOP occupants are more likely to sustain fatal thoracic injuries than in-position occupants.

(a) (b)

Figure 5.1. Recommended OOP test positions: (a) position 1 ; (b) position 2 [14]

Another influential factor reported is the influence of airbag friction on the kinematics of the upper body region [16, 17]. The study undertook by Kamiji and Kawamura [15] was conducted using computer simulation on a 3-year old dummy model. They concluded the head's direction of twist is significantly affected by the friction between the head and the airbag. However, the study did not investigate the dummy responses when subjected to various friction coefficients. Park et al. [12] conducted a number of computer simulations and experimental tests on the OOP interaction using the 3-year old dummy. Using the low-risk airbag deployment body block tests, they concluded that friction coefficient is among one of the most influential factor in injury causation. In an extensive airbag review by Khan et al. [17], it was also reported on several studies that friction between the airbag and occupant are among one of the contributing factor in analyzing OOP scenarios.

The last factor that is reported to have significant effect on OOP occupant injuries is the airbag's fabric permeability. Roychoudhury et al. [18] conducted an investigation by simulating the effect of deploying airbag on OOP using 5^{th} percentile female dummy. This study concluded that the increase of airbag leakage, also known as fabric permeability, has direct contribution of the change in the thorax injury criteria. Besides that, they demonstrated that under certain inflator conditions, altering the airbag material does not contribute to the change in thorax injuries. Rekveldt et al. [19] conducted a study on the influence of airbag fabric permeability on the head acceleration and neck loads. By varying the permeability coefficient from 0.042 and 0.1, it was shown that the neck loads and head acceleration reduced significantly with higher fabric permeability. The study also suggested that permeability of 0.08 and above can result in a too soft deployment of airbag.

Although airbag systems may have been designed and evaluated accurately, experimental testing must be carried out later in the design process. However, evaluating different prototypes and experimental setups are usually costly and undesirable. Therefore, numerical

simulations are very desirable in investigating wide range of airbag designs and design parameters. Optimization of the design can also lead to significant reduction in experimental cost. Having the ability to accurately predict OOP injuries from a deploying airbag is crucial in the design process for automotive safety industry. Due to the vast influential factors in governing an airbag system, determining the most important factors proved to be challenging. Hence, the selection of factors for this study is based on various studies reported in the literature. Many investigators have analyzed the injury levels of the OOP occupants when subjected to a single design parameter. Hence, analyzing the interaction between these factors and their combined effects on injury levels needs further investigation. The main objective of this work is to investigate the combined effect of various influential factors on OOP injury levels from a deploying airbag and to develop a set of injury prediction model based on the response surface regression model.

5.3 Methodology

This study involves modeling and analysis of the injury potential of a 3-year old from a deploying airbag using the multi-body dynamic code, MADYMO 7.4.2. The 3-year old dummy utilized in this study is a validated MADYMO Hybrid-III ellipsoid model [21]. The numerical setup consists of a facet vehicle interior, airbag system and multi-body (MB) mathematical dummy model. Due to complexity of the airbag system, the simulation model is validated in terms of the injury criteria with similar simulation and experimental study by Kamiji et al. [15]. Once the validation is completed, the first part of the study involves investigating the effect of one factor on one output (injury level) through multiple simulation iterations. The second part of this study is focused on the development of the response surface methodology (RSM) to investigate the interactions of several factors and their relationship with the injury responses. The RSM is developed using the statistical tool,

Design Expert 7 [21]. The regression model generated from the RSM can be used to predict and optimize any response of interest without the need for simulation runs.

Based on the main factors reported, the factors under considerations are the friction between airbag and dummy, OOP test configurations, fabric permeability and its range of interest are listed in Table 5.1.

Table 5.1. The DoE Factors and Variables

Design Factors	**Range of Variables**
Friction coefficient, μ	0.00, 0.20, 0.40, 0.60, 1.00
Fabric permeability, $\wp$	0.02, 0.04, 0.06, 0.10
OOP test positions	Position 1, Position 2

5.3.1 Vehicle interior and airbag model for evaluating injuries to OOP occupants

The vehicle model setup for this study consists of a simple representation of a generic vehicle interior. The vehicle's interior components, as shown in Figure 5.2(a), include a windshield, airbag system, dashboard, solid bench and floor. The windshield and dashboard components are of extreme importance in determining the response of the airbag because the inflated airbag typically takes the shape of these components. Figure 5.2(b) illustrates the dimension parameter of the test layout. The height and depth of the airbag system relative to the head's center of mass is 0.21m and 0.23m respectively and the airbag deploying angle is 84 degrees. The airbag system used in this study is a top-mounted system. The kinematics of the airbag system is represented in Figure 5.3 and it is clearly shown that the airbag began to take the form of the opening between the windshield and the dashboard after 30ms of deployment time.

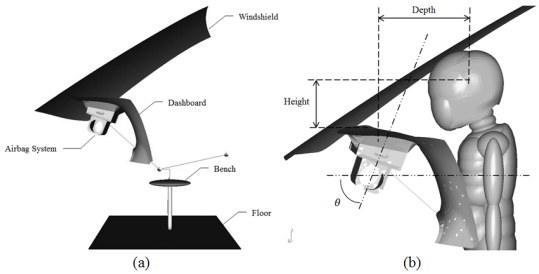

Figure 5.2. (a) Vehicle components (b) Dimensional parameters of OOP simulation setup

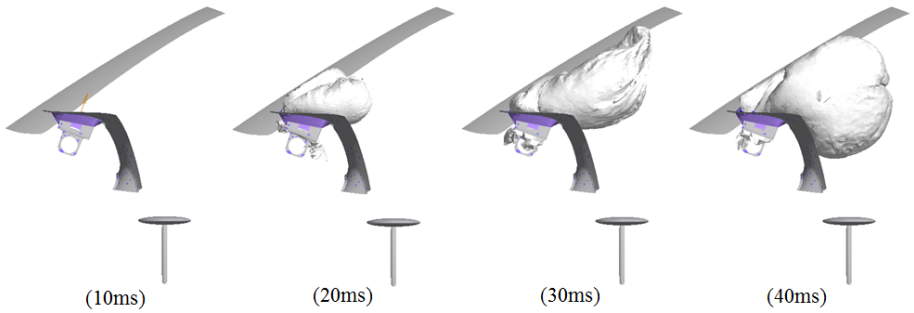

Figure 5.3. Kinematics of the deployment of frontal airbag

5.3.2 Validation of airbag model using injury criteria

The airbag model is simulated and validated with similar study by Kamiji et al. [15] using a Hybrid-III 3-year old dummy in OOP position 1. Figure 5.4 shows the similarity of the model setup from Kamiji et al. [15] and from this study. Due to the lack of specification for airbag system deployment angle, the angle of the windshield and distance of the dummy relative to the airbag system, assumptions are made and the design parameters are adjusted to match the overall kinematics of the head and the dynamic forces acting on the neck with the published data.

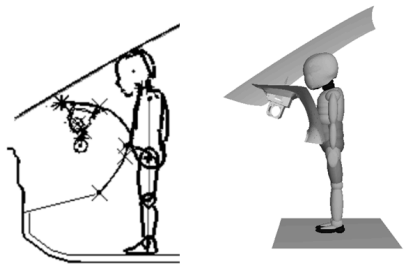

Figure 5.4. Model setup for airbag simulation on out-of-position 3-year old dummy from Kamiji et al. [15] (left) and from this study (right)

The friction coefficient between the airbag and the dummy model is set at 0.3 and the fabric permeability is set at 0.06. Figure 5.5(a) and (b) illustrates the simulated kinematic responses from Kamiji et al. [15] and this study respectively. It can be seen that the head is only slightly rotated at 20ms. At 30ms, the kinematic of the upper torso and the head suggest that the airbag is fully deployed and has full contact with the dummy's thoracic body region. At 40ms, the airbag forced the upper torso to rotate backward further. From this validation

analysis, it is found that the dummy's kinematics responses are very sensitive to small changes in friction coefficient and fabric permeability.

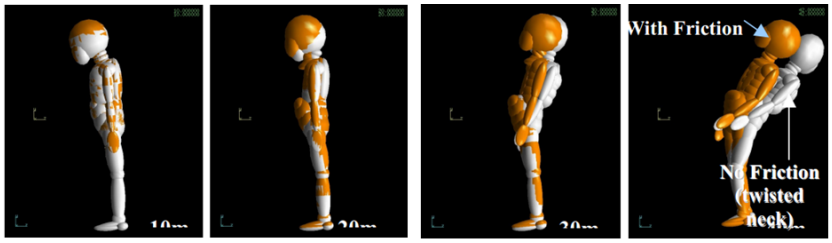

(10ms) (20ms) (30ms) (40ms)

a) Simulated kinematics for the 3-year old from Kamiji et al. [15]

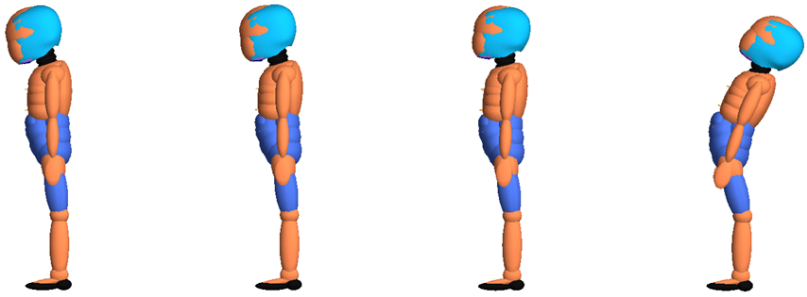

(10ms) (20ms) (30ms) (40ms)

b) Simulated kinematics for the 3-year old from this study

Figure 5.5. Simulated kinematics for the out-of-position 3-year old dummy model in position 1 configuration

The comparison of the neck loadings can be seen in Figure 5.6(a) and (b). It is shown that the performance of the 3-year old's injury responses correlates well with experimental and simulation results by Kamiji et al. [15]. The peak neck moment from this study correlates very well with Kamiji's experimental results. While the neck moment from Kamiji's simulated and experimental results begin shortly after 10ms, the simulated neck moment from this study begin at a later time of 17ms. Similarly, the neck force shows reasonable correlation with experimental and simulation results from Kamiji et al. [15]. Additionally, it can be seen that the dynamic responses from this study falls within the window of the experimental and simulated results from Kamiji et al. [15]. Therefore, the numerical model developed for this study is suitable for examination of the injury responses for the 3-year old.

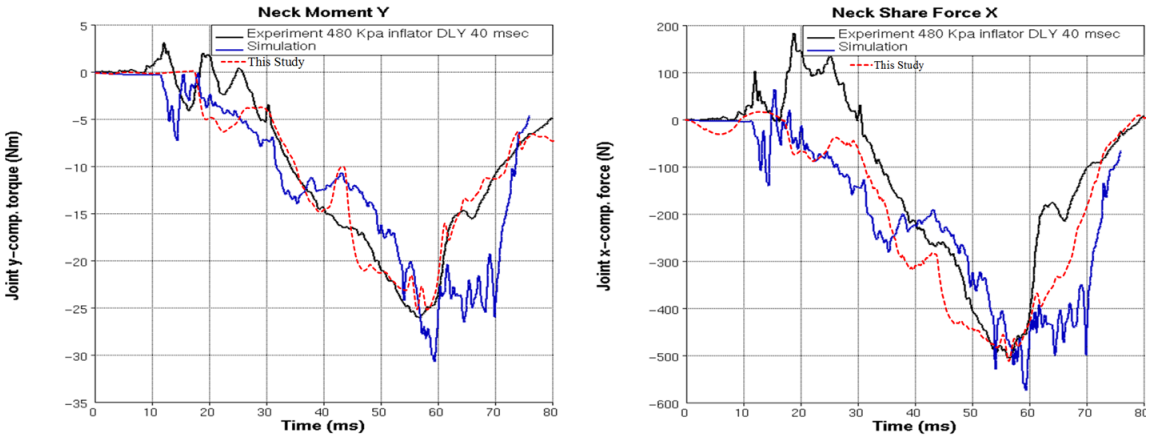

(a) (b)

Figure 5.6. Comparison of the dynamic responses of the 3-year old's neck from this study and from Kamiji et al. [15]: (a) neck y-moment ; (b) Neck x-force from this study and from Kamiji et al.

5.4 Results and Discussions

To avoid repetitive graphs, the kinematics for the 3-year old OOP test with the friction coefficient of 0.5 and fabric permeability of 0.06 for test positions 1 and 2 are illustrated in Figure 5.7(a) and (b). The airbag fabric is made transparent to increase clarity. It can be seen from the simulated kinematics that potentially high injury levels are expected to the 3-year old head and neck body regions. In general, neck injuries of type tension-extension or hyperextension is expected where the head is accelerated backwards and tension force at the lower neck. Therefore, analyzing the injury responses at the head and neck body regions are of primary interest in this study.

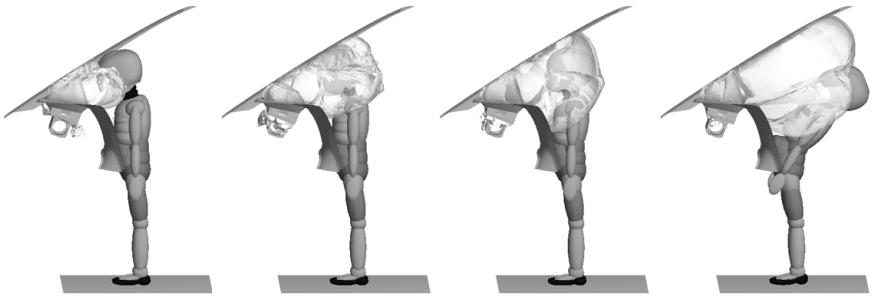

a) Simulated kinematics for position 1 from this study

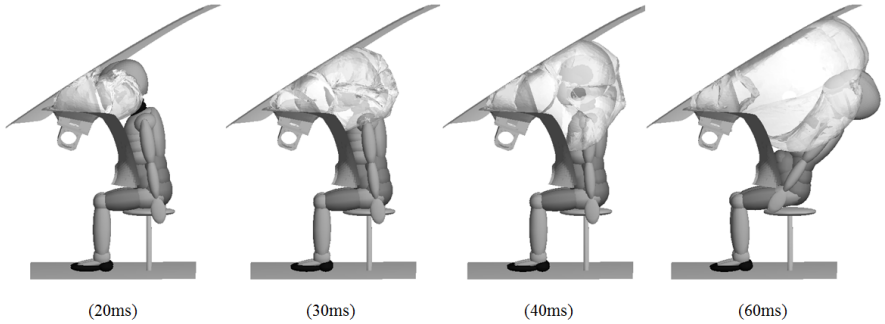

b) Simulated kinematics for position 2 from this study

Figure 5.7. Simulated kinematics for position 1 and position 2 with friction of 0.5 and fabric permeability of 0.06

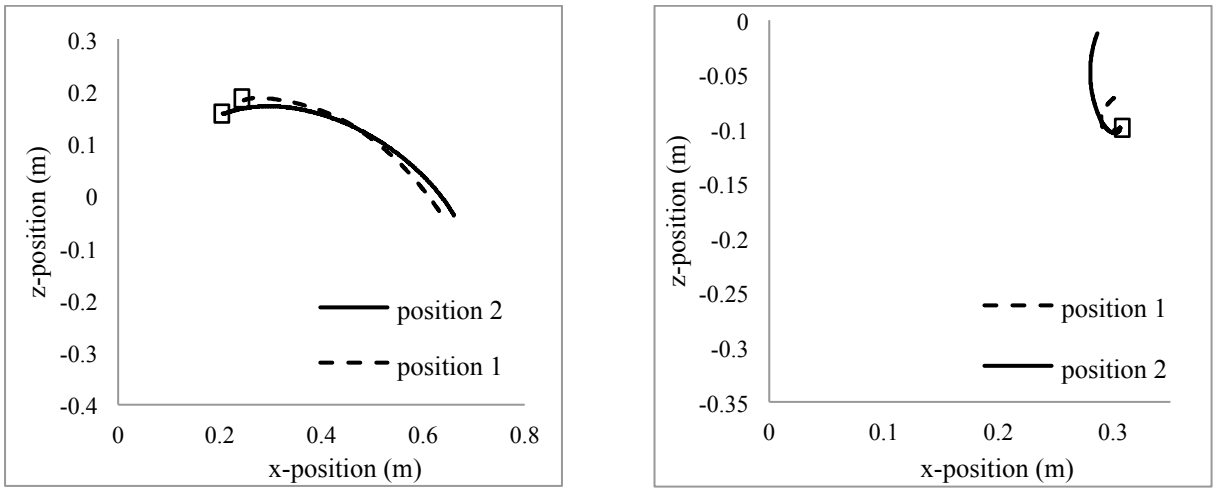

(a) (b)

Figure 5.8. Head and pelvic trajectories with friction of 0.5 and fabric permeability of 0.06: (a) path of head ; (b) path of pelvic

The path of the head and pelvic body with friction and permeability set to 0.5 and 0.06 respectively is illustrated in Figure 5.8(a) and (b). Each trajectory is plotted from 0 to 80ms with respect to the original coordinate system that is located at the airbag module. It can be seen that the head trajectories for both positions are quite similar in shape and magnitude. On the other hand, the trajectory of the pelvic for both positions suggests that the torso and pelvic body regions undergo upwards counter-clockwise rotation. The displacement and rotation of the pelvic for position 2 is larger than that of position 1. The generic rotational response of the three body regions for the two test positions are illustrated in Figure 5.9. The rotation of the upper body and tibia are approximately the same for both test cases, the

rotation of the femur for position 1 is minimal while the femur is rotated counter-clockwise and upwards for position 2.

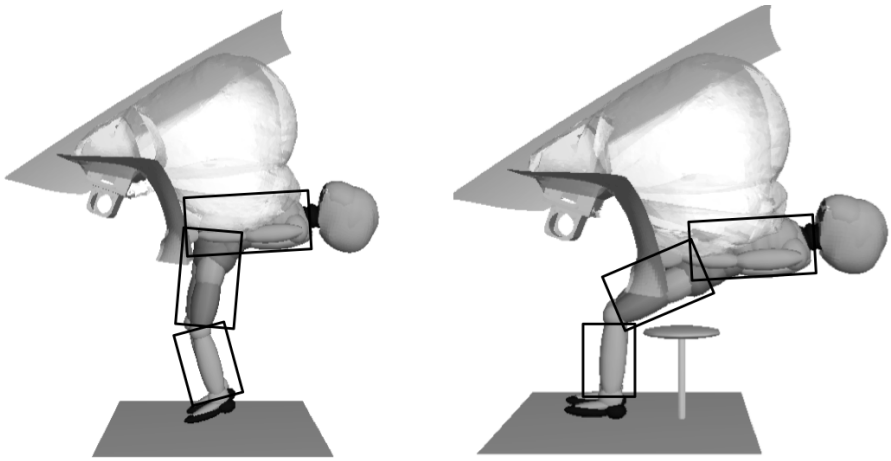

(a) (b)

Figure 5.9. After-impact configuration (80ms) with friction of 0.5 and fabric permeability of 0.06. (a) position 1 ; (b) position 2

The ATD Injury Assessment Reference Value (IARV) for the 3-year old child is used to evaluate the occupant injuries for all scenarios. The value of 570 has been specified for the HIC_{36} as the threshold associated with severe injuries for 3-year old. Similarly, the N_{ij} value of 1.0 and lower neck tension and compression loadings of 1130N and 1380N are the injury thresholds for the neck region [22]. Since the primary impact of the airbag is on the head and neck as shown in the kinematics figure, the injury assessments are focused only on the head and neck regions. The complete simulated injury levels are tabulated in Table 5.2 and 5.3. The red highlights as seen in these tables indicates injury level above the IARV threshold and the yellow highlights indicates that the injury level is within 80 percent of the IARV threshold. Conjointly, the graphical interpretations of the influence of these three factors under investigation are shown in Figures 5.10 (a) – (h).

The simulated results show that the HIC_{36} increases with higher friction coefficient and lower fabric permeability for both OOP test configurations. Although the simulated kinematics showed that the neck should undergo hyperextension type of injuries, the complete analysis indicates that the neck may also undergo compression loading due to the

influence of membrane force. The influence of membrane forces will be discussed later. Regardless of friction and fabric permeability levels, it is shown that neck tension loading generally occurs at test position 2 and compression loading tends to favor test position 1. Both neck axial loadings decreased with increasing fabric permeability. In the case of neck injury criteria, N_{ij}, it is shown that N_{ij} values, ranging from 0.2 to 1.0, increases with higher friction for position 2, but have reverse effect for position 1. On the other hand, the N_{ij} values are generally lower with higher fabric permeability. In general, the injury levels are higher in position 2 compared to position 1 mainly due to the closer positioning of the dummy relative to the airbag system.

Table 5.2. Influence of friction coefficient on injury levels

	Position 1				**Position 2**			
Friction	HIC_{36}	N_{ij}	Tension (N)	Compression (N)	HIC_{36}	N_{ij}	Tension (N)	Compression (N)
0.00	159	1.69	576	2908	198	1.23	719	1989
0.25	154	1.66	518	2309	429	0.83	1069	298
0.50	786	0.73	1319	356	698	1.02	1256	5
0.75	796	0.75	900	813	941	1.21	1685	5
1.00	825	0.8	855	1101	1043	1.31	1920	151

Table 5.3. Influence of fabric permeability on injury levels

	Position 1				**Position 2**			
Permeability	HIC_{36}	N_{ij}	Tension (N)	Compression (N)	HIC_{36}	N_{ij}	Tension (N)	Compression (N)
0.02	485	2.42	1167	3410	1110	1.25	1764	66
0.04	331	2.03	900	2835	915	1.46	1723	5
0.06	198	1.3	787	1738	198	0.83	1100	5
0.08	41	1.3	211	1939	231	0.60	580	141
0.10	66	0.35	308	342	117	0.52	555	6

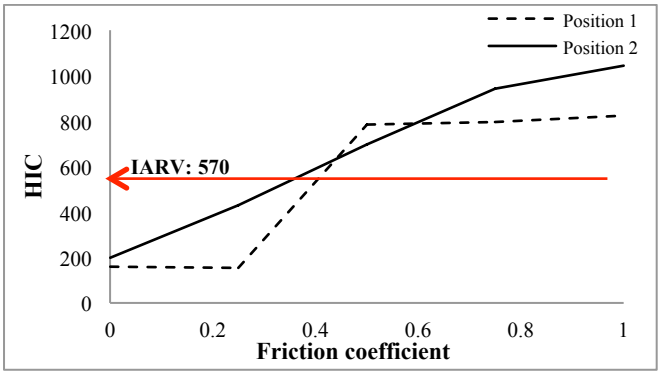

(a) Influence of friction on HIC_{36}

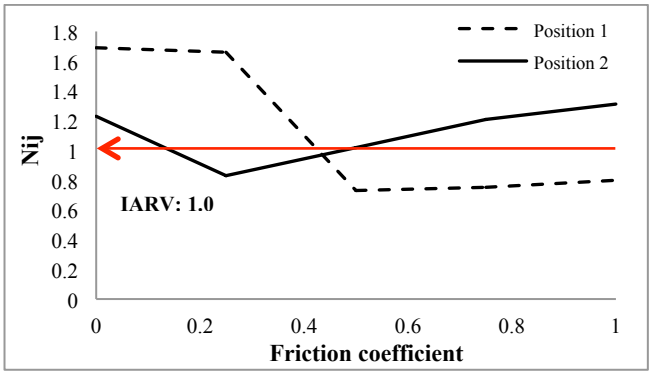

(b) Influence of friction on N_{ij}

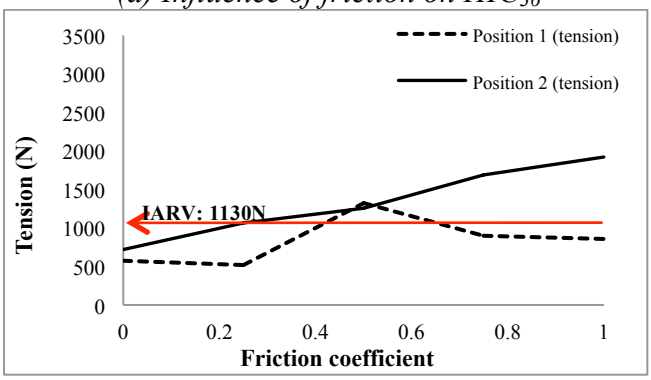

(c) Influence of friction on neck tension

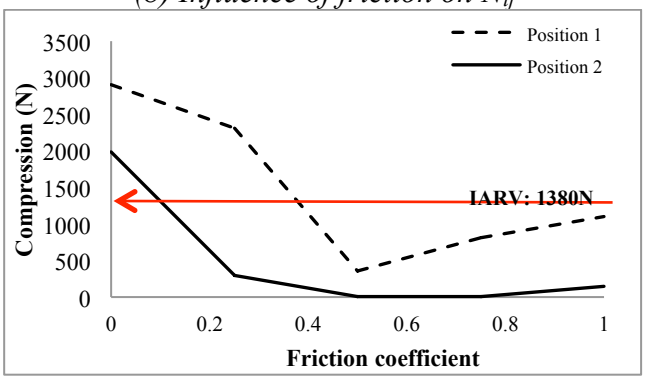

(d) Influence of friction on neck compression

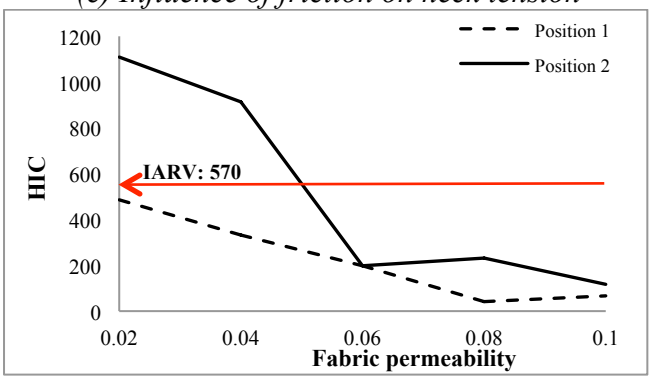

(e) Influence of fabric permeability on HIC

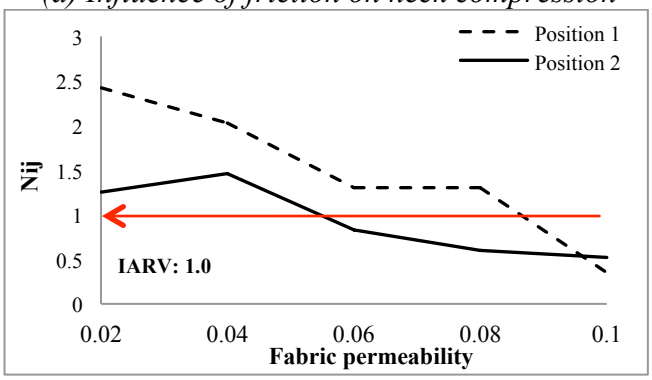

(f) Influence of fabric permeability on N_{ij}

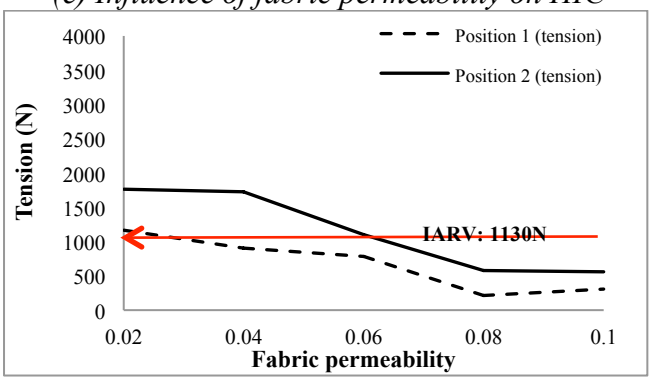

(g) Influence of fabric permeability on neck tension

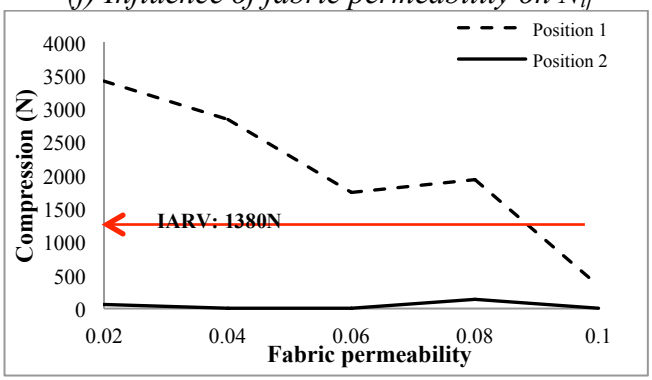

(h) Influence of fabric permeability on neck compression

Figure 5.10. 3-year old OOP occupant test for various injury levels under the influence of the three factors

5.4.1 Influence of membrane force

As discussed previously, the expected injury loading to the neck is of type hyperextension where the neck is accelerated and rotated backwards by the deploying airbag. However, previous analysis from this study proved that this does not hold true for all scenario. Membrane force or phase is a process that occurs later in the airbag deployment stage that typically acts above the center of gravity of the head and generate a download force.

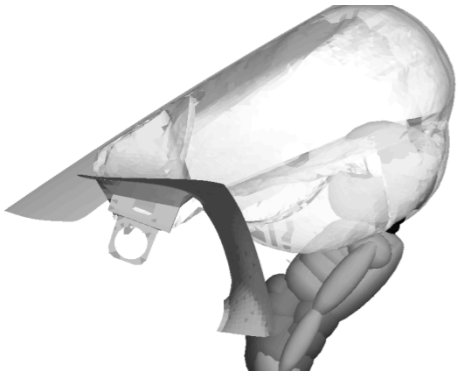

Figure 5.11. Effect of membrane force at 60ms after deployment, position 2, friction of 0.25 and permeability of 0.06

Figure 5.11 represents the effect of membrane force in generating compression loading to the neck. It is shown that the membrane force moved to wrap around and depressed the head. Hence, compression loading is generated. In addition, it is shown from previous analysis in this study that the membrane force is more significant for OOP test position 1 compared to test position 2. It is demonstrated that as friction coefficient between the dummy and the airbag reduces, the tendency of the deploying airbag to slide above the head, taking the shape of the head, increases. Additionally, as the fabric permeability increases, the chances for a compression loading due to membrane force increases. In test position 2, where the head is positioned closer to the airbag module, the punch out force typically forces the head to rotate backwards more quickly than that of position 1; hence, the chances of membrane force effect is lesser. The effect of membrane force on the occupant

seems to be strongly influenced by the occupant's vertical position especially if the occupant's initial head position is below the airbag module.

5.4.2 Prediction model using response surface methodology

Traditionally, typical experiments are designed to evaluate the effect of one variable on one response. As such, the relationships between factors are ignored and predicting the effect of combined parameters on a particular response poses considerable challenges. Therefore, the D-optimal response surface method (RSM) can be used to establish a relationship between multiple inputs (factors) and outputs (responses) that can be used to predict a response(s), and also to optimize the design. The D design is particularly suitable because the qualitative factors have more than two levels. Additionally, the necessary simulation runs for a D design are always lower than traditional full- or fractional factorial designs. In this study, the design model is of type quadratic and the fitting of the regression model takes the form of:

$$y = \beta_0 + \beta_1 x_1 + \beta_2 x_2 + \beta_3 x_3 + \beta_{11} {x_1}^2 + \beta_{22} {x_2}^2 + \beta_{33} {x_3}^2 + \beta_{12} x_1 x_2 + \beta_{13} x_1 x_3 + \beta_{23} x_2 x_3 + \epsilon \quad (5.1)$$

where y is the response; β_i and x_i $(i = 1,2,3)$ are the vector of unknown coefficient and factors. With the consideration of model such as (1), the relationship between y and x_i can be used to predict response values over a range of control variables. Additionally, optimization of the response can be determined by observing the settings of x_i that result in the maximum or minimum over a region of interest. More information on the mathematical basis of the D design can be found in [23, 24].

The injury levels sustain by the 3-year old in an OOP test can be determined using the polynomial model. To avoid repetitive figures, Figure 12(a) and (b) depict the response surfaces for the lower neck tension for OOP test position 1 and 2. These figures are plotted based on the third degree polynomial model interaction between the selected factors and the lower neck tension loading. In broad terms, the injury response can be optimized (minimize)

with low friction and high fabric permeability. Similarly, the fitted model also suggest that the dummy experienced generally higher neck tension in OOP test position 2 when compared to OOP test position 1. The various injury level of the dummy can be drawn based on similar methodology as listed in Table 4. All the DoE fitted model listed in Table 4 yielded high R-square indicating a good prediction model where all the injury levels are well fitted within the regression lines.

Table 5.4. The fitted model for 3-year old injury level

HIC_{36}	Position 1	$1238.5 + 1992.6\mu - 27923.9\mathcal{p} - 17850.8\mu\mathcal{p} - 34.6\mu^2 + 150130\mathcal{p}^2$
	Position 2	$973.3 + 2805.8\mu - 22633.23\mathcal{p} - 28692.8\mu\mathcal{p} - 34.5\mu^2 + 150135\mathcal{p}^2$
N_{ij}	Position 1	$2.9 - 3.2\mu - 19.1\mathcal{p} + 11.7\mu\mathcal{p} + 1.97\mu^2$
	Position 2	$2.3 - 2.3\mu - 19.1\mathcal{p} + 12\mu\mathcal{p} + 1.8\mu^2$
Neck Tension (N)	Position 1	$1542.1 + 1001.4\mu - 15323.5\mathcal{p} - 11456.8\mu\mathcal{p} - 1262.6\mu^2 + 20526.6\mathcal{p}^2\mu$
	Position 2	$1676.6 + 1709.2\mu - 15323.5\mathcal{p} - 11456.8\mu\mathcal{p} - 1262.6\mu^2 + 20526.6\mathcal{p}^2\mu$
Neck Compression (N)	Position 1	$5618.5 - 15861.81\mu - 42150\mathcal{p} + 194178\mu\mathcal{p} + 13099\mu^2 - 179764\mathcal{p}^2$
	Position 2	$3898.8 - 15861.81\mu - 42150\mathcal{p} + 194178\mu\mathcal{p} + 13099\mu^2 - 179764\mathcal{p}^2$

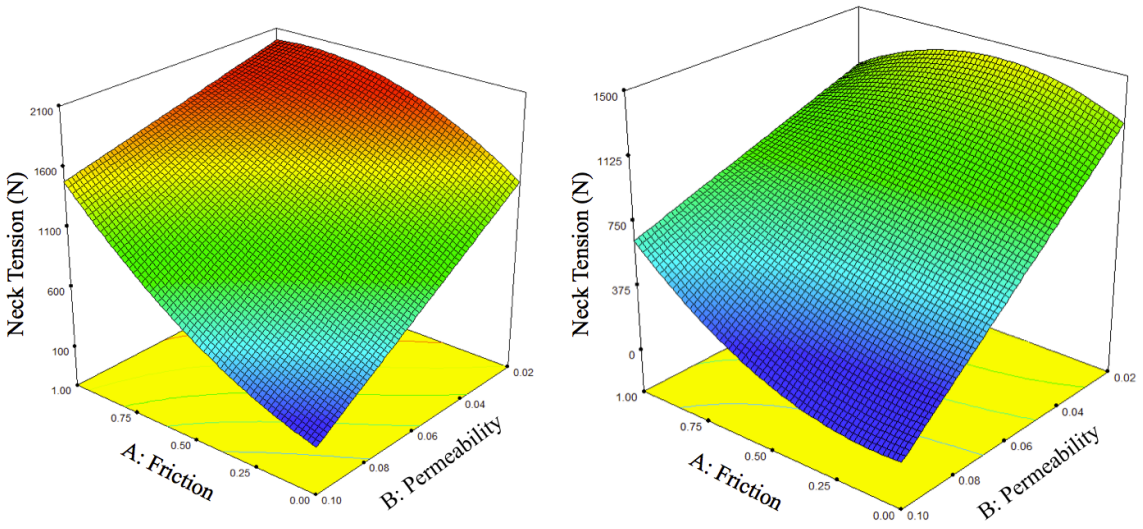

(a) (b)

Figure 5.12. Response surface for neck tension: (a) position 1 ; (b) position 2

In order to examine the accuracy and the robustness of the prediction model, the observed injury levels obtained from MADYMO simulated are compared to the fitted model as shown in Tables 5.5 - 5.8. Four test scenarios are randomly selected for each injury category. It is shown that the prediction model is able to predict the HIC_{36} values, the lower neck tensions and N_{ij} values to within 10 percent of the observed value. This reinforces the confidence in the predictive capability of the fitted model. Next, it is observed from Table 8

that the lower neck compression prediction model is the least robust. The high percentage of error at the OOP test position 2 indicated that the prediction model is not acceptable for estimating the neck compression. In previous discussion on the topic of membrane force, it is demonstrated that OOP occupants are susceptible to membrane force at combination of low friction and high permeability. The high percentage error in the neck compression are of this factor combinations. Additionally, it is shown that neck compression is negligible in test position 2. Hence, the neck compression analysis for position 2 is a gray area. The prediction model of the neck compression showed good correlation between the predicted values and observed values at OOP test position 1.

Table 5.5. Predicted versus observed HIC_{36} injury level

	OOP Position 1		OOP Position 2	
	μ=0.3 p=0.02	μ=0.6 p=0.03	μ=0.25 p=0.06	μ=0.6 p=0.03
Observed HIC_{36} (MADYMO)	1125	1337	429	1694
Predicted HIC_{36} (RSM)	1228	1398	425	1597
Error (%)	9.15	4.56	0.93	5.73

Table 5.6. Predicted versus observed N_{ij} injury level

	OOP Position 1		OOP Position 2	
	μ=0.4 p=0.07	μ=0.3 p=0.06	μ=0.25 p=0.06	μ=0.6 p=0.03
Observed N_{ij} (MADYMO)	1.03	1.30	0.81	1.29
Predicted N_{ij} (RSM)	0.93	1.18	0.89	1.21
Error (%)	9.71	9.23	9.88	6.20

Table 5.7. Predicted versus observed lower neck tension

	OOP Position 1		OOP Position 2	
	μ=0.5 p=0.04	μ=0.3 p=0.06	μ=0.6 p=0.03	μ=0.4 p=0.06
Observed Tension (MADYMO)	1083	1290	1857	1230
Predicted Tension (RSM)	1058	1245	1803	1159
Error (%)	2.31	3.49	2.91	5.77

Table 5.8. Predicted versus observed neck compression

	OOP Position 1		OOP Position 2	
	μ=0.6 $\wp$=0.03	μ=0.1 $\wp$=0.06	μ=0.1 $\wp$=0.08	μ=0.25 $\wp$=0.06
Observed Comp. (MADYMO)	1099	1838	333	298
Predicted Comp. (RSM)	1106	2024	481	361
Error (%)	0.64	10.12	44.44	21.14

5.5 Conclusion

This study demonstrated the ability of the response surface methodology to adequately describe the injury responses of OOP children from a frontal deploying airbag. For this purpose, a generic facet vehicle interior was developed using the MADYMO multi-body dynamic code. The injury levels for the 3-year old dummy in an OOP scenario were predicted from the numerical model, and the results were validated with similar experimental and simulated study reported in the literature. The validated model was then used for a parametric study to analyze the effects of individual variables on the injury response of the dummy. The factors or variables identified in this study include the fabric permeability, the friction between dummy and airbag, and OOP test positions.

Overall, the results from the parametric study of the influence of one factor on the injury response indicated that low friction between the airbag and the dummy and high fabric permeability caused significantly lesser injury to the head and neck body regions of the 3-year old. However, the neck axial compression was found to be highly sensitive to the airbag membrane force, which can occur at low friction coefficient and high fabric permeability. It was also shown that the axial loadings vary for each setup configurations. It is important to note that the material selection of the airbag influence its friction and permeability coefficients.

Finally, a regression model generated from the response surface was developed to predict the injury responses of the 3-year old. The response surface method was used to quantify the

relationships between the multiple factors on the injury responses. It was shown the N_{ij}, HIC_{36} and lower neck tension loadings of the observed values correlated well with the prediction model. The prediction model for the neck compression loading were the least robust as it did not predict the dummy's compression loading in OOP test position 2. It was concluded that the compression loading were caused by the membrane phase of the airbag. Overall, the prediction model is proven to be adequate in the predicting the injury responses for the OOP 3-year old child. By taking advantage of the predictive capability of the response surface method, the injury levels sustain by 6-year old and smaller females can also be investigated. Further research may also include a more detail study on quantifying the influence of membrane forces in affecting the dynamic responses of the occupant.

5.6 References

[1] US. National Highway Traffic Safety Administration (NHTSA), 2012, "An Analysis of Recent Improvement to Vehicle Safety," DOT HS 811 572, Washington, DC.

[2] US. National Highway Traffic Safety Administration (NHTSA), 2009, "Lives Saved Calculations for Seat Belts and Frontal Air Bags," DOT HS 811 206, Washington, DC.

[3] US. National Highway Traffic Safety Administration (NHTSA), 2012, "Lives Saved in 2011 by Restraint Use and Minimum Drinking Age Laws," DOT HS 811 702, Washington, DC.

[4] Kindelberger, J., Chidester, A., Ferguson, E, 2002, "Air Bag Crash Investigations," 18th International Technical Conference on the Enhanced Safety of Vehicles, Paper No. 299, Nagoya, Japan.

[5] Prasad, A. K., Samaha R. R., Louden, A., 2002, "Side Air Bag Research: Static Testing of Side Impact Air Bags Using Three and Six Year Old Hybrid III Dummies and the 12 Month CRABI Dummy," National Highway Traffic Safety Administration, Washington, DC.

[6] Rains, G. C., Prasad, A., and Summers, L., 1998, "Assessment of Advanced Air Bag Technology and Less Aggressive Air Bag Designs Through Performance Testing," 16th International Technical Conference on the Enhanced Safety of Vehicles, Paper No. 98-S5-0-06, Windsor, Canada.

[7] Bass, C. R., Crandall, J. R., and Pilkey, W. D., 1998, “Out-of-Position Occupant Testing (OOPS3 Series),” University of Virginia, Automobile Safety Laboratory.

[8] Noureddine, A., Digges, K., Eskandarian, A., and Bedewi, N., 1998, "Analysis of airbag depowering and related parameters in out of position environment," *International Journal of Crashworthiness, 3:3, 237-248, DOI: 10.1533/cras.1998.0073.*

[9] Agaram, V., Kang, J., Nusholtz, G., Kostyniuk, G., 2001, “Hybrid III Dummy Neck Responses to Air Bag Loading,” 17th International Technical Conference on the Enhanced Safety of Vehicles, Paper No. 469, Amsterdam, The Netherlands.

[10] ISO, 1998, “Road Vehicles – Test procedures for evaluation out-of-position vehicle occupant interactions with deploying air bags,” ISO/TR 10982:1998.

[11] Prasad, A., Maltese, M., and Louden, A., 2002, “Injury Risks From Advanced Air Bags in Frontal Static Out-of-Position Tests," 18th International Technical Conference on the Enhanced Safety of Vehicles, Paper No. 427, Nagoya, Japan.

[12] Prasad, A., Louden, A., and Pack, R., 2003, “Evaluation of Frontal Air Bag Performance,” 19th International Technical Conference on the Enhanced Safety of Vehicles, Paper No. 05-0395, Washington, DC.

[13] Watson, B. and Cronin, D. S., 2011, "Side impact occupant response with varying positions," *International Journal of Crashworthiness, 16:5, pp. 569-582, DOI:10/180/13588265.2011.616079.*

[14] Annonymous, “Air Bag Aggressiveness Testing,” National Highway Traffic Safety Administration, Washington, DC.

[15] Kamiji, K., and Kawamura, N., 2001, “Study of Airbag Interference with Out-of-Position Occupant by Computer Simulation” 17th International Technical Conference on the Enhanced Safety of Vehicles, Paper No. 374, Amsterdam, The Netherlands.

[16] Park, W., and Hong, S., 2004, “A study on the modeling technique for the passenger OOP simulation,” 10th International MADYMO Users Meeting Conference.

[17] Khan, M.U., and Moatamedi, M., 2008, "A review of airbag test and analysis," *International Journal of Crashworthiness, 13:1, 67-76, DOI: 10.1080/13588260701731674*

[18] Roychoudhury, R., Sun, D., Hamid, M. and Hanson, C., 2000, “5th Percentile Driver OOP computer simulation”, SAE 2000 World Congress, Detroit, Michigan.

[19] Rekveldt, M., 2002, “Airbag Modeling for Out-of-position: Numerical Approach and Advance Airbag Test”, MADYMO User Conference 2002.

[20] MADYMO model manual, Release 7.4.1, TNO Road-Vehicles Research Institute, January 2012.

[21] Design-Expert, Release 7, Sate-Ease – Statistics Made Easy. www.stateease.com

[22] Lund, A. K., 2003, "Recommended Procedures for Evaluating Occupant Injury Risk from Deploying Side Airbags," A joint project of Alliance, AIAM, AORC and IIHS. Insurance Institute for Highway Safety, Arlington, Virginia.

[23] Khuri, A. L., and Mukhopadhyay, S., 2010, "Response Surface Methodology," Wiley Interdisciplinary Reviews: Computational Statistics, Vol. 2, Issue 2., pp.128-149.

[24] Chu, Y., Han, I., and Han, C., 2002, "Improved Evolutionary Operation Based on D-optimal Design and Response Surface Method," *Korean J. Chem Eng. 19(4), pp.535-544.*

CHAPTER SIX

FINITE ELEMENT APPROACH IN ESTIMATING DRIVER FATALITY RATIO OF A FLEET OF LTV STRIKING A PASSENGER CAR BASED ON VARIOUS OBJECTIVE MEASUREMENTS IN SIDE-IMPACT ACCIDENTS

6.1 Introduction

Many investigators has examined many mathematical models for describe the behavior of multi-vehicle crashes. Some traditional methods used to understand vehicle collisions are the spring-damper model, piecewise linear stiffness method and hybrid lumped mass model. To date, the most accurate method of presenting the non-linear behavior of vehicle crashes is through the use of finite element methods. The response of the vehicles in multi-vehicle crashes is influenced by their structural stiffness, mass and physical geometry. These parameters then influence the severity of the crash. The crash compatibility of multi-vehicle is a subject devoted to examine and quantify the crash severity of vehicle-to-vehicle crash. Examples of crash situations that give rise to incompatibility are: a small passenger car colliding with a large car or trucks (LTVs); a collision of a passenger car or LTVs with pedestrian or cyclist.

Issues on multi-vehicle collisions and its affect on the crash compatibleness need to be investigated to further improve the crashworthiness of future vehicles. Incompatible crash behavior can be approached in three distinct ways, namely, geometrical compatibility, stiffness compatibility and mass compatibility [1]. Many investigators have conducted researches on the compatibility and aggressivity of vehicles using experimental and computer simulations. Moradi et al. [2] that the mass ratio between two colliding vehicle in frontal crashes cannot be utilized to accurately define the occupants relative fatality risks. In another

[5] Part of this chapter will be published in the following source:
Y.Y. Tay, A. Papalatha, L.V.S.P.C. Koneru, R. Moradi, and H.M. Lankarani, "A Finite Element Approach in Estimating Driver Fatality Ratio of a Fleet of LTV Striking a Passenger Car Based on Vehicle's Intrusion, Acceleration and Stiffness Ratios in Side-Impact Accidents," *Journal of Mechanical Science and Technology,* 2014.

study conducted by Moradi et al. [3], they examined and quantified the geometrical characteristics of a large truck with side-guard with the injury potential of occupants in the small car, and it was shown that installation of side guards for large trucks are essential for reducing injury risks and intrusion into the passenger cabin of the small car. Watanabe et al. [4, 5] demonstrated the effect of stiffness matching on crash compatibility for SUVs-to-passenger cars and concluded that structural deformation can be reduced by matching the stiffness on both cars but could worsen at higher impact speeds. In addition, Hirayama et al. [6] designed a set of experimental aimed at investigating the crash compatibility of light cars with and without multiple load paths striking a heavy car. It was shown that light cars with multiple load paths are more crash compatible with heavy cars owing to better energy absorbing capability and improved structural interaction.

The goal of this chapter is investigate the relative driver fatality risks of occupants in a multi-vehicle crash. In the first part of this chapter, various mathematical models that can describe the dynamic responses and behavior of two colliding vehicles are investigated. In the second part of this study, the dynamic responses of two vehicles are accurately defined using finite element code, LS-DYNA. This is accomplished by selecting a wide-range of light trucks and vans (LTVs) as the bullet vehicle and a passenger car as a target vehicle. Next, the structural and dynamic properties of the two colliding vehicles are examined and correlated to the relative occupant fatality risks, also known as driver fatality ratio (DFR). The primary objective of this study is to propose three objective measurements in estimating the DFR, namely, by using intrusion, deceleration and stiffness ratio of two colliding vehicles. For this methodology to be consistent and accurate in predicting the DFR for vehicles that are not presented in this study, the objective measurements are combined to form a combined DFR estimation model. By carrying this methodology further, the combined DFR method is also utilized to estimate the DFR for newer passenger car. With the ability to predict DFR of

various vehicles, the proposed methodology may hold merits for optimizing the aggressivity and crash compatibility of newer vehicles with the fleet of on-road vehicles.

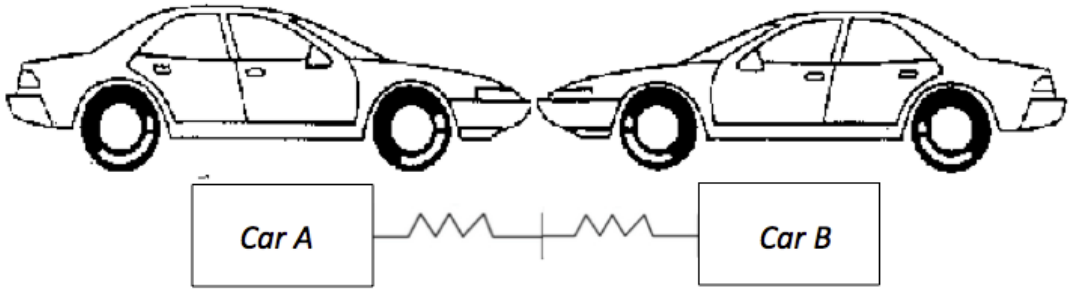

Figure 6.1. Illustration of multi-vehicle crash and its representation using a simple spring-mass model

6.1.2 Kinematics and dynamics linear stiffness

A frontal-impact accident of two vehicles is illustrated in Figure 6.1. The simplest assumption to determine the kinematics of a vehicle is to assume that the collision is purely inelastic. This assumption implies that the elastic deformations of the vehicles are neglected and the plastic deformation of the car must be large, which is the case for most vehicle crashes. Using stereomechanics and zero coefficient of restitution, the conservation of linear momentum can be described as:

$$m_a v_a + m_b v_b = v_f(m_a + m_b) \tag{6.1}$$

where m_a and v_a is the weight and velocity of the first vehicle; m_b and v_b is the weight and velocity of the second vehicle; and v_f is the final velocity of both vehicles. The closing speed or speed difference, denoted as v_c, of both colliding vehicles is basically $v_c = v_a - v_b$; hence, the ΔV for colliding vehicles is:

$$\Delta V_a = -\frac{m_b}{m_a + m_b} v_c \tag{6.2}$$

$$\Delta V_b = \frac{m_a}{m_a + m_b} v_c \tag{6.3}$$

It can be seen that if m_b is assumed to the larger and heavier vehicle, the partner vehicle will experience a higher ΔV or acceleration. Once the initial and final speed are established, the kinetic energy, K_e, at the pre- and post-crash can be expressed as:

$$K_e = K_{e,initial} - K_{e,final} = \frac{1}{2}\frac{m_a}{m_a+m_b}{v_c}^2 \tag{6.4}$$

the deformation energy, U_d, can then be determined using the conservation of energy, $E = U_d + KE = 0$:

$$U_d = \frac{1}{2}\frac{m_a}{m_a+m_b}x^2 \tag{6.5}$$

where x is the static crush or the post-crash deformation of the structure. It is important to note that the deformation energy in a multi-vehicle crash is not necessary the same for both the colliding vehicles. On the contrary, the available deformation energy, depicted by the area under the force-deflection curve, for smaller vehicle is often much lower than that for LTVs. Hence, deceleration and intrusion effects are often transmitted more to the smaller vehicle, rendering higher fatality risks to its occupants.

In addition to the preceding method in quantifying the deformation energy of a vehicle, the force-deflection method is perhaps the most widely used technique to quantify stiffness. Other parameters such as coefficient of restitution, dynamic and static crush of the structures can also be extracted from the force-deflection curve. Steyer et al. [15] showed that the force-deflection curve could be categorized in two stages, namely, the loading phase and the rebound or hysteresis phase. They indicated that the final load of the occupant cabin strength should be high enough to avoid structural collapse. For this study, only the stiffness at the loading phase is considered. To obtain the force-deflection curve, the barrier total force is recorded and plotted against the dynamic crush of the vehicle. Next, the linear slope of the curve, which represents the stiffness of the vehicle, is obtained through the least square method over a range of selected displacement. In the past, investigators have examined the

stiffness using the crush ranging from 0 to 300 mm; however, observation of real world crashes suggested that the stiffness at lower levels of crush is more accurate [16, 17]. The linear stiffness approach, as shown using Figure 6.2, uses the range of crush of 0 to 120 mm for the formulation of the linear stiffness. It is obvious that this linear stiffness approach is dependent on the range of displacement selected. The goal in crash compatibility research is to utilize this deformation energy effectively so that occupants in both colliding vehicles have analogue chances of survival, and this can be achieved by adjusting the stiffness or load paths of a car.

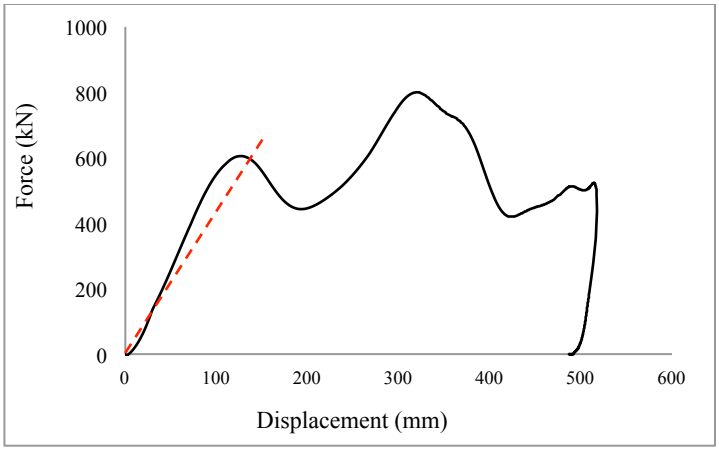

Figure 6.2. Illustration of vehicle stiffness using linear stiffness approach

Besides the linear stiffness method, the conservation of energy can be used to estimate the stiffness of a vehicle by assuming that the energy dissipated is fully converted to crush energy. In a rigid barrier crash where the common velocity is zero, the area under the force-deflection curve depicts the crush energy. Which leads to the following equation:

$$E = \frac{1}{2}mv^2 = \int_0^{c_d}(k_d x)dx \tag{6.6}$$

where m is the mass of the car; k_d is the dynamic stiffness of the car; x is the crush depth of the car and c_d is the dynamic crush of the car. This describes the loading phase of the force-crush curve; the unloading of hysteresis phase can also be derived in the similar manner. In a multi-vehicle crash, the common velocity is not zero like the rigid barrier test. The common velocity in a vehicle-to-vehicle crash can be approximated at the time of maximum dynamic

crush. During the period of common velocity at high impact velocity, the structure undergo inelastic crush and the coefficient of restitution is zero. Hence, the common velocity, v_c, can be determine with the conservation of momentum:

$$v_c = \frac{m_1 v_1 + m_2 v_2}{(m_1 + m_1)} \tag{6.7}$$

where v_i and m_i $(i = 1\,, 2)$ are the velocities and masses of both colliding cars. So, the absorbed energy can be calculated as:

$$E = \frac{1}{2} m_1 ({v_1}^2 - {v_c}^2) = \int_0^{c_d} (k_d x) dx \tag{6.8}$$

Lastly, the static stiffness can be calculated using the residual crush of the vehicle. However, static stiffness does not account for the initial elastic behavior or the hysteresis phase in the force-crush curve. The static stiffness in a rigid barrier test can be defined as:

$$k_s = \frac{mv^2}{x_s} \tag{6.9}$$

where x_s is the residual crush that can be obtained from the post-crash of the vehicle.

The National Highway of Traffic Administration (NHTSA) has devoted a test program to evaluate the force-deflection curves using experimental test for a fleet of on-road vehicles. The force-deflection curve is obtained using a full-frontal impact US-NCAP test with load-cells mounted on the rigid wall. The force-deflection curves data are available to public and are available on NHTSA's website [7].

The dynamic analysis of the multi-vehicle crash described at Figure 6.1, the motion can be assumed to be sinusoidal, and the displacement response is given as:

$$\underline{x}(t) = \frac{\Delta V}{\omega_e} sin(\omega_e t) \begin{bmatrix} 1 \\ mass_{ratio} \end{bmatrix} + v_f \begin{bmatrix} t \\ 1 \end{bmatrix} \tag{6.10}$$

where v_f is given in Equation (6.1) ; v_c is the speed difference of both vehicles ; ω_e is the natural frequency ; and $mass_{ratio}$ is the mass ratio of both vehicles. The spring system has a parallel configuration and the equivalent stiffness can be used to define the ω_e, as:

$$\omega_e = \sqrt{\frac{K_1 K_2}{(K_1+K_2)}\left(\frac{m_a+m_b}{m_a m_b}\right)} \tag{6.11}$$

Next, the velocity can be defined by differentiating Equation (6.8) and a subsequent differentiation will give the acceleration:

$$\underline{\dot{x}}(t) = \underline{v}(t) = \frac{\Delta V}{\omega_e}\omega_e cos(\omega_e t)\begin{bmatrix}1\\ mass_{ratio}\end{bmatrix} + v_f\begin{bmatrix}1\\1\end{bmatrix} \tag{6.12}$$

$$\underline{\ddot{x}}(t) = \underline{a}(t) = -\frac{\Delta V}{\omega_e}{\omega_e}^2 sin(\omega_e t)\begin{bmatrix}1\\ mass_{ratio}\end{bmatrix} \tag{6.13}$$

Now, the maximum dynamic crush of the system and its the total collision time can be defined as:

$$C = \frac{\Delta V}{\omega_e} \tag{6.14}$$

$$t_c = \frac{\pi}{2\omega_e} \tag{6.15}$$

It is very clear that the duration of the multi-vehicle crash, t_c, is a function of mass and stiffness. The determination of the kinematic and dynamic response using the linear stiffness method is highly simplified. It is obvious that the front-end structure of a vehicle is more complex, which requires multiple mass and spring system to properly define the system. The lumped parameter model provides a better approximation of the vehicle's response. Pawlus et al. [8] further developed this model to analyze other dynamic responses of the vehicle such as the loading and unloading stiffness, vehicle impact and rebound speed. Results from their study indicated quite reasonable correlation of the spring-mass model with the experimental test.

6.1.3 Characterization of vehicle crashes using lumped parameter model

Prior to the advancement in the finite element analysis, the spring-mass-model (SPM) is an efficient method of representing a vehicle's kinematics and dynamics using combinations of spring, dampers and point mass. It is important to stress that the SPM is not applicable to all crash modes since the model's formulation is based on the vehicle's crash

pulse. Figure 6.3, adopted from [9], illustrates a simplified representation of the dynamic response of a vehicle in a full-frontal crash; where m_1 and m_2 describe the chassis and the passenger compartment masses, and the energy absorbers are represented as spring stiffness, k_i, and damper coefficient, c_i (i=1,2).

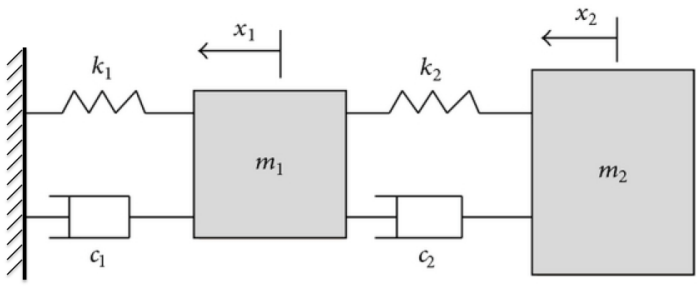

Figure 6.3. A full-frontal crash representation using spring-mass-model

The dynamic equations of motions of this PSM are:

$$m_1\ddot{x}_1 + (c_1 + c_2)\dot{x}_1 + (k_1 + k_2)x_1 - c_2\dot{x}_2 - k_2x_2 = 0 \tag{6.16}$$

$$m_2\ddot{x}_2 + c_2\dot{x}_2 - k_2x_2 - c_2\dot{x}_1 - k_2x_2 = 0 \tag{6.17}$$

To satisfy Equations (6.16) and (6.17), the solution to this ODE for x_1 and x_2 can be expressed as:

$$x_i = C_i e^{st} = \begin{bmatrix} x_1 \\ x_2 \end{bmatrix} e^{st} \tag{6.18}$$

where C_i and s are some complex numbers. And by substituting Equation (6.18) into Equations (6.16) and (6.17), the solution can be defined as:

$$R_1C_1 - R_2C_2 = 0 \tag{6.19}$$

$$Q_2C_2 - Q_1C_1 = 0 \tag{6.20}$$

where, $R_1 = m_1s^2 + (c_1 + c_2)s + (k_1 + k_2)$; $R_2 = c_2s + k_2$; $Q_2 = m_2s^2 + c_2s - k_2$; $Q_1 = c_2s + k_2$. Next, Equation (6.19) and (6.20) can be combined to form:

$$R_1Q_2 - R_2Q_1 = 0 \tag{6.21}$$

By substituting R_1, R_2, Q_1 and Q_2 into Equation (6.19) and (6.20), the matrix characteristics matrix can be formed:

$$\begin{bmatrix} m_1 s^2 + (c_1 + c_2)s + (k_1 + k_2) & c_2 s + k_2 \\ c_2 s + k_2 & m_2 s^2 + c_2 s - k_2 \end{bmatrix} \begin{bmatrix} C_1 \\ C_2 \end{bmatrix} = \begin{bmatrix} 0 \\ 0 \end{bmatrix} \tag{6.22}$$

To obtain a non-trivial solution, where C_i cannot be zero, the determinant of the LHS matrix must vanish. Hence, the final form of the solution can be represented as:

$$s^4 + ts^3 + us^2 + vs + w = 0 \tag{6.23}$$

where,

$$t = \frac{m_1 c_1 + m_2 (c_1 + c_2)}{m_1 m_2} \tag{6.24}$$

$$u = \frac{m_1 k_1 + m_2 (k_1 + k_2) + c_1 c_2}{m_1 m_2} \tag{6.25}$$

$$v = \frac{k_1 c_1 + k_2 c_2}{m_1 m_2} \tag{6.26}$$

$$v = \frac{k_1 k_2}{m_1 m_2} \tag{6.27}$$

The 4th order polynomial equation needs to be solved to obtain the four roots. The three combination of roots are given as:

a) two pairs of complex conjugates;

b) one pair of complex conjugates and two pairs real and negative roots

d) four pairs of real and negative roots.

These four roots will give the damping, frequency, amplitude and phase parameters, which can then be utilized to form a close-form displacement equation for displacement, x_1 and x_2. A detailed discussion on obtaining these parameters is discussed in [9]. Many researchers have utilized this SPM in describing the non-linear behavior of the vehicles in crashes [10, 11]. To increase the accuracy in predicting the dynamic responses of a vehicle, the SPM method can be rather complex as shown in Figure 6.4 (a) and (b).

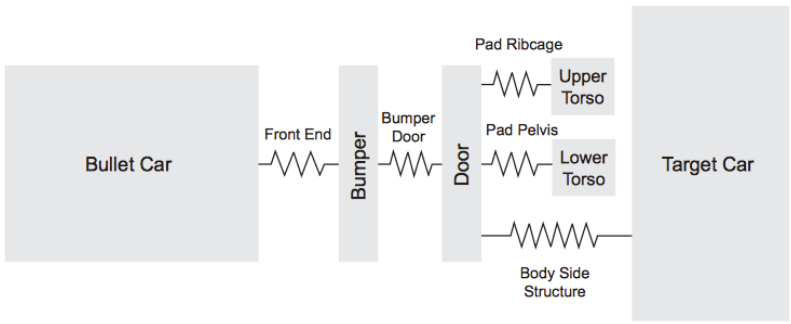

(a)

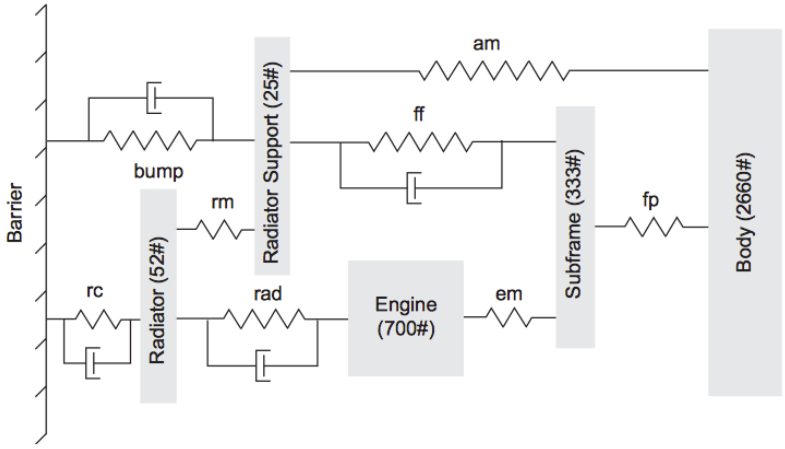

(b)

Figure 6.4. SPM for (a) multi-vehicle side-impact accident ; (b) full-frontal impact test [12]

The limitations of utilizing SPM model in predicting the response of the vehicle is that it requires prior knowledge on the stiffness and damper coefficient that can accurately define the structure of the vehicle. These parameters can be determined experimentally or obtain from pre-existing finite element models. Furthermore, the one-dimensional analysis using SPM technique is no longer sufficient for optimizing the vehicle's design. Finite element methods provide a more powerful technique in identifying the dynamic responses of the vehicle, and more. In addition, finite element methods allow a better spatial visualization of the pre- and post-crash of the vehicle model.

6.2 Applications to Multi-Vehicle Crashes using Finite Element Method

The earliest work in quantifying vehicle compatibility is introduced by Gabler et al. [1], by using the aggressivity metric method (AM). The AM method is determined through statistical crash data gathered from the Fatality Analysis Reporting System (FARS) and the General Estimate System (GES) databases to determine the number of fatalities and crashes.

More importantly, the AM method provided a general overview on the aggressiveness of a particular LTV when compared to a passenger vehicle. By establishing the concept that LTVs are highly incompatible with passenger cars, NHTSA proposed a driver fatality ratio (DFR) based on accident databases to compute the DFR for specific LTVs-to-passenger vehicle crash scenarios. The five LTVs are categorized into full size van, full size pickup, utility vehicle, minivan and small pickup [13].

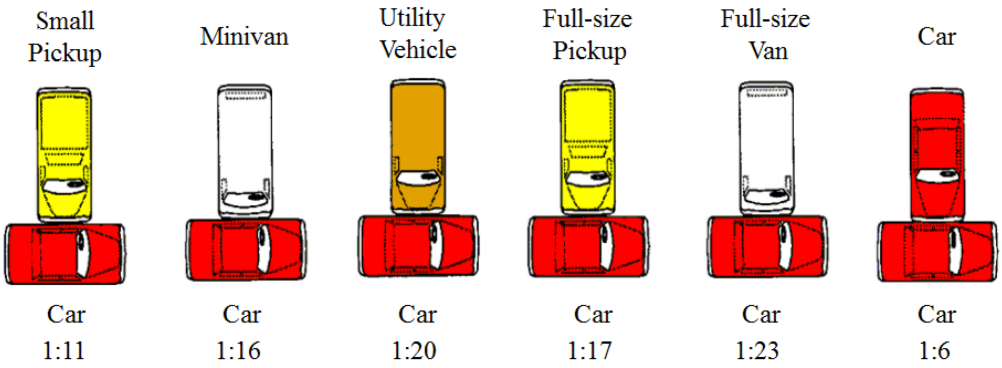

Figure 6.5. Driver fatality ratio of LTVs-to-passenger car in side-impacts accidents [14]

Figure 6.5 represents the DFR for various LTVs-to-passenger car crashes. The DFR introduced by NHTSA is based on actual FARS statistical data. In addition, the DFR is age adjusted to represent 26 – 55 year old drivers to eliminate any unreliable data [14]. Because the proposed DFR is based on actual crash data, no standard procedure is available for predicting the DFR for newer fleet of vehicles. In addition, DFR represents an overall fatality risk for each class of vehicle where differentiating the DFR for a other specific vehicle-to-vehicle crash is not possible. Therefore, it is important to develop a prediction method that can be validated using the statistical DFR provided and to predict the DFR for any specific vehicle-to-vehicle crash. A study conducted by Moradi et al. [2] proposed that passenger compartment intrusion ratio of any two colliding vehicles in a frontal-impact accident can be used to estimate the DFR. Currently, no DFR estimation model has been developed for side-impact accidents. Therefore, three objective measurements are identified, namely, intrusion ratio, deceleration ratio and stiffness ratio, of the two colliding vehicles in side-impact

accident to form a combined DFR estimation model. The side-impact accident reconstruction is conducted using the finite element solver, LS-DYNA.

6.2.1 Objective measurements in estimating DFR

Three objective measurements are identified to have high influence to the DFR. In the first proposed method, the use of intrusion ratio in estimating DFR is a relatively straightforward process. The intrusions into the bullet and target vehicles are measured at various locations and the intrusion ratio determines the estimated DFR. Due to the diverse design of different cars, some structural components might be in the direct loading path of the crash or might be of different stiffness. Hence, it is crucial to obtain the intrusion measurements from as many locations as possible. The intrusion to the target vehicle is measured at the B-pillar at three different locations, namely, the cushion reference point, the window sill point and the head reference point. Equivalently, the intrusion to the bullet vehicle is measured at the engine top, the foot-well or lower occupant compartment and at the A-pillar. Illustrated in Figure 6.6 is the graphical representation of the locations for measuring intrusions.

The second proposed method is depicted by the deceleration ratio transmitted between the target and bullet vehicles. Similarly, the transmitted deceleration values are measured using accelerometers located at three locations for both the target and bullet vehicles as illustrated in Figure 6.7, the accelerometers are located at three locations for both the target and bullet vehicles. Due to the inaccuracy of measuring the deceleration from nodal or element points of the vehicle model, solid rigid-bodies are created to represent the accelerometers. By measuring deceleration values from the rigid-body accelerometers, noisy and unreliable data can be eliminated. Equations (6.28) and (6.29) represent the intrusion ratio and the deceleration ratio:

$$DFR_{estimate}^{intrusion} = \alpha \left(\frac{Intrusion\ depth\ in\ the\ bullet\ vehicle}{Intrusion\ depth\ in\ the\ target\ vehicle} \right) \tag{6.28}$$

$$DFR_{estimate}^{deceleration} = \beta\left(\frac{Deceleration\ of\ the\ bullet\ vehicle}{Deceleration\ of\ the\ target\ vehicle}\right) \quad (6.29)$$

where α and β represent the unknown weight factor for vehicle's intrusion depth and deceleration. The third proposed method of estimating DFR using stiffness ratio is discussed in the subsequent section.

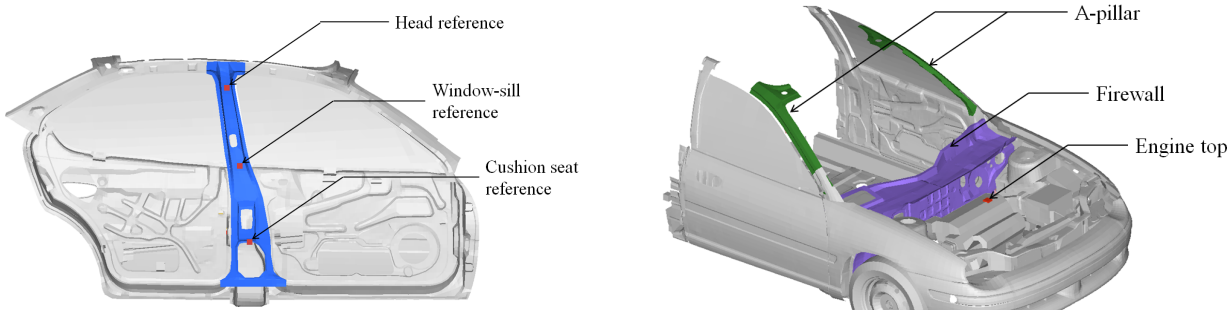

(a) (b)

Figure 6.6. Locations for measuring intrusions for (a) Target vehicle ; (b) Bullet vehicle

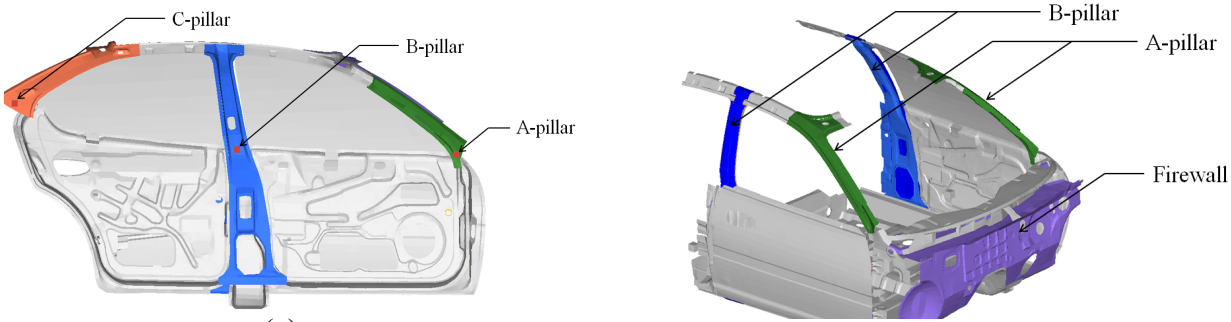

(a) (b)

Figure 6.7. Locations for measuring deceleration for (a) Target vehicle ; (b) Bullet vehicle

The third proposed method in estimating DFR is the linear stiffness method. The stiffness of a vehicle is generally higher with increasing mass, although no significant correlation has been determined. However, the concept on vehicle stiffness is a not very well defined as measuring the stiffness of a complex structure, such as a vehicle, has posted considerable challenges. A study by Gabler et al. [14] correlated the stiffness and mass of the vehicle with the aggressivity metric and it was shown that vehicles with higher stiffness and mass are generally more aggressive. In general, crashworthiness of vehicles deals with the energy absorption capability of a structure, denoted as the area under the force-displacement curve. In order to maximize this characteristic, the structures and load paths should be

arranged to deform with large volume reaching plasticity. To obtain the force-deflection curve for the bullet vehicles, the U.S. full-frontal regulatory program is utilized for the full-frontal simulation test [18]. Similarly, the force-deflection curve for the passenger car is obtained using a side-impact test in accordance to the IIHS side-impact protocol [19]. By comparing the stiffness of the two colliding vehicles, its stiffness ratio can be used to estimate the DFR. The stiffness ratio can be calculated using Equation (6.30):

$$DFR_{estimate}^{stiffness} = \gamma\left(\frac{Stiffness\ of\ the\ bullet\ vehicle, K_{Bullet}}{Stiffness\ of\ the\ target\ vehicle, K_{Target}}\right) \tag{6.30}$$

where, K_{Bullet} represents the front-end stiffness of the bullet vehicle; K_{Target} represents the side-structure stiffness of the target vehicle; and γ is an unknown weight factor for the stiffness ratio. By utilizing similar methodology by Moradi et al. [3], the intrusion ratio, deceleration ratio and stiffness ratio can be combined to estimate the DFR. Hence, the DFR can be estimated as:

$$DFR_T^B = DFR_{estimate}^{intrusion} + DFR_{estimate}^{deceleration} + DFR_{estimate}^{stiffness} \tag{6.31}$$

Using Equation (6.31), the combined DFR analysis based on these three approaches warrants lower redundancy and increases the robustness of this prediction model. By adjusting the value weight factors, α, β and γ, the relative priorities of each component in affecting the DFR can be established.

6.2.2 Finite element reconstruction for the multi-vehicle side-impact crash

The fleet of vehicles used in this study is developed and validated by National Crash Analysis Center [20]. It is reported that the NCAC's FE vehicle models are in good agreement with the NHTSA's experimental data. The finite element setup of different vehicle-to-vehicle in a side-impact crash is illustrated in Figure 6.8. Also illustrated in that figure is the categorization of the LTVs and passenger vehicle. The side-impact protocol used to reconstruct the side-impact crash is the Federal Motor Vehicle Safety Standard (FMVSS) No. 214, where the bullet vehicle strikes the target vehicle at 53.9*kph* (33.5*mph*) crabbing at

27 degrees angle. The passenger vehicle is assigned as the target vehicle and it is held constant throughout the study while the bullet vehicles are varied.

The non-linear finite element code, LS-DYNA is utilized to solve the non-linear behavior of the crash scenario. LS-PREPOST and Hyperview are the post-processing tools used to extract the results. The required boundary conditions and parameters are defined to control the stability of the numerical models. Additionally, the required contact card *CONTACT_AUTOMATIC_SURFACE_TO_SURFACE is assigned to define the contact between the bullet and target vehicle. For the vehicle-to-vehicle contact parameters, the static and dynamic coefficient of friction is set at 0.40 to reduce noisy results and the friction decay coefficient is set at zero. The time-step is defined to be small and the total termination time is set at 20*ms* to capture all the impact events.

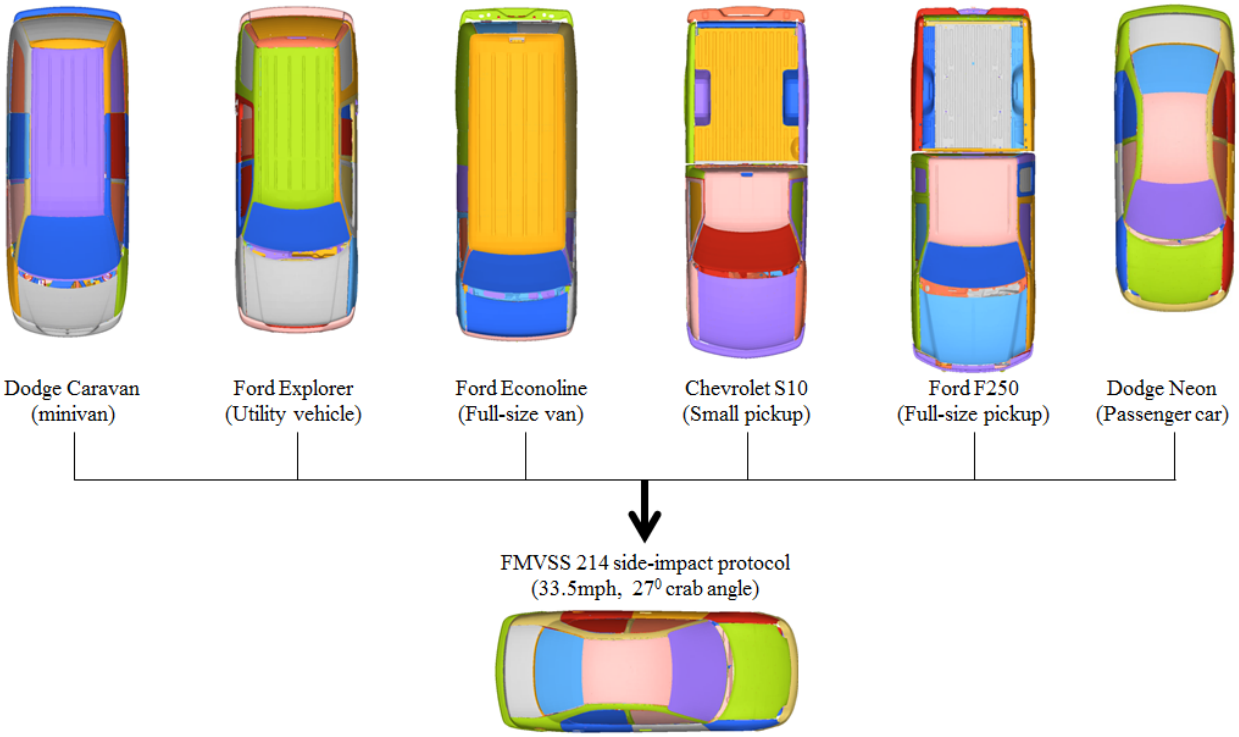

Figure 6.8. Reconstruction of side-impact accident using finite element method

6.2.3 Results and discussions

The intrusion depth and deceleration of the bullet and target vehicle are measured at various locations and the results are shown in Tables 6.1 and 6.2 respectively. The post-crash deformation of the LTV-to-vehicles is illustrated in Figure 6.11. From the results, it is shown that regardless of the statistical DFR severity ranking, the intrusions and decelerations transmitted to the bullet vehicles are generally lower than that of the target vehicle. This type of behavior is expected from side-impact accidents because the structural supports and crush depth for the side-structure are much lower than the front-end of the vehicle. The post-crash deformation of both vehicles suggests that the front-end of the bullet vehicle is generally stiffer than the side structure of the target vehicle. Therefore, the difference in stiffness and the overall geometrical incompatibility of both colliding vehicles in side-impact accidents always results in higher intrusion and acceleration values to the smaller target vehicle than to the bullet vehicle.

Based on the intrusion levels, it is clearly shown that with higher DFR severity ranking, the intrusion to the target vehicle's head reference point increases while the intrusion to the bullet vehicle's engine top decreases. By cross examining the intrusion ratio of different locations, it is shown that ratio of the intrusion measured at the head reference point for the target vehicle and the intrusion measured at the engine top for the bullet vehicle yielded good estimation of DFR. In fact, no other combination of the intrusion ratio yielded good correlation with the statistical DFR. In addition, the average intrusion ratio based on the summation of all combination intrusion ratios also provided poor estimation of statistical DFR. For the target vehicle, intrusion measurements obtained from the engine top provides consistent results due to its location is located in front of the occupant cabin, that is at similar locations for other vehicles. Contrary, the locations for the foot-well and A-pillar vary significantly from vehicles to vehicles.

For the target vehicle, the intrusions measured at the cushion seat and window sill reference point are too sensitive to the various front-end height of the target vehicles. The intrusion to the head reference yielded higher consistency and is less sensitive to the front-end height of the target vehicle. Unlike frontal-accidents where under-ride of the target vehicle may occur when the ride height difference is high, side-impact accidents mostly occurred with the point of impact below the head reference point. Therefore, the intrusion measurement to the bullet vehicle is measured at the head reference point and the result indicated good robustness and reliability.

The deceleration ratios are found to be almost analogous with the statistical DFR, and the average of the deceleration ratios are found to be in good agreement with the statistical DFR. It is shown that the decelerations are the highest at the B-pillar for all crash scenario follow by the decelerations at the C and then A-pillar. Once again, due to the higher stiffness at the front-end of a vehicle, bulk of the impact energy is transmitted to the target vehicle causing the target vehicle to undergo higher acceleration. The proposed methodology that estimates the DFR using the intrusion and deceleration ratios of two colliding vehicles has shown to correlate well with the statistical DFR.

Table 6.9. Summary of ***intrusion ratios*** for different crash scenario with target vehicle as ***Dodge Neon***

Crash Scenario (Bullet vehicle)	Target Vehicle Intrusions [*mm*]			Bullet Vehicle Intrusions [*mm*]			DFR (statistics)	DFR (Intrusion Ratio)
	Head Ref.	Window-Sill	Seat Ref.	Firewall	Engine Top	A-pillar		
Dodge Neon	348.6	425.5	442.7	37.2	60.3	11.0	1:6	**1:5.8**
Chevy S10	388.2	491.9	464.4	19.4	39.1	8.0	1:11	**1:9.9**
Dodge Caravan	388.0	514.5	564.1	13.2	23.9	3.5	1:16	**1:16.2**
Ford F250	433.9	574.9	451.9	6.1	24.0	1.4	1:17	**1:18.1**
Ford Explorer	468.5	610.8	576.0	11.4	22.1	3.4	1:20	**1:21.2**
Ford Econoline	460.0	423.6	393.1	12.4	21.3	8.3	1:23	**1:21.6**

Table 6.10. Summary of ***deceleration ratios*** for different crash scenario with target vehicle as ***Dodge Neon***

Crash Scenario (Bullet vehicle)	Target Vehicle Acceleration [*G's*]			Bullet Vehicle Acceleration [*G's*]			DFR (statistics)	DFR (Deceleration Ratio)
	A-pillar	B-pillar	C-pillar	A-pillars	B-pillars	Firewall		
Dodge Neon	26.0	56.7	37.3	5.8	4.2	6.1	1:6	**1:7.4**
Chevy S10	22.2	59.2	40.4	5.3	3.9	5.5	1:11	**1:8.3**
Dodge Caravan	31.0	57.7	44.1	3.5	2.7	3.3	1:16	**1:14.1**
Ford F250	54.3	50.5	50.1	3.5	2.3	3.0	1:17	**1:17.5**
Ford Explorer	36.0	68.9	66.7	3.8	3.3	2.3	1:20	**1:18.2**
Ford Econoline	73.2	62.4	66.8	3.1	3.7	1.8	1:23	**1:23.3**

The stiffness curve for the target vehicle is obtained by using the US-NCAP full frontal test protocol. On the other hand, the stiffness curve for the bullet vehicle is obtained using the IIHS side-impact test protocol. The reaction forces of the rigid wall and moving deformable barrier are recorded and plotted against the instantaneous intrusion into the occupant compartment. The force-deflection graphs are illustrated in Figures 6.9 and 6.10 for the bullet and target vehicle respectively.

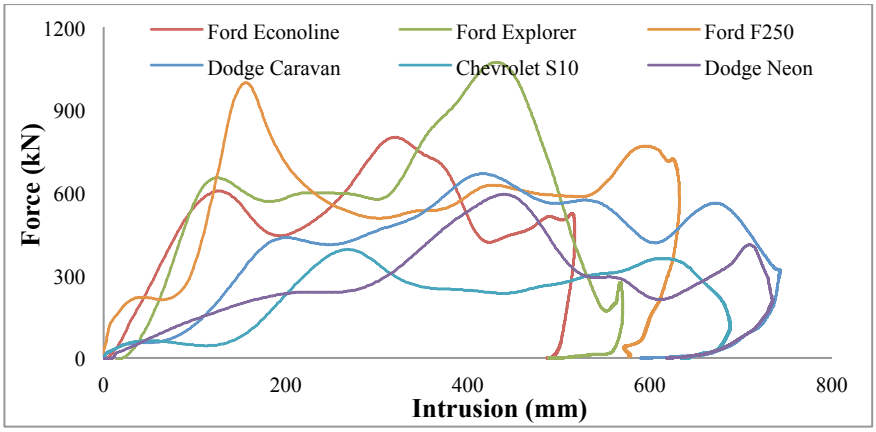

Figure 6.9. Force-deflection curve for various ***target vehicles*** obtained using the US-NCAP full-frontal test protocol

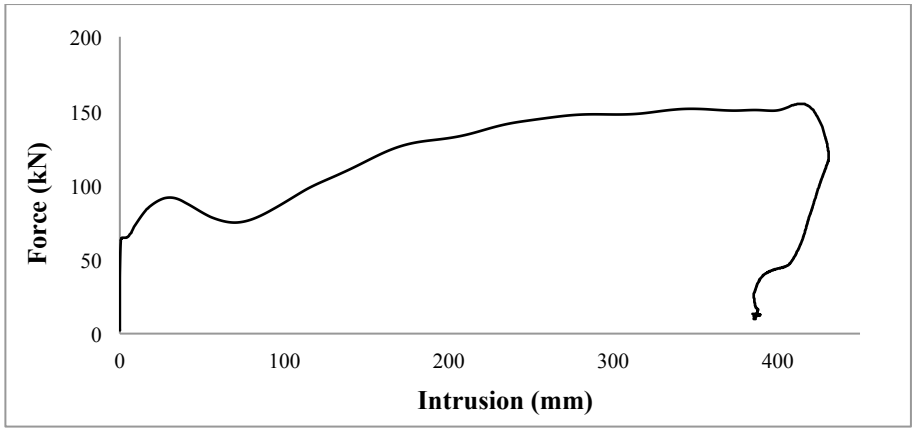

Figure 6.10. Force-deflection curve for ***Dodge Neon*** obtained using FMVSS 214 side-impact test protocol

Based on these two stiffness graphs, the stiffness can be determined through the slope of the curve. By utilizing the linear stiffness method and selecting the intrusion range of 0 to 120mm to be constant, the stiffness can be determined and the result is shown in Table 6.11. It is clearly shown that by using Equation (6.31), the estimated DFR based on stiffness ratio performs very poorly with the statistical DFR. However, this can be corrected by introducing a stiffness scale factor:

$$Adjusted\ DFR_{estimate}^{stiffness} = \gamma \cdot \mathrm{C} \cdot \left(\frac{Stiffness\ of\ the\ bullet\ vehicle, K_{Bullet}}{Stiffness\ of\ the\ target\ vehicle, K_{Target}}\right) \quad (6.32)$$

where C is the dimensionless stiffness scale factor. With the modified Equation (11), the adjusted estimated DFR certainly correlate better with the statistical DFR.

Based on the results, it is apparent that Ford Econoline is highly crash incompatible with Dodge Neon while Chevy s10 is quite compatible with Dodge Neon. For the Chevy s10-to-Dodge Neon and Dodge Caravan-to-Dodge Neon crash scenario, the stiffness ratio correlates poorly with the statistical DFR. Based on the stiffness graph as illustrated in Figure 6.9, the front-end stiffness for Dodge Caravan and Chevrolet s10 is lower from approximately 0 to 100mm intrusion and higher from approximately 100 to 220mm intrusion, and this explains the poor correlation for this two crash scenarios. In another word, the challenges in choosing an accurate intrusion range presents itself as one of the limitations in

utilizing the linear stiffness method, and that the interpretation of the vehicle stiffness is highly dependent on the range of intrusion chosen for the analysis.

Table 6.11. Summary of ***stiffness ratios*** for different crash scenario with target vehicle as ***Dodge Neon***

Crash Scenario (Bullet Vehicle)	**Bullet Vehicle Front-end Stiffness, K_{bullet}**	**Target Vehicle Side-structure Stiffness, K_{target}**	**DFR (statistics)**	**DFR (Stiffness Ratio)**	**Adjusted DFR (Stiffness Ratio)**
Dodge Neon	1386	1155	1:6	**1:1.2**	**1:6.0**
Chevy S10	647		1:11	**1:0.6**	**1:3.0**
Dodge Caravan	1334		1:16	**1:1.2**	**1:6.0**
Ford Explorer	4844		1:20	**1:4.2**	**1:21.0**
Ford F250	3857		1:17	**1:3.3**	**1:16.5**
Ford Econoline	5324		1:23	**1:4.6**	**1:23.0**

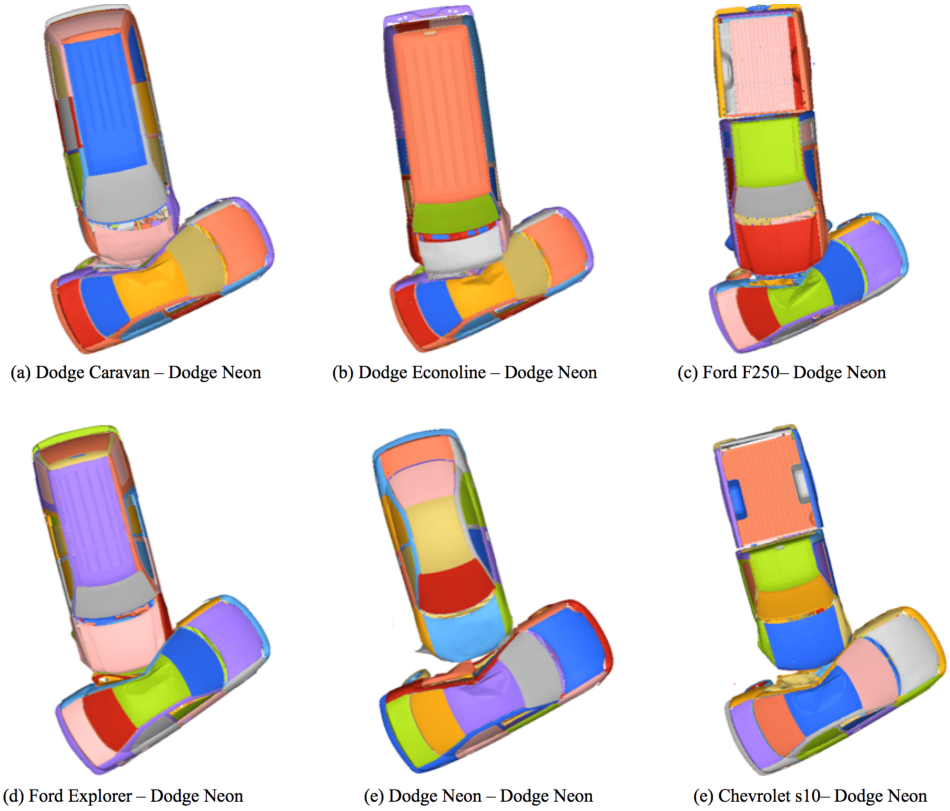

(a) Dodge Caravan – Dodge Neon (b) Dodge Econoline – Dodge Neon (c) Ford F250– Dodge Neon

(d) Ford Explorer – Dodge Neon (e) Dodge Neon – Dodge Neon (e) Chevrolet s10– Dodge Neon

Figure 6.11. Post-crash of different vehicle-to-vehicle crash configurations with Dodge Neon as target vehicle

It is conclusive that estimating the DFR using linear stiffness method as proposed in this study is only somewhat accurate. Therefore, by utilizing Equations (6.28), (6.29) and (6.30), it can be inferred at γ is negligible and cannot be used as a reliable component in the formulation of the combined DFR analysis. By setting α and β to be 0.5 assuming both

intrusion and acceleration have equal effect on the driver fatality, the combined DFR estimation model can be described as:

$$DFR_T^B \approx \alpha\left(\frac{Intrusion\ depth\ the\ bullet\ vehicle}{Intrusion\ depth\ the\ target\ vehicle}\right) + \beta\left(\frac{Deceleration\ of\ the\ bullet\ vehicle}{Deceleration\ of\ the\ target\ vehicle}\right) \quad (2.33)$$

As previously discussed, the relative priorities of the components can be adjusted by adjusting the α and β values. Instead of using the equal weight factors, the α and β can be adjusted to a 0.6 and 0.4 ratio to give higher priority to the intrusion ratio. The selection of these weight factors solely depends on the contribution of these parameters to the injury potential of the occupants

Table 6.12. ***Combined DFR estimation model*** with target vehicle as ***Dodge Neon***

Crash Scenario (Bullet Vehicle)	**DFR (statistics)**	**DFR (Intrusion Ratio)**	**DFR (Deceleration Ratio)**	**Combined DFR (Estimated)**
Dodge Neon	1:6	1:5.8	1:7.4	**1:6.6**
Chevy S10	1:11	1:9.9	1:8.3	**1:9.1**
Dodge Caravan	1:16	1:16.2	1:14.1	**1:15.2**
Ford F250	1:17	1:18.1	1:17.5	**1:17.8**
Ford Explorer	1:20	1:21.2	1:18.2	**1:19.7**
Ford Econoline	1:23	1:21.6	1:23.3	**1:22.5**

By extending this methodology further, the combined DFR estimation model is utilized to estimate the DFR for a newer passenger car in side-impact accident. In order to maintain consistency, the fleet of vehicles used as bullet vehicles is similar to the previous simulation test. However, the vehicle selected as the target vehicle is the Toyota Yaris FE model. Similarly, the intrusion measurements for both target and bullet vehicles are taken at similar locations as the previous test. Last but not least, the DFR improvement for the Toyota Yaris, when compared to Dodge Neon, is also analyzed.

The intrusion ratio and deceleration ratio are illustrated in Tables 6.13 and 6.14. Based on intrusion levels, it is clearly shown that the intrusions to the target and bullet vehicle are significantly reduced with the Toyota Yaris when compared to Dodge Neon. In terms of the estimated DFR severity ranking, the simulation with Toyota Yaris is consistent with the DFR ranking with Dodge Neon as the target vehicle, where full-size van, full-size

pickup, utility vehicle and minivan ranked the highest DFR followed by small pickup and passenger car. Similarly, the intrusion and deceleration ratios can be combined using Equation (6.33) and the estimated DFR is shown in Table 6.15. It is clearly shown that the estimated DFR for the newer target vehicle is improved significantly when compared to older target vehicle. In terms of quantitative improvements, the estimated DFR for full-size-van-to-passenger car crash has the highest improvement, which correlates to approximately 50 percent reduction in DFR while the estimated DFR for minivan-to-passenger car crash yielded the lowest improvement of only 10 percent in DFR reduction.

The significant structural improvements to Toyota Yaris, when compared to older vehicles such as Dodge Neon, have increased the crashworthiness of the side-structure, which resulted in lesser deformation and deceleration transmitted to the occupant cabin.

Table 6.13. Summary of ***intrusion ratios*** for different vehicle scenario with target vehicle as ***Toyota Yaris***

Crash Scenario (Bullet vehicle)	**Target Vehicle Intrusions [*mm*]**			**Bullet Vehicle Intrusions [*mm*]**			**DFR (Intrusion Ratio)**
	Seat Ref.	**Head Ref.**	**Window-Sill**	**Foot-well**	**Engine Top**	**A-pillar**	
Toyota Yaris	114.7	**98.7**	119.6	22.5	**35.3**	24.7	**1:2.8**
Chevy S10	97.7	**101.0**	100.4	7.3	**15.7**	0.3	**1:6.4**
Dodge Caravan	234.8	**257.7**	271.7	9.2	**19.2**	1.9	**1:13.4**
Ford F250	274.1	**250.4**	299.4	0.5	**17.4**	0.3	**1:14.4**
Ford Explorer	292.5	**129.7**	218.7	8.1	**13.5**	0.1	**1:9.6**
Ford Econoline	251.4	**175.2**	261.0	8.2	**10.3**	0.6	**1:16.9**

Table 6.14. Summary of ***deceleration ratios*** for different crash scenario with target vehicle as ***Toyota Yaris***

Crash Scenario (Bullet vehicle)	**Target Vehicle Acceleration [*G's*]**			**Bullet Vehicle Acceleration [*G's*]**			**DFR (Deceleration Ratio)**
	A-pillar	**B-pillar**	**C-pillar**	**A-pillars**	**B-pillars**	**Firewall**	
Toyota Yaris	18.3	51.7	28.7	5.0	11.3	6.8	**1:4.3**
Chevy S10	15.1	74.6	26.0	6.9	7.1	7.8	**1:5.3**
Dodge Caravan	26.1	85.4	39.9	3.6	3.5	3.9	**1:13.8**
Ford F250	28.4	59.0	46.2	4.1	3.2	3.9	**1:11.9**
Ford Explorer	22.0	56.1	40.1	4.0	3.5	4.0	**1:10.3**
Ford Econoline	33.3	76.5	65.5	4.6	5.0	4.6	**1:12.3**

Table 6.15. ***Combined DFR estimation model*** with target vehicle as ***Toyota Yaris***

Crash Scenario (Bullet Vehicle)	DFR (statistics)	DFR (Intrusion Ratio)	DFR (Deceleration Ratio)	Combined DFR (Estimated)	*Percent Improvement [%]
Dodge Neon	1:6	1:2.8	1:4.3	**1:3.4**	43.3
Chevy S10	1:11	1:6.4	1:5.3	**1:5.9**	46.4
Dodge Caravan	1:16	1:13.4	1:13.8	**1:13.6**	15.0
Ford F250	1:17	1:14.4	1:11.9	**1:13.2**	22.4
Ford Explorer	1:20	1:9.6	1:10.3	**1:10.0**	50.0
Ford Econoline	1:23	1:16.9	1:12.3	**1:14.6**	36.5

* Percent improvement of the DFR by comparing the DFR for Toyota Yaris with Dodge Neon as the target vehicle

6.4 Conclusions

The primary objective of this study was to develop a DFR estimation model for a fleet of LTVs striking a passenger car in a side-impact collision using finite element approach. The non-linear finite element software, LS-DYNA, was used for the side-impact accident reconstructions. In this process, three quantitative methods, namely, the intrusion ratio, deceleration ratio and stiffness ratio were proposed and correlated with the statistical DFR. Next, a combined DFR estimation model was presented to increase the reliability and robustness of the model. The numerical simulations and results have shown the intrusion and deceleration ratios correlated quite well with the statistical DFR. On the contrary, the stiffness ratio approach was a "prove-of-concept" and selecting a suitable displacement range has posted considerable challenge. Additional research work needs to be done to examine a proper algorithm to quantify the vehicle's stiffness. Some of the methods that could potentially be used to correlate the vehicle's stiffness with the statistical DFR are to analyze the stiffness using piecewise linear approximation by discretizing the force-deflection curve into three separate regions: before buckling, after buckling and when the occupant cabin starts to deform. However, the linear stiffness approach may be applicable to frontal car-to-car crash where the difference in stiffness may be lesser.

By using the proposed combined DFR estimation model, a final set of simulations were replicated by replacing the Dodge Neon with Toyota Yaris as the target vehicle, and the

identical fleet of bullet vehicles from the previous study were utilized. The purpose of this simulation test was to evaluate the structural performance of newer passenger cars by quantifying its DFR when impacted by LTVs. It was shown that the crashworthiness of the Toyota Yaris performed significantly better than the Dodge Neon. This was reflected on the significant reduction ranging from 10 to 50 percent in the estimated DFR. The strength of utilizing the proposed methodology in estimating DFR is in the initial design process of newer vehicles. With this, automotive engineers can calculate and estimate the DFR of newer vehicles with the current fleet of on-road vehicles, and necessary changes can be made to decrease its aggressivity. In turn, injury potential to vehicle occupants can be reduced.

6.5 References

[1] Gabler, H., and Hollowell, W., 1998, "The Aggresivity of Light Trucks and Vans in Traffic Crashes," 1998 SAE-980909, Detroit, Michigan.

[2] Moradi, R., Setpally, R., Lankarani, H.M., 2013, “Use of Finite Element Analysis for the Prediction of Driver Fatality Ratio Based on Vehicle Intrusion Ratio in Head-On Collisions," Applied Mathematics, pg 56-63. DOI: 10.4236/am.2013.45A007.

[3] Moradi, R., Septally, R., and Lankarani, H. M., 2011, “Influence of the Truck Side Under-ride Guard Height on Cabin Intrusion and Injury Potentials of the Small Car Occupants in Car/Heavy-Truck Side Crashes,” International Journal of Vehicle Structures and Systems (IJVSS), special issue on Fracture mechanics and Crashworthiness, - Part II, IJVS1019, Vol. 3, No. 3, pp. 169-177.

[4] Watanabe, T., Hirayama, S., Obayashi, K., and Okabe, T., “Research on Stiffness Matching Between Vehicles for Frontal Impact Compatibility,” NHTSA, Paper No. 05-0302, Washington DC.

[5] Watanabe, T., Hirayama, S., Obayashi, K., and Okabe, T., “Second Report of Research on Stiffness Matching Between Vehicles for Frontal Impact Compatibility,” NHTSA, Paper No. 07-0261, Washington DC.

[6] Hirayama, S., Obayashi, K., and Okabe, T., “Compatibility for Frontal Impact Collisions Between Heavy and Light Cars,” NHTSA, Paper No. 454., Washington DC.

[7] Annonymous, "Vehicle Crash Database", National Highway Traffic Administration, Washington DC., http://www-nrd.nhtsa.dot.gov/database/veh/veh.htm (retrieved: Jan, 2014).

[8] Pawlus, W., and Karimi, H.R., 2011, "Mathematical modeling of a vehicle crash test based on elasto-plastic unloading scenarios of spring-mass models," *Int J Adv Manuf Tech., DOI 10.1007/s00170-010-3056-x.*

[9] Huang, M., *Vehicle Crash Mechanics*, CRC Press, 2002: Florida, 2002. Print.

[10] Munyazikwiye, B. B., Karimi, H. R., and Gunnar, K., 2013, "Mathematical Modeling of Parameters Estimation of Car Crash Using Eigensystem Realization Algorithm and Curve-Fitting Approaches," *Mathematical Problems in Engineering Vol. 2013, http://dx.doi.org/10.1155/2013/262196.*

[11] Witold Pawlus, Hamid Reza and Kjell Gunnar Robbersmyr, 2011,"Application of viscoelastic hybrid models to vehicle crash simulation," *International Journal of Crashworthiness, 16:2, 195-205, DOI: 10.1080/13588265.2011.553362.*

[12] Bois, P. D., Chou, C.C., Fileta, B.B., Khalil, T.B., King, A.L., Mahmood, H.F., Mertz, H.J., and Wismans, J., 2004, "Vehicle Crashworthiness and Occupant Protection," American Iron and Steel Institute.

[13] Joksch, H., Massie, D., and Pichler, R., 1998, "Vehicle Aggressivity: Fleet Characterization Using Traffic Collision Data", NHTSA, DOT HS 808 679, DOT-VNTSC-NHTSA-98-1, Washington DC.

[14] Gabler, H. C., Hollowell, W., 1998, "NHTSA's Vehicle Aggressivity and Compatibility Research Program," NHTSA Paper Number 98-S3-O-01, Washington DC.

[15] Steyer, C., and Delannoy, P., 1998, "Proposal to Improve Compatibility in Head on Collisions," 16th International Technical Conference on Enhanced Safety of Vehicles, Paper No. 98-S3-O-05, Windsor.

[16] Diggs, K., and Eigen, A., 2001, "Measurements of Stiffness and Geometric Compatibility in Front-to-Side Crashes," The 17th ESV Conference Proceedings, Amsterdam, The Netherlands.

[17] Augestein, J., Perdeck, E., Bowen, J., Stratton, J., Horton, T., Rao, A., Digges, K., Malliaris, A., and Steps, J., 2000, "Injury Patterns in Near-Side Collisions," SP-1518, SAE Paper No. 2000-01-0634, Michigan, MI.

[18] Annonymous, 2002, "Frontal Crashworthiness Evaluation – Guidelines for Rating Structural Performance," Insurance Highway Institute for Highway Safety, Arlington, VA.

[19] Annonymous, 2012, "Side Impact Crashworthiness Evaluation Crash Test Protocol," Insurance Highway Institute for Highway Safety, Version VI, Arlington, VA.

[20] Finite Element Model Archive, National Crash Analysis Center, George Washington State University http://www.ncac.gwu.edu/vml/models.html (retrieved: November 2013).

CHAPTER SEVEN

CONCLUSIONS AND RECOMMENDATIONS

7.1 Conclusions

The primary objective of this thesis was aimed at contributing to the body of knowledge in the field of vehicle crashworthiness by introducing several new technologies to improve the passive safety of road vehicles in side-impact accidents with the ultimate goal of reducing the injury levels of vehicle occupants. The goal of this thesis was achieved by investigating the safety performance of advance airbag systems with the implementation of pre-crash sensing algorithm, structural performance of vehicle side-impact structures with the inclusion of high-energy absorbing cellular materials in the door panels in side-impact accidents, development of injury prediction model to estimate injuries to out-of-position occupants caused by frontal- and side- deploying airbags, and parametric study on vehicle aggressivity and estimation of driver fatality ratio in side-impact accidents.

The studies of vehicle crashworthiness, structural integrity analysis, impact injury biomechanics and injury prediction models have drawn significant interest from investigator and researchers from both the automotive and academia industry. Over the past few decades, occupant safety in road vehicles has improved tremendously. The focus on the field of vehicle crashworthiness have shifted from designing phase to the optimize phase, where researchers are beginning to predict and optimize the behavior of vehicles when subjected to various crash scenario. Today, the advancement in computational efficiency and finite element solver have transformed the way investigator conduct research work. Finite element analyses have shown to be highly accurate in predicting the non-linear behavior of vehicle crashes. This technique eliminates the need to conduct experimental runs, which can be very costly and time consuming.

In chapter two, the dynamic behavior of vehicles' side-structure with the inclusion of high-energy absorption cellular paddings was investigated. The objective measurements used to evaluate the structural performances were the intrusion depth of the B-pillar, transmitted acceleration and energy-absorption characteristics of the side-structure. It was shown that the transmitted acceleration and intrusion depth with the inclusion of CONFOR Green were reduced by approximately 20 and 30 percent, respectively. Similarly, the energy absorbed by the side-structure was increased by 25 percent with the inclusion of celular paddings. One of the concerning issue with side-impact accidents is the limited crush space of the side-structure. This severely limits the energy absorption capability of the side-structure through the means of structural deformation. Hence, this study highlights the importance utilizing high-energy absorbing cellular paddings in critical parts of the vehicle to reduce the intrusion and deceleration transmitted into the occupant cabin.

In chapter three, the effect of implementing pre-crash sensing algorithm to pre-deploy airbag prior to actual crash is quantified using injury levels sustain by occupants in side-impact accidents. The injury criteria used to quantify the injury levels of occupants were head injury criteria, thoracic trauma index, pelvic acceleration, and rib deflections. The side-airbag was modeled as a generic airbag with a bell curve inflator model, and a moving deformable barrier impacts the vehicle at various impact speeds. The primary hypothesis of this study is that current airbag systems may not have sufficient amount of time to reach fully inflated stage at high speed crashes; hence, reducing the injury protection capability of the airbag system. At all simulated test speeds, it was found that the injury levels of the occupants were significantly reduced with the pre-deployment of airbag. Furthermore, the reductions in the injury levels were more significant at high speed tests compared to low speed tests. Quantitatively, the injury potentials to the rib deflection was reduced by 11 percent, TTI(d)

by 20 percent, VC by 4 percent, pelvic force by 26 percent and pelvic acceleration by 29 percent, with the implementation of pre-crash sensing for the 50mph side-impact crash speed.

In chapter four and five, the injury levels of out-of-position occupants caused by frontal- and side- airbags were investigated. A set of injury prediction model was then developed using Design-of-Experiment methodologies, namely, the full-factorial design and response surface method. The objective measurements determined to have significant effects on the occupants' injury levels caused by a side-airbag were airbag fully inflated depth, airbag mass flow rate, and airbag permeability. Similarly, the airbag permeability, occupants' initial position, and friction coefficient between the occupant and airbag were determined as the influential factors for the frontal-airbag. The purpose of these studies was aimed at developing injury prediction models for the out-of-position occupants using full-factorial and response surface methodologies. It was found that the regression model obtained from the proposed methodologies were sufficient and accurate in predicting the injury levels of the occupants. This study also provided valuable design guidelines for the manufacturers of airbag systems.

Chapter six investigated the dynamic response of vehicles in a multi-vehicle crash. In the first part of this case study, various mathematical models to formulate the response of the vehicle in a full-frontal crash were investigated. It was shown that lumped mass model was quite accurate in predicting the kinematics and dynamics of a vehicle. In the second part of this case study, which forms the core of this chapter, involved analyzing the structural behavior of various multi-vehicle crashes. Due to the accuracy of finite element analysis, this method was utilized for the reconstruction of the side-impact accidents. A set of multi-vehicle crashes was conducted on a fleet of LTVs striking a passenger car in a side-impact accident. Next, the structural responses, such as, the acceleration, intrusion and stiffness ratios, of both the colliding vehicles were utilized to estimate the driver fatality ratio. The

main conclusion from this study was that the transmitted deceleration and intrusion of both vehicles were in good agreement with the statistical DFR, and can be used to predict the DFR for newer vehicles.

This thesis presented some of the new technologies that can be utilized in improving the passive safety of vehicle systems. However, several processes such as verification on the feasibility of the design in terms of manufacturing point-of-view, experimental tests, and cost-benefit analysis, must be performed before the implementation of these new technologies to future road vehicles. The preceding studies were made possible with the use of powerful and highly efficient finite element and multi-body analysis tools. Finally, the primary objective of this thesis was achieved with these proposed methodologies.

7.2 Recommendations

The research work presented in this thesis can be extended to future research, and they are summarized below:

- The work on the driver fatality risks can be extended to include various injury parameters to form a more robust DFR estimation model. Special attention must be paid to the weighting factors for determining the priorities of the intrusion and deceleration ratio in the combined DFR estimation model.
- This study investigated the structural behavior of a vehicle with the inclusion of cellular paddings. Future studies may include examining the influence of cellular paddings on the injury response of occupants. The arrangement and combinations of various these paddings also governs a new study. Also, the dynamic response of the vehicle with the installation of these paddings in the aft-side-door should be also be investigated.
- Special attention must be paid to the robustness of the response surface methodology in estimating the injury risks of out-of-position occupants from

frontal deploying airbag. This can be achieved by examining other techniques such as Kriging meta-model for comparison purposes.

- This thesis focused primarily on analysis of mechanical systems using multi-body dynamics and finite element method. However, special attention can be paid to the use of flexible body for impact analysis. If successful, flexible body may be feasible to various impact applications.
- Active safety software such as TASS Pre-Scan can be utilized to further develop on the concept of utilizing pre-crash sensing algorithm to pre-deploy the side-impact airbags.